The role of HCN channels in the prenatal development of the cerebral cortex in the mouse (*Mus musculus*, Linnaeus 1758)

I n a u g u r a l – D i s s e r t a t i o n

zur

Erlangung des Doktorgrades

der Mathematisch-Naturwissenschaftlichen Fakultät

der Universität zu Köln

vorgelegt von

Anna Katharina Schlusche

aus Frankfurt am Main

Köln

2017

Berichterstatter:	Prof. Dr. Ulrich Benjamin Kaupp Prof. Dr. Mats Paulsson
Tag der mündlichen Prüfung:	7. Dezember 2016

Zusammenfassung

Die Entwicklung des Gehirns folgt einem komplexen Muster, dessen Störung im Menschen zu einem heterogenen Spektrum an Erkrankungen, inklusive der schwerwiegenden Lissenenzephalie oder Mikrozephalie, führen kann.

Grundlegende Prozesse der kortikalen Entwicklung sind die Proliferation der neuralen Stamm- und Vorläuferzellen, deren Differenzierung in die verschiedenen neuronalen Subtypen und Gliazellen, sowie die Migration dieser differenzierten Zellen zu ihren endgültigen Ziellokalisationen. Diese Vorgänge werden neben anderen Signalen durch die elektrische Aktivität des Gehirns reguliert, welche wiederum durch die intrinsischen und extrinsischen Eigenschaften der einzelnen Zellen determiniert wird.

Ein Modulator der intrinsischen biophysikalischen Eigenschaften der Zelle ist der Hyperpolarisations-aktivierte und zyklisch Nukleotid-modulierte (HCN) Kanal und der durch ihn vermittelte Ionenstrom, I_h.

In der vorliegenden Arbeit wurden zum ersten Mal die Expressionsprofile der vier verschiedenen HCN-Untereinheiten während der embryonalen Vorderhirnentwicklung in der Maus analysiert. Diese Analysen offenbarten ein entwicklungsspezifisches Expressionsprofil, wobei die HCN3- und HCN4-Subtypen vor allem im embryonalen Gehirn eine Rolle spielen, wohingegen HCN1 und HCN2 die höchste Expression im postnatalen und adulten Vorderhirn zeigen.

Des Weiteren konnte mittels Expression einer dominant-negativen HCN Untereinheit eine Untereinheiten-unspezifische Ablation des durch HCN-Kanäle vermittelten Ionenstroms (I_h) erzielt und damit die Funktion des Stroms in der embryonalen Entwicklung untersucht werden. Die embryonale Ablation des I_h führte zu einer Mikrozephalie, die durch eine starke Verringerung der Proliferation und zeitlich veränderter Differenzierung der neuralen Stamm- und Vorläuferzellen verursacht wurde. Die Migration der jungen Neurone hingegen war nicht beeinträchtigt.

In *in vitro* Experimenten mit primären kortikalen Stammzellkulturen konnten ebenfalls eine reduzierte Proliferation und veränderte Differenzierung als Folge der pharmakologischen Inhibition des I_h nachgewiesen werden.

Zusammenfassend zeigt diese Arbeit damit erstmalig eine entscheidende Rolle der HCN-Kanäle und des durch sie vermittelten I_h in der Proliferation und Differenzierung von neuralen Stamm- und Vorläuferzellen.

Abstract

The development of the brain requires a complex sequence of processes, and any disturbances in these processes can lead to severe disorders such as lissencephaly and microcephaly.

The involved events, which include the proliferation of neural stem and progenitor cells, the differentiation into a variety of neuronal subtypes and glial cells, as well as the migration of differentiated cells to their final localization, are tightly regulated. Among other mechanisms, the electrical activity of the brain, which is determined by extrinsic and intrinsic properties of neurons and glia, significantly contributes to the spatial and temporal control of these processes.

The hyperpolarization-activated and cyclic nucleotide-gated (HCN) channels and the current (I_h) mediated by them, have important functions in modulating the intrinsic biophysical properties of many cell types, including neurons.

This work presents the first detailed investigation of the endogenous subtype expression of HCN subunits in the embryonic forebrain. The analysis demonstrated a subtype switch, with HCN3 and HCN4 expression present during embryonic development, and HCN1 and HCN2 being the major subunits in the postnatal and adult mouse forebrain.

To study the functional significance of the early embryonic expression of HCN subunits, I_h was inhibited by a dominant-negative HCN (HCN-DN) subunit, resulting in a subunit-unspecific ablation of the current. Forebrain-specific embryonic expression of the transgenic subunit using the EMX1 promoter resulted in a severe microcephaly phenotype. The investigation of early cortical developmental processes revealed an impaired proliferation and differentiation of neural stem and progenitor cells in HCN-DN-expressing transgenic mice, but no impaired migration.

In agreement with these findings, *in vitro* experiments using primary neural stem cells from the embryonic rat cortex showed a reduced proliferation and altered differentiation when I_h was pharmacologically blocked.

In summary, this is the first work to show an involvement of the HCN3 and/or HCN4 subtype-mediated I_h in the proliferation and differentiation of neural stem and progenitor cells in the mammalian cerebral cortex.

Table of content

1 Introduction

The cerebral development is a complex process requiring a tight temporal and spatial regulation. Disturbances in any of the underlying processes can lead to severe malformations and disorders of the brain, such as microcephaly, lissencephaly, and cortical heterotopia, which can each be associated with epilepsy and mental retardation (Ross and Walsh, 2001; Francis et al., 2006; Pang et al., 2008). To better understand the pathophysiology of these debilitating diseases, a gain in knowledge of the exact mechanisms controlling cortical development is crucial.

1.1 Cortical Development

The formation of the cortical structures can be divided into three major steps:

The proliferation of neural stem cells;
Their differentiation into neurons and glial cells;
The migration of differentiated cells into cortical layers.

Cortical pyramidal neurons originate from the ventricular zone (VZ), where the highest proliferation activity occurs between embryonic days (E) 10 and E17 in the mouse embryo (Takahashi et al., 1993; Molyneaux et al., 2007). They differentiate from so-called neuroepithelial cells, which sheet the neural tube during early cerebral development and give rise to neural progenitor cells, the so-called radial glial cells (RG) (Kriegstein and Goetz, 2003). RGs possess a marked apicobasal polarity and are characterized by the expression of glial markers (Choi and Lapham, 1978; Kriegstein and Goetz, 2003).

Two major types of RG progenitor cells (apical and basal progenitors) can be distinguished by the location of their somata during mitosis (Taverna et al., 2014). The apical progenitors proliferate close to the lumen of the ventricle and can be divided into apical RGs (aRG) and apical intermediate progenitors (aIP) (Tyler and Haydar, 2013; De Juan Romero and Borrell, 2015). The basal progenitors consist of the basal RGs (bRG) - which exists only in a rather small population in the rodent brain – and the basal intermediate progenitors (bIP). Both basal cells lose contact with the ventricle and form the subventricular zone (SVZ) located on the apical side of the VZ (Figure 1-1) (Shitamukai et al., 2011; Wang et al., 2011; De Juan Romero and Borrell, 2015).

While aRGs maintain their ability to proliferate throughout development and divide both symmetrically (self-renewing) and asymmetrically (generating neurons or IPs) (Noctor et al., 2004), the IPs and the bRGs almost exclusively perform symmetrical

neurogenic divisions and, thus, divide in a self-consuming manner (Haubensak et al., 2004; Noctor et al., 2004; Wang et al., 2011; Tyler and Haydar, 2013).

In contrast to pyramidal neurons, inhibitory interneurons originate from the ganglionic eminence (GE) in the dorsal forebrain. Interneurons exhibit a different transcription profile that allows the two types of neurons to be differentiated from each other early in development (Anderson et al., 1999; Letinic et al., 2002; Fishell and Rudy, 2011).

After the peak neurogenesis is complete, the gliogenesis starts shortly before birth. During brain development, the SVZ gains in importance compared to the VZ, which is reflected by the increasing thickness of the SVZ and the simultaneous decrease in the VZ, as well as by the fact that most glial progenitor cells (gIP) proliferate in the SVZ (Figure 1-1). Astrocytes derive from three major cell pools. One astrocytic population is generated directly from RGs after their final division and translocate into the upper cortical layers to transform into astrocytes (Figure 1-1) (DeAzevedo et al., 2003; Noctor et al., 2004). Additionally, an overlapping progenitor pool for neuro- and gliogenesis is located in the SVZ, which generates astrocytes as early as on E15 (Noctor et al., 2004; Gao et al., 2014; Siddiqi et al., 2014). Furthermore, most of the astrocytes in the postnatal rodent brain in layers I - IV are generated locally by the division of mitotically active astrocytes (Ge et al., 2012). Oligodendrocytes that appear early on in cortical development descend from the GE. From E12.5 to E15.5, they are generated in the medial GE and anterior entopeduncular area and, at a later stage, descend from the lateral and caudal GE (Kessaris et al., 2006). As of postnatal day (P) 0, oligodendrocytes are generated in the SVZ of the dorsal telencephalon (Kessaris et al., 2006). In the adult rodent cortex, most oligodendrocytes originate from the lateral and caudal GE or SVZ (Levison and Goldman, 1993; Kessaris et al., 2006).

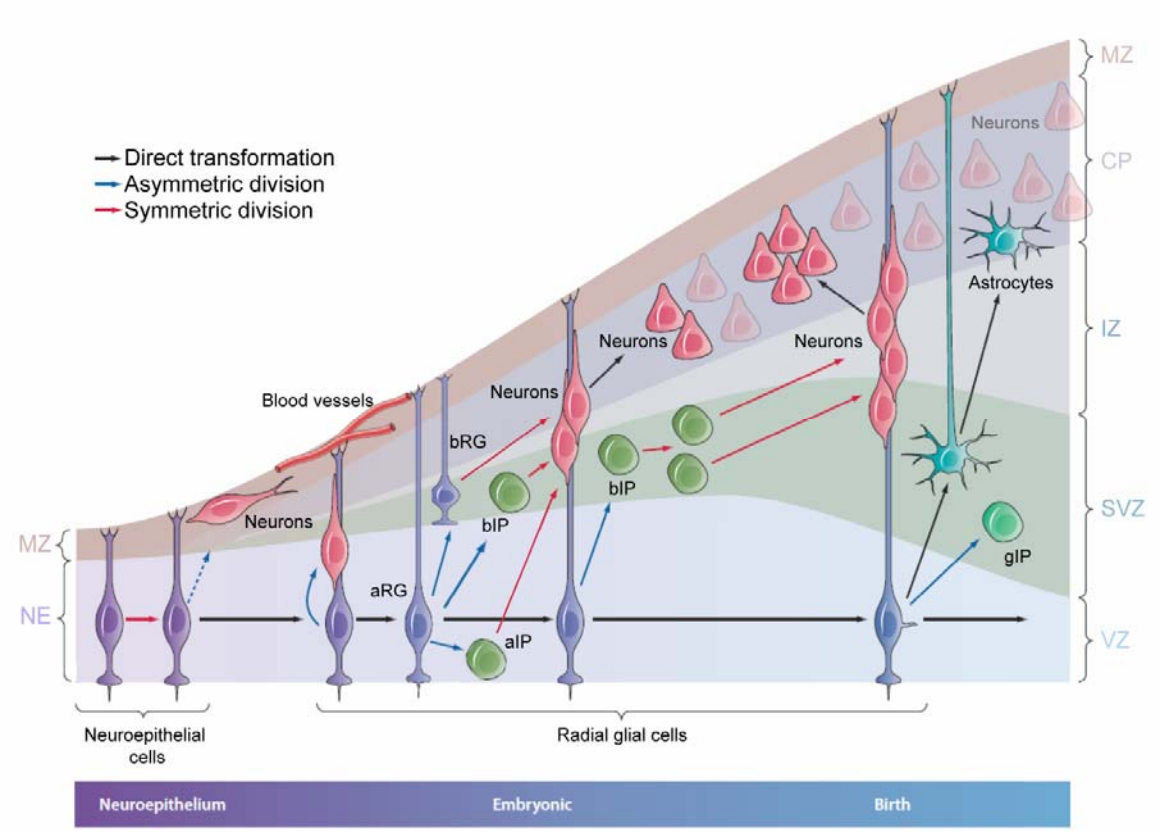

Figure 1-1 Processes of cortical development

Neuroepithelial cells in the neuroepithelium (NE) divide and transform into radial glial cells. Both cell types extend their processes through the cortical wall to the marginal zone (MZ). Apical radial glial cells (aRG) can divide asymmetrically to generate neurons and symmetrically to establish apical intermediate progenitors (aIP), the basal radial glial cell (bRG) and basal intermediate progenitor (bIP) pools. bRG, bIPs and aIPs divide mostly symmetrically into neurons that migrate along the RGs generating the cortical plate (CP). Around birth, the neurogenesis is complete and gliogenesis starts. After their last division, RGs transform into astrocytes and translocate into the CP. Oligodendrocytes and further astrocytes are generated by the glial IPs (gIP) in the thickened subventricular zone (SVZ). (VZ: ventricular zone; IZ: intermediate zone); modified from (Kriegstein and Alvarez-Buylla, 2009).

To reach their predetermined location in the newly formed cortical structure, neurons have to migrate. The earliest born excitatory neurons keep a long process to the basal membrane of the pial surface and migrate outward by somal translocation to form the preplate, which is generated at approximately E10 in the rodent brain (Nadarajah and Parnavelas, 2002; Marín et al., 2010). Subsequently born neurons migrate via locomotion along these radial glia cells (Rakic, 1972; Nadarajah and Parnavelas, 2002), thereby splitting the preplate into the marginal zone and subplate, forming together the cortical plate (Kriegstein and Noctor, 2004). The intermediate zone is established by the afferents of neurons from subcortical and cortical regions, building a white matter tract (Rakic, 2009). The cortical plate thickens by newly generated neurons in an inside-out fashion so that neurons born at a later stage

migrate past their older siblings (Rakic, 1974). The latest generated neurons reach their destination in layers II /III shortly before birth (Taniguchi et al., 2012). As the cortex thickens, the SVZ is formed, and the VZ decreases in size so that the postnatal proliferation occurs exclusively in the SVZ (Nadarajah et al., 2001).

Cortical interneurons migrate tangentially from the GE along the intermediate zone/SVZ or the marginal zone, followed by radial migration into the cerebral cortex (Anderson et al., 2001; Ang et al., 2003).

Once the neurons have reached their destination, contacts with neighboring and distant neurons are established by the formation and pruning of synapses.

1.2 Electrical activity in developmental processes

The above-mentioned developmental processes are controlled at numerous molecular and functional levels. Proliferating, differentiating, and migrating cells respond to internal and external cues guiding these cells through brain development. Within an electrically active organ such as the brain, which is composed of cells equipped with the ability to receive, convert, and transmit electrical signals, the spontaneous electrical activity and the bioelectrical properties of the cell's membrane play an important role in brain development (Spitzer, 2006; Rosenberg and Spitzer, 2011). Neuronal electrical activity depends on the extrinsic properties of neurons, e.g. neurotransmitter release, and the intrinsic biophysical properties, e.g. ion channel composition of the different cell types (Moody and Bosma, 2005).

Of note, electrical activity is not only limited to the generation of action potentials but includes the ion flux through the cell membrane mediated by a variety of ion channels in general.

1.2.1 Proliferation

Proliferation is a strictly regulated mechanism that can become part of pathological processes when it is deregulated. It is controlled by a variety of extrinsic and intrinsic cues mediating cellular responses via, among other factors, secondary messengers. Calcium is one of the most important second messengers and can modulate cell proliferation in a variety of different cell types. During the cell cycle, calcium transients are needed for the transition from G1 to S phase, and for the initiation and maintenance of mitosis (Berridge, 1995; Capiod, 2011). An increase in cytoplasmic calcium can be induced by voltage-gated calcium channels (VGCC; T- and L-type), or by calcium release from intracellular stores, mainly the endoplasmatic reticulum (ER) (Capiod, 2011).

Calcium transients were detected in proliferating cells in the rodent VZ *in situ* (Owens and Kriegstein, 1998). In those cells, transients are not dependent on neurotransmitters, such as glutamate and γ-aminobutyric acid (GABA), or on VGCC activity, but seem to rely exclusively on internal calcium stores. These fluctuations in calcium concentrations synchronize in varying sizes of cell clusters and in individual cells (Owens and Kriegstein, 1998). An increase in intracellular calcium concentration can also be detected in RGs, in which the inositol 1,4,5-trisphosphate (IP_3) pathway is coupled to the internal calcium stores of the ER (Weissman et al., 2004). Furthermore, inhibition of these calcium transients decreases the proliferation rate (Weissman et al., 2004; Lin et al., 2007), as reflected by a reduction in S-phase cells. These observations suggest a role for calcium fluctuations at the transition between G1 and S phase (Weissman et al., 2004; Resende et al., 2010). Due to the tight coupling of proliferating progenitor cells in the VZ by gap junctions, the calcium waves lead to a synchronization of the cell cycle progression (Bittman et al., 1997).

Besides calcium signaling, the proliferation of neuronal precursor cells can be modified by external cues such as neurotransmitters. GABA and glutamate have diverse roles in the regulation of neural proliferation. Both neurotransmitters can increase neural proliferation in the VZ, while they decrease proliferation in the SVZ (Haydar et al., 2000). It is further known that the reduction in proliferation is facilitated by $GABA_A$ and α-amino-3-hydroxy-5-methyl-4-isoxazolepropionic acid (AMPA)/kainate receptors, which mediate a depolarization of the cell membrane that leads to an increase in intracellular calcium through VGCC and, consequentially, to a decrease in DNA synthesis (LoTurco et al., 1995; Haydar et al., 2000). The negative effect of GABA on the proliferation of primary cortical stem cells was also shown in cell culture experiments (Antonopoulos et al., 1997). The prominent inhibitory effect of GABA and glutamate on neural proliferation can cause a substantial reduction in proliferation in the SVZ, which masks the pro-proliferative effect of these neurotransmitters in the VZ (Haydar et al., 2000).

Apart from ionotropic receptors, proliferating neuronal precursor cells mainly express calcium-dependent and voltage-gated potassium channels (Mienville and Barker, 1997; Hallows and Tempel, 1998; Picken Bahrey and Moody, 2002). Potassium channels are also expressed in other proliferating cells, including different cancer cell lines, and are believed to influence the cell cycle progression by modulating the membrane potential (Blackiston et al., 2009; Urrego et al., 2014).

1.2.2 Differentiation

The differentiation of neural precursor cells into neurons of different fate and morphology as well as into glial cells is a strictly regulated process with internal and external cues that has a distinct temporal and spatial order (Desai and McConnell, 2000; Rowitch and Kriegstein, 2010). The various differentiation steps are highly sensitive to changes in ion concentration in the cell environment, and depend on the ability of the cells to react to such alterations.

The differentiation of neurons is determined by the acquisition of a neurotransmitter type and the establishment of biophysical properties by the different neuron types, mainly by ion channel composition. In embryonic *Xenopus laevis* neurons and primary embryonic rat neurospheres, two different calcium transients were observed (Gu and Spitzer, 1995; Ciccolini et al., 2003). On the one hand, the global calcium transients spreading through the whole cell and modulating ion channel and neurotransmitter maturation and, on the other hand, calcium events, which are mostly local processes and modulate neurite outgrowth (Gu and Spitzer, 1995; Ciccolini et al., 2003). The pattern of the global calcium transients can be correlated to the neuronal cell type in *Xenopus laevis* spinal cord neurons. Furthermore, suppression of this activity leads to the expression of excitatory neurotransmitters (namely glutamate and acetylcholine), while an increase in this activity induces an inhibitory neurotransmitter type (glycine and GABA), independent of their genetic fate (Borodinsky et al., 2004). These experiments show that the activity level can predominate other developmental cues. Also, Brosenitsch and Katz showed that the expression of tyrosine hydroxylase is dependent on a combination of the transcription factor Phox2 and the depolarizing activity *in vitro* and *in vivo*, suggesting a role for electrical activity in dopaminergic cell fate (Brosenitsch and Katz, 2002). For all of these findings, there is only a short time window during brain development in which electrical activity plays an important role.

In addition to the determination of the neuronal fate, the final morphology with dendritic outgrowth and axonal pathfinding is also regulated by patterns of spontaneous activity and calcium transients (Katz and Shatz, 1996; Tang et al., 2003; Hanson and Landmesser, 2004; Kalil et al., 2011). Furthermore, the establishment of their axonal and dendritic connections (Spitzer, 2006; Chen and Kriegstein, 2015) and the formation of new synapses (Ben-Ari, 2006; Wang and Kriegstein, 2009) depend on spontaneous neuronal activity, and is needed for the establishment of adult patterns of connectivity within developing networks (Khazipov and Luhmann, 2006).

Although the differentiation of glial cells shows distinct machinery defining the oligodendrocytic or astrocytic cell fate, it also shares some mechanisms among the

different cell types. The calcium-sensing receptor (CaSR) is upregulated during oligodendrogenesis in the rodent brain (Ferry et al., 2000; Chattopadhyay et al., 2008). Facilitated by the CaSR, extracellular calcium mediates the commitment of neural precursor cells to oligodendrocytic precursor cells, their proliferation, and their maturation by an unknown mechanism (Chattopadhyay et al., 2008). During this process, calcium is acting as a primary messenger, instead of assuming its predominant role as a secondary messenger.

Much less is known about the role of calcium in astroglial differentiation. In the pituitary adenylate cyclase-activating polypeptide (PACAP) pathway, which, upon activation, is promoting the astrocytic cell fate, calcium is needed as a second messenger (Vallejo, 2009). Furthermore, expression of neuregulin-1 suppresses the glial cell fate by a presenilin–dependent pathway. Interestingly, presenilin is known to have a function in calcium homeostasis (Honarnejad and Herms, 2012), which led to the hypothesis that calcium waves in RGs are not only needed for the proliferation of neurogenic precursor cells but also for the inhibition of the astroglial cell fate (Leclerc et al., 2012).

Both glial cells have in common that their proliferating precursor cells express delayed rectifying and transient potassium channels, as well as sodium channels (Kressin et al., 1995; Bordey and Sontheimer, 1997; Chvatal et al., 1997; MacFarlane and Sontheimer, 2000; Higashimori and Sontheimer, 2007). The cell cycle exit is accompanied by upregulation of the Kir4.1 channel, leading to a hyperpolarized membrane potential and the subsequent differentiation into glial cells (Higashimori and Sontheimer, 2007).

1.2.3 Migration

One modulatory mechanism of the migration of neurons in the rodent brain is dependent on the early secretion of different neurotransmitters. The mechanisms differ between the radial and tangential migration of excitatory and inhibitory neurons, and between the various brain regions. In the rodent cortex, the migration of neurons is mainly regulated by paracrine secretion of the two major neurotransmitters glutamate and GABA (Demarque et al., 2002; Manent et al., 2005).

In migratory pyramidal cells, the main glutamatergic receptor is the N-methyl-D-aspartate (NMDA) receptor (Behar et al., 1999; Reiprich et al., 2005), whereas interneurons express mainly AMPA/kainate receptors (Manent and Represa, 2007). For radially migrating excitatory neurons, glutamate is a chemoattractant mediating cell migration towards the outer layer of the cortical plate (Behar et al., 1999; Hirai et al., 1999; Reiprich et al., 2005). Compared to their mature siblings, the membrane potential of immature dissociated cerebellar neurons is in a more depolarized state.

This depolarization removes the magnesium block of NMDA receptors, while their subsequent activation mediates a calcium influx (Hirai et al., 1999; Gerber et al., 2010).

The role of GABA in the modulation of migration of cortical neurons is more complex than that of glutamate. While the early post-mitotic neurons in the VZ/SVZ express the ionotropic $GABA_A$ and $GABA_{A/C}$ receptors - which promote migration from the germinal zones into the IZ - neurons migrating through the IZ react via the metabotropic $GABA_B$ receptor, which is needed to enter the cortical plate (Behar et al., 1998, 2000). In the upper cortical plate, neurons express $GABA_A$ receptors, which mediate a stop signal and, concomitantly, a decrease in the migration rate (Behar et al., 1998, 2000). GABA-evoked migratory responses are also dependent on calcium influx (Heck et al., 2007). In mature neurons, GABA is the main inhibiting neurotransmitter in the forebrain, while in immature neurons GABA is depolarizing. The depolarizing GABA effect is due to an increased intracellular chloride concentration in the immature brain, mediated by a differential expression of chloride transporters (Ben-Ari, 2002). It has been shown that this so-called GABA switch is needed in interneurons to alter the GABA response from a pro-migratory signal to a stop signal (Bortone and Polleux, 2009; Inoue et al., 2012).

Furthermore, serotonin was identified as an inhibitor of radial migration (Riccio et al., 2012).

Both glutamate and GABA increase the intracellular calcium concentration, which strongly influences migration (Behar et al., 1996; Hirai et al., 1999). It is known that the calcium influx in granule cells of the cerebellum is mediated by the voltage-gated N-type calcium channels. The amplitude and frequency of these calcium transients are correlated to the mode of migration, with a high intracellular calcium concentration promoting the migration (Komuro and Rakic, 1996).

In addition to calcium channels, small sodium currents and delayed potassium currents, but no hyperpolarization-activated currents, were detected in migrating neurons of the murine cortex (Picken Bahrey and Moody, 2002). By ablating the function of the leak potassium current mediated by the KCNK channel, migration of the pyramidal cells is impaired (Bando et al., 2014). This ablation leads to altered calcium handling in the migrating cells (Bando et al., 2014).

1.3 HCN channels

As described above, early electrical activity is of great importance to all processes of cortical development. For a developing neuron to be responsive and to process electrical signals, the intrinsic biophysical properties are essential. The hyperpolarization-activated cyclic nucleotide-binding non-selective cation (HCN) channel is of high relevance to the determination of these properties.

1.3.1 Structure and function of HCN channels

The HCN channel is a tetrameric channel belonging to the superfamily of voltage-gated potassium channels (Ludwig et al., 1998; Kaupp and Seifert, 2001). Each subunit consists of six transmembrane domains (S1-S6) with S4 as a voltage sensor containing positively charged arginine and lysine residues (Figure 1-2) (Gauss et al., 1998; Ludwig et al., 1998). The pore region is located between S5 and S6 with the glycine – tyrosine – glycine (GYG) motif, which is characteristic of the selectivity filter in potassium channels. In contrast to strictly potassium-conducting channels, the HCN channel contains a cysteine residue in front of the GYG motif spaced by an isoleucine. This is presumably the cause of the additional sodium permeability of the channel (Macri et al., 2012). At the intracellular C-terminus, a C-linker connects the S6 domain with the cyclic nucleotide-binding domain (CNBD) (Figure 1-2) (Wainger et al., 2001; Zagotta et al., 2003). HCN channels can assemble into homo- or heteromeric tetramers (Figure 1-2) (Ulens and Tytgat, 2001; Much et al., 2003).

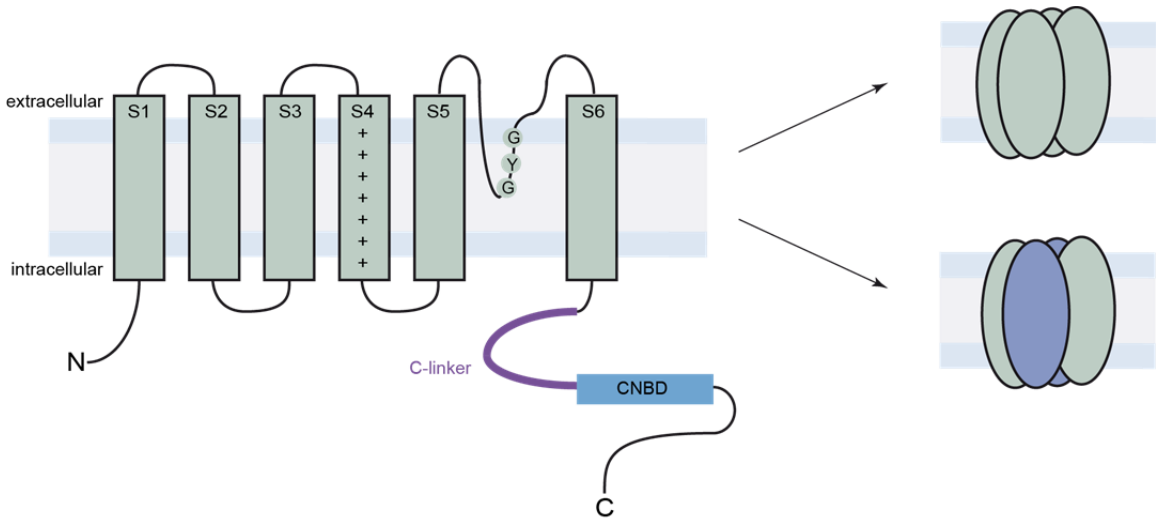

Figure 1-2 HCN channels

Each HCN subunit consists of six transmembrane domains (S1 –S 6) with a positively charged voltage sensor in S4. The pore region is located between S5 and S6 with the GYG motif as a selectivity filter characteristic of potassium channels. At the C-terminus, the cyclic nucleotide-binding domain (CNBD) is connected via the C-linker to S6, mediating the cyclic nucleotide modulation. Four subunits form a homo- or heteromeric tetramer.

In both the rodent and the human genomes, four different genes encode HCN subunits (HCN1 to 4) (Ludwig et al., 1998; Santoro et al., 1998; Stieber et al., 2005). The distinct subtypes show specific kinetics, with the HCN1 channel exhibiting the fastest activation (Santoro et al., 1998), HCN2 and HCN3 being intermediate in their response (Ludwig et al., 1999; Stieber et al., 2005), and HCN4 being the slowest reacting subtype (Ludwig et al., 1999; Seifert et al., 1999). In addition to the different activation and deactivation dynamics of the channel subtypes, the response to cyclic nucleotides varies as well. HCN2 and HCN4 subtypes show the strongest effect on cAMP application (Ludwig et al., 1999; Seifert et al., 1999), while HCN1 reacts only slightly to cAMP (Santoro et al., 1998), and HCN3 shows no effect of cyclic nucleotide binding (Stieber et al., 2005).

The function of HCN channels and the h-current (I_h) mediated by them, is strongly dependent on the spatial distribution of the HCN subunits in neuronal compartments, which substantially varies between individual neuronal subtypes.

In the cortex and hippocampus, HCN channels are mainly expressed in distal dendrites (Lörincz et al., 2002), where they contribute to the integration of postsynaptic potentials and, thus, to the regulation of functional connectivity (Magee, 1999; Williams and Stuart, 2000; Huang et al., 2009).

In a variety of cell types in different brain regions such as the hippocampus, thalamus, and cerebellum, HCN channels are mainly distributed along the soma and presynaptic terminals of axons (Luján et al., 2005; Boyes et al., 2007), influencing the membrane properties and neurotransmitter release (Lupica et al., 2001; Ludwig et al., 2003; Boyes et al., 2007). Also, I_h can contribute to the frequency control of the pacemaker, due to its depolarizing action upon hyperpolarization (Brown and Difrancesco, 1980). This was shown in the thalamus and in the heart (Brown and Difrancesco, 1980; McCormick and Pape, 1990; Mesirca et al., 2014).

In heterologous systems and in some cell types such as stellate cells of ventral cochlear nucleus, the I_h can be separated into an instantaneous current I_{ins}, which is voltage-independent, and a steady-state current I_{ss}, which is slowly activated upon hyperpolarization (Macri et al., 2002; Proenza et al., 2002; Rodrigues and Oertel, 2005; Aponte et al., 2006). It is not yet known whether the I_{ins} is a leak conductance or a second channel population (Macri et al., 2002; Proenza and Yellen, 2006).

1.3.2 Expression patterns of the different HCN subtypes

While I_h has crucial functions in the heart and brain, this work will mainly be focused on the latter.

All four HCN subtypes can be found with different expression patterns in the rodent brain, which was investigated at the RNA and protein levels (Moosmang et al., 1999; Notomi and Shigemoto, 2004). The highest expression of HCN1 can be found in the neocortex, hippocampus, superior colliculus, cerebellum, and brain stem (Moosmang et al., 1999; Santoro et al., 2000; Lörincz et al., 2002; Notomi and Shigemoto, 2004). The HCN2 subtype is ubiquitously expressed throughout the brain with prominent labeling in the thalamus and brain stem (Ludwig et al., 1998; Moosmang et al., 1999; Santoro et al., 2000; Notomi and Shigemoto, 2004). Of all the HCN subtypes, HCN3 exhibits the weakest expression in the brain, with only a slight increase in expression in the olfactory bulb, piriform cortex, habenular nucleus, and hypothalamus (Moosmang et al., 1999; Notomi and Shigemoto, 2004). HCN4 has a distinct expression pattern with prominent labeling in the olfactory bulb, habenular complex, and substantia nigra, and with the highest expression in the thalamus (Moosmang et al., 1999; Seifert et al., 1999; Santoro et al., 2000; Notomi and Shigemoto, 2004).

1.3.3 Regulation of HCN channels

HCN-channel activity is regulated by different molecules, kinases, and other proteins.

The best-investigated regulators are the cyclic nucleotides, mainly cAMP and, with a lower binding affinity, cGMP. Upon binding of cyclic nucleotides to the CNBD, the activation curve shifts towards more depolarized membrane potentials leading to a more positive half-maximal activation. This effect is caused by the release of auto-inhibition, probably mediated by the C-linker (Figure 1-2) (Wainger et al., 2001; Wicks et al., 2010). Additionally, cAMP traps the channel in the open state, which results not only in faster activation but also in slower deactivation (Wicks et al., 2010). The small effect of cAMP binding to HCN1 is due to a pre-existing disinhibition of the subunit (Chow et al., 2012). Another small molecule with the same effect on HCN channels, i.e. a depolarization shift of the activation curve and an alteration in channel kinetics, is mediated by phosphatidylinositol 4,5-bisphosphate (PIP_2) (Pian et al., 2006; Zolles et al., 2006). PIP_2 acts independently of cAMP and shows the same effect on HCN1, 2, 3, and 4 (Pian et al., 2006; Zolles et al., 2006; Ying et al., 2011). Both molecules lead to an activation of I_h at physiological membrane potentials. Furthermore, intracellular protons shift the activation curve to more hyperpolarized potentials and cause a decrease in channel opening (Munsch and Pape, 1999; Zong et al., 2001). This results in a reduction of I_h due to acidification and to an increase in the current facilitated by alkalization of the intracellular milieu (Munsch and Pape, 1999; Zong et al., 2001). Moreover, I_h is modulated by extracellular protons in a manner similar to that observed with intracellular acidification. Expressed in taste buds, HCN channels function as a receptor for sour taste (Stevens et al., 2001). In addition, a decrease in the extracellular chloride concentration reduces I_h and decelerates the opening kinetics in HCN2 and HCN4 channels (McCormick and Pape, 1990; Frace et

al., 1992; Wahl-Schott et al., 2005). Interestingly, a reduction in intracellular chloride concentration increases the instantaneous component without affecting the steady state I_{ss} (Mistrík et al., 2006).

In addition to small molecules, phosphorylation of kinases can also regulate HCN channels. HCN1 was discovered by the binding to a Src tyrosine kinase (Santoro et al., 1997). Later it was shown that Src kinase phosphorylation at the C-linker in HCN2 and HCN4 shifts the activation curve to more positive potentials and accelerates the activation kinetics (Zong et al., 2005; Arinsburg et al., 2006; Li et al., 2009). The phosphorylation site is conserved in all four subtypes.

Like other ion channels, the function of HCN channels is dependent on the correct subcellular localization. There are different accessory subunits and proteins that are needed to determine the final localization of the HCN subunits. Some exhibit additional regulatory functions, but all interact via the C-terminus of the channel subunit. HCN1 interacts with filamin A. Upon binding, the channel forms clusters and can be endocytosed, resulting in a decrease in current density (Gravante et al., 2004; Noam et al., 2014). Additionally, there is a deceleration of channel kinetics and a hyperpolarization shift of the activation curve (Gravante et al., 2004). From interaction studies, it is known that HCN2 can bind to the neuronal scaffolding proteins tamalin, S-SCAM, and Mint2 (Kimura et al., 2004). These scaffolding proteins are essential for trafficking and localization of several membrane proteins. Furthermore, HCN2 interacts with the potassium channel regulator protein 1 (KCR1), which results in a suppression of channel activity in the heart (Michels et al., 2008). In the rodent brain, HCN3 interacts with the potassium channel tetramerization domain-containing protein 3 (KCTD3), which increases the HCN3 cell surface expression and, thereby, its current density (Cao-Ehlker et al., 2013). An interaction with caveolin-3 is known for HCN4 in the sinoatrial node of the heart (Barbuti et al., 2004). This interaction places the channel into lipid rafts, facilitating proximity to modulating proteins such as adrenergic receptors (Barbuti et al., 2004, 2007). It is open to speculation whether the detected depolarizing shift of the activation curve caused by the destabilization of the lipid rafts is due to the disrupted interaction with caveolin-3, or due to hitherto unknown proteins in the rafts (Barbuti et al., 2004). HCN1, 2, and 4 interact with the MinK-related protein 1 (MiRP1) or KCNE2, resulting in an acceleration and increase of I_h, as well as in a higher cell surface expression of the protein in the heart and brain (Brandt et al., 2009; Ying et al., 2012). The tetratricopeptide repeat containing the Rab8b-interacting protein (TRIP8b) interacts with all four HCN subtypes and regulates trafficking and gating of the HCN channel (Santoro et al., 2004, 2011). To date, nine splice variants of TRIP8b with various binding effects on the channel are known to result in the up- or downregulation of the cell surface expression in distinct cellular locations (Lewis et al., 2009; Santoro et al.,

2009). In addition, TRIP8b antagonizes cAMP binding to the C-terminus of the channel subunit, resulting in a negative shift of the activation curve and in a reduced channel opening probability (Santoro et al., 2009; Zolles et al., 2009; Hu et al., 2013; DeBerg et al., 2015). It is still unknown whether this is the only impact on channel gating or whether TRIP8b also has a cAMP-independent mechanism (Zolles et al., 2009).

1.3.4 Knockout mouse models of the different HCN subunits

Knockout models of all four HCN subtypes are currently being analyzed. Their phenotypes vary due to the distinct expression profiles of the various HCN subtypes.

A global HCN1 knockout shows an increase in seizure susceptibility and severity, independent of the induction protocol, without displaying spontaneous epileptiform activity in the murine brain (Huang et al., 2009; Santoro et al., 2010). Also, these mice show enhanced hippocampus-dependent learning and memory but impaired motor learning (Nolan et al., 2003). Furthermore, an anti-depressant effect was observed in behavioral tests with *Hcn1* knockout mice (Lewis et al., 2011). In the visual system, HCN1 is widely expressed in the retina. Upon genetic ablation, the retinal response to light is prolonged, leading to altered vision (Knop et al., 2008). Moreover, because of the expression of HCN1 channels in dorsal root ganglia, their role in neuropathic pain was investigated. *Hcn1* knockout mice show a decrease in cold allodynia (Momin et al., 2008). In addition, HCN1 knockout mice exhibit bradycardia with sinus arrhythmia and sinus pauses (Fenske et al., 2013).

In line with the expression pattern of HCN2, *Hcn2* knockout mice show spontaneous absence epilepsy with reduced locomotion and sinus dysrhythmia (Ludwig et al., 2003). Likewise, a spontaneously occurring mutation in the *Hcn2* gene resulting in the absence of the HCN2 subtype causes absence epilepsy, ataxia, and an anti-depressant effect in so-called apathetic mice (Chung et al., 2009; Lewis et al., 2011). Due to the severity of the global knockout of *Hcn2*, the genetic deletion in a subtype of somatosensory neurons was established and investigated, showing a decrease in inflammatory thermal hyperalgesia and neuropathic pain (Emery et al., 2011).

The knockout of the auxiliary subunit TRIP8b shows deficits in motor learning, an anti-depressant effect, and mild absence epilepsy (Lewis et al., 2011; Heuermann et al., 2016).

Global *Hcn3* knockout mice presumably have a cardiac phenotype with an increase in T waves in the electrocardiogram, indicating a decelerated cardiac repolarization (Fenske et al., 2011).

The global knockout of *Hcn4* leads to an embryonically lethal phenotype, due to the absence of the main cardiac pacemaker, and causes severe bradycardia (Stieber et al., 2003).

1.3.5 HCN channels and disease

Although alterations in HCN channels and I_h are known to be involved in a variety of physiological and pathological processes in the nervous system, such as in pain (Lewis and Chetkovich, 2011) and Parkinson's disease (Chan et al., 2011), this work will be focused on the impact of I_h on epilepsy.

In different animal models of genetic and induced epilepsies, e.g. febrile seizures, temporal lobe epilepsy, or absence epilepsy, I_h was shown to be either increased or decreased, depending on the temporal or regional specificity of the experiments (see 1.3.4) (Chen et al., 2001; Jung et al., 2007; Dyhrfjeld-Johnsen et al., 2009; Kanyshkova et al., 2012).

In humans with severe chronic epilepsy, changes can be observed in HCN expression and current density in the hippocampus and neocortex (Bender et al., 2003; Wierschke et al., 2010). In addition to the alteration in I_h, which is likely to be secondary to epilepsy, genetic variations and triple proline deletions in HCN1 and HCN2 were detected in patients with generalized seizures or febrile seizures (Tang et al., 2008; Dibbens et al., 2010). Recently, mutations in the HCN1 subtype and a variety of comorbidities were found in patients with epileptic encephalopathies, which altered the HCN1 properties expressed *in vitro* in heterologous cells (Nava et al., 2014). The severe neurological phenotypes associated with HCN1 mutations point to an important effect of I_h on brain development.

In the heart, HCN channels and I_h can be changed depending on the progression of the disease, or they can constitute a genetic risk factor for the onset of the disease (see 1.3.4) (Herrmann et al., 2015; Verkerk and Wilders, 2015)

1.3.6 HCN expression and function in the developing rodent

Depending on the neuronal activity, changes occur in HCN subunit expression and localization in the cell during postnatal development. The adjustment of the neuron's biophysical properties is an essential prerequisite for the establishment and maturation of networks (Vasilyev and Barish, 2002; Brewster et al., 2006; Surges et al., 2006; Bender and Baram, 2008). However, the prenatal impact of I_h on cortical development remains unknown and has yet to be elucidated.

In the developing heart, HCN channel-mediated pacemaker currents are crucial for cardiac development and, thereby, for the viability of the embryo (see 1.3.4) (Stieber

et al., 2003). The same lethality was observed in mice that were deficient in the cyclic nucleotide-binding site in the CNBD of the HCN4 subtype, suggesting that the enhancement of HCN4 activity due to cAMP binding is an essential feature in the development of the cardiac system (Harzheim et al., 2008). Surprisingly, *Hcn4* deletion with an expression onset in the adult mouse shows only a mild cardiac phenotype with no alteration in mortality (Herrmann et al., 2007), suggesting an important role for the HCN4 subtype in cardiac development.

Of note, HCN expression was already detected in murine embryonic stem cells (Wang et al., 2005). While the impact of HCN channels on stem cell proliferation was described, the mechanisms underlying disturbed cell cycle regulation remain to be explored (Lau et al., 2011).

1.4 Hypothesis

This project is aimed at investigating the function of I_h in the prenatal development of the murine cortex based on a transgenic approach with a dominant-negative HCN subunit, ablating the I_h in a subunit-independent manner. To evaluate the early embryonic development, the EMX1 promoter was used to express the transgene in a forebrain-specific manner from E10 onward. This approach possibly altered the biophysical properties of the neuronal precursors, shedding new light on the impact of electrical competence on early developmental processes. Additionally, *in utero* electroporation was applied to further dissect specific prenatal time periods and processes. The combined evidence of these *in vivo* data and *in vitro* experiments - using rat cortical stem cell cultures and blocking I_h pharmacologically with ZD7288 – show the role of I_h in the early development of neuronal stem cells, progenitor cells, and early neurons.

This data provide novel insight into the impact of HCN channel activity on early prenatal developmental processes of the brain.

2 Material

2.1 Substances

All chemicals used in this work are from Carl Roth or Sigma-Aldrich if not otherwise stated.

5-Bromo-2'-deoxyuridine (BrdU); *in vitro*	Fluka
Betaisodona	mundipharm
Bovine serum albumin	PAA
Buprenorphine	RB Pharmaceuticals
Caprofen	Norbrook Laboratories /Bayer
Chemiblocker	Merck Millipore
DAPI Fluormount-G	Southern Biotech
DMEM/F-12 medium	Gibco
dNTPS	PANBiotech
Fluormount	Southern Biotech
Gadolinium	Insight agents
Hoechst 33342	Invitrogen
Human recombinant fibroblast growth factor (FGF)	Invitrogen
Isofluran	AbbVie
Ketamin	Albrecht
L-glutamine, N2-supplement	Gibco
Luminata™ Crescendo Western HRP Substrate	Merck Millipore
Lysis buffer (genotyping)	Peqlab
Midori Green Advance	Biozym
Milk powder	Heirler
NeuroTrace® 500/525	Molecular Probes
NeuroTrace® 530/615	Molecular Probes
Normal goat serum	Vector
NuPAGE® MOPS SDS running buffer	Life technologies

NuPAGE® transfer buffer	Life technologies
OCT	Sakura
PAN ladder 1 (DNA marker)	PANBiotech
Penicillin/Streptomycin	Gibco
Picrinic Acid	AppliChem
Sodium pyruvate	Gibco
Spectra™ Multicolor broad range protein ladder	Fermentas
Taq Polymerase	Applied Biosystems
Tris pH 7.4	AppliChem
Triton X 100	USBiological
Tween20	AppliChem
Vidisic	Bausch und Lomb
Xylazin	Eurovet

2.2 Buffers

Bath solution	135 mM NaCl 5 mM KCl 5 mM HEPES 2 mM $CaCl_2$ x 2H2O 2 mM $MgCl_2$ x 6H2O 10 mM Glucose 20 mM Sucrose pH 7.4 (NaOH)
Carrier solution	1 % Horse Serum 0.2 % BSA 0.5 % Triton X-100
Electrode solution	5 mM KCl 135 mM K^+-Gluconate 10 mM HEPES 0.2 mM NaGTP 2 mM $MgCl_2$ x 6H2O 2 mM ATP (Mg-Salt) 0.1 mM EGTA pH 7.3 (KOH)
HCN-IHC solution	5 % Chemiblocker 0.5 % Triton X-100 in PB

Lysis Buffer (genotyping)	0.4 mg/ml proteinase K in lysis buffer
PCR buffer (10x)	0.2 M Tris pH 7.9 0.5 M KCl
Phosphate buffer (PB) 0.1 M	14.41 g Na_2HPO_4 x $2H_2O$ 2.62 g NaH_2PO_4 x H_2O ad 1 l pH 7.4
Phosphate buffered saline (PBS)	3 M NaCl 161 mM Na_2HPO_4 x 2 H2O 39 mM KH_2PO_4
Sodium citrate buffer	10 mM Sodium citrate in PBS pH 9 (NaOH)
Sucrose buffer	0.32 M Sucrose 1 mM EDTA 5 mM Tris HCl pH 7.4 + freshly added Proteinase Inhibitor Cocktail (1:100)
Tris buffered saline (TBS)	100 mM Tris pH 7.4 50 mM NaCl

2.3 Antibodies

2.3.1 Primary Antibodies

Antigen	**Clone**	**Species**	**Producer**
WB			
HCN1	N70/28	mouse	neuromab
HCN2	75-111	mouse	neuromab
HCN3	75-175	mouse	neuromab
HCN4	75-150	mouse	neuromab
Hemagglutinin (HA)	12CA5	mouse	Roche
IHC and ICC			
Cleaved Caspase 3	AF835	rabbit	R and D Systems
CNPase	11-5B	mouse	Sigma
GFAP	GA5	mouse	Millipore
HCN4	PG2-1AY	rat	AG Kaupp/Wachten

Ki67	AB15580	rabbit	Abcam
Nestin	rat-401	mouse	Millipore
NeuN	A60	mouse	Chemicon
TuJ1	TuJ-1	mouse	R and D Systems
BrdU (ICC)	BU-33	mouse	Sigma-Aldrich
Sox2	MAB2018	mouse	R and D Systems

2.3.2 Secondary antibodies

Antigen	**Conjugate**	**Species**	**Producer**
GFP	A488	Rabbit	Molecular Probes
Goat	A546	Donkey	Molecular Probes
Mouse	HRP	Sheep	Dianova/Jackson
Mouse	A488	Goat	Molecular Probes
Mouse	A546	Goat	Molecular Probes
Mouse	fluorescein	Goat	Invitrogen
Rabbit	A546	Goat	Molecular Probes
Rabbit	fluorescein	Goat	Invitrogen
Rat	A488	Goat	Molecular Probes
Rat	A546	Goat	Molecular Probes

2.4 Primer Sequences

2.4.1 Genotyping

Cre	5’ - AAA CGT TGA TGC CGG TGA ACG TGC - 3’
	5’ - TAA CAT TCT CCC ACC GTC AGT ACG - 3’
HCN4	5‘ - GGC ATG TCC GAC GTC TGG CTC AC - 3‘
	5’ - TCA CGA AGT TGG GGT CCG CAT TGG - 3’

tTA2	5’ - CCA TGT CTA GAC TGG ACA AGA - 3’
	5’ - CTC CAG GCC ACA TAT GAT TAG - 3’
Ai9	5’ - AAG GGA GCT GCA GTG GAG TA - 3’
	5’ - CCG AAA ATC TGT GGG AAG TC - 3’
	5’ - GGC ATT AAA GCA GCG TAT CC - 3’
	5’ - CTG TTC CTG TAC GGC ATG G - 3’
NEXCre	5’ - CCG CAT AAC CAG TGA AAC AG - 3’
	5’ - GAG TCC TGG AAT CAG TCT TTT TC - 3’
	5’ - GAG TCC TGG AAT CAG TCT TTT TC - 3’

2.5 Kits

BCA assay	Thermo Fisher
CytoSelect™ 24-Well Cell Migration Assay	Cell Biolabs
EndoFree Plasmid Maxi Kit	Quiagen
GeneUp Total RNA Mini Kit	Biotechrabbit
KAPA SYBR FAST universal Kit	Peqlab
LDH Cytotoxicity Assay Kit	Thermo Scientific
LIVE/DEAD Cell-Mediated Cytotoxicity Kit	Life technology
QuantiTect Reverse Transription Kit	Quiagen
TissueScan Developmental Mouse Tissue qPCR Array	Origin

3 Methods

3.1 Animals and husbandry

All experimental procedures were approved by the „Behörde für Gesundheit und Verbraucherschutz“ of the City State of Hamburg, and by the „Landesamt für Natur, Umwelt und Verbraucherschutz Nordrhein-Westfalen“, Germany. Animals (mice, *Mus musculus*) were kept in type II long plastic cages under standard housing conditions (21 ± 2 °C, 50-70 % relative humidity, and food and water ad libitum, nesting material as well as a cart box houses and wood for chewing were provided in the cologne facilities). Mice were kept on an inverted 12:12 light:dark cycle and fed with Sniff, Las Vivendis or Altromin food. In experiments with doxycyclin treatment 200 mg/kg doxycycline was included into the Sniff food. Transgenic mouse lines used, were the following

C57BL/6-$^{Emx1tm1(cre)Ito}$ ROSA26$^{tm(tTA)}$ Tg$^{(tetO\text{-}Hcn4GYS,\text{-}EGFP)}$ further on called EMX-HCN-DN,

C57BL/6- Emx1$^{tm1(cre)Ito}$ Gt(ROSA)26$^{Sortm9(CAG\text{-}tdTomato)Hze}$ further on called EMX-Ai9,

C57BL/6- Emx1$^{tm1(cre)Ito}$ ROSA26$^{tm(tTA)}$ Tg$^{(tetO\text{-}Hcn4573X,\text{-}EGFP)}$ further called EMX-HCN-573X,

C57BL/6- Neurod6$^{tm1(cre)Kan}$ ROSA26$^{tm(tTA)}$ Tg$^{(tetO\text{-}Hcn4GYS,\text{-}EGFP)}$ further called NEXCre-HCN-DN.

NEXCre mice were a kind gift from Prof. Klaus-Armin Nave, Max-Planck-Institute Göttingen. As wild-type mice C56Bl/6J were analyzed.

3.2 Genotyping of transgenic mouse lines

To genotype the different transgenic mice, polymerase chain reactions (PCR) were performed. Tail or ear biopsies were lysed overnight in 100 µl lysis buffer at 54 °C. To inactivate the added proteinase K, samples were incubated at 85 °C for 45 min. Thereafter, a PCR was performed using a Biometra T3 Thermocycler.

The different PCRs to genotype the different mouse lines can be seen in **Table 3-1**.

Mouse line	PCR
EMX1-HCN-DN	Cre, tTA2, HCN4
NEXCre-HCN-DN	NEXCre, tTA2, HCN4
EMX-Ai9	Cre, Ai9
EMX-HCN-SND	Cre, tTA2, HCN4

Table 3-1 Performed PCRs for genotyping the used mouse lines

For all primer sequences see the material section. To validate the existence of the Cre locus in the different EMX1 driven mouse lines the following PCR assay without dimethyl sulfoxide (DMSO) was performed:

Forward primer (50 pmol)	0.5 µl
Reverse primer (50 pmol)	0.5 µl
MgCl2 (50 mM)	2.0 µl
10 x PCR-Buffer	5.0 µl
dNTPs	0.5 µl
Taq-Polymerase	0.5 µl
DNA-Template	2.0 µl
H2O	ad 50 µl

In **Table 3-2** the optimal PCR program to detect the Cre locus is shown.

	Temperature [°C]	Time	Cycle
Initial denaturation	95	5 min	1
Denaturation	95	30 s	2-30
Annealing	55	45 s	
Elongation	72	45 s	
Final elongation	72	5 min	31

Table 3-2 PCR program used to detect the Cre transgene

The tTA2, HCN4, NEXCre, and Ai9 loci were genotyped with the following PCR assay supplemented with DMSO:

Forward primer (50 pmol)	0.5 µl
Reverse primer (50 pmol)	0.5 µl
MgCl2 (50 mM)	2.0 µl
DMSO	2.5 µl
10 x PCR-Buffer	5.0 µl
dNTPs	0.5 µl
Taq-Polymerase	0.5 µl
DNA-Template	2.0 µl
H2O	ad 50 µl

To determine, if the genotype is hetero – or homozygous the NEXCre and Ai9 PCR assays were performed, using four primers for AI9 and three primers for NEXCre. See material section for detail.

The PCR program yielding the highest amplification for the tTA2 transgene is shown in **Table 3-3**.

	Temperature [°C]	**Time**	**Cycle**
Initial denaturation	95	5 min	1
Denaturation	95	30 s	2-30
Annealing	58	45 s	
Elongation	72	45 s	
Final elongation	72	5 min	31

Table 3-3 PCR program to detect the tTA2 transgene

For the HCN4 transgene the optimal PCR program is shown in **Table 3-4.**

	Temperature [°C]	**Time**	**Cycle**
Initial denaturation	95	5 min	1
Denaturation	95	30 s	2-30
Annealing	60	30 s	
Elongation	72	30 s	
Final elongation	72	5 min	31

Table 3-4 PCR program to validate the HCN4 transgene

To detect the NEXCre locus the PCR program shown in **Table 3-5** was used.

	Temperature [°C]	Time	Cycle
Initial denaturation	95	5 min	1
Denaturation	95	30 s	2-30
Annealing	54	30 s	
Elongation	72	30 s	
Final elongation	72	5 min	31

Table 3-5 PCR program to detect the NEXCre locus

The tdTomato in the Ai9 mouse line was detected by the PCR program shown in **Table 3-6**.

	Temperature [°C]	Time	Cycle
Initial denaturation	95	5 min	1
Denaturation	95	30 s	2-30
Annealing	61	45 s	
Elongation	72	45 s	
Final elongation	72	5 min	31

Table 3-6 PCR program to validate the Ai9 genotype

To detect the PCR product an agarose gel electrophoreses was performed using 2–3 % agarose gels with 0.004 % Midori Green Advance (Biozym) to detect double stranded DNA. The sizes of the detected DNA bands for the different genotypes were compared with the marker PAN ladder 1 and are shown in **Table 3-7**.

PCR product	Size [bp]
Cre	214
tTA2	597
HCN4	350
NEXCre	WT 770, Mut 520
Ai9	WT 297, Mut 196

Table 3-7 PCR products and their sizes in base pairs [bp]

3.3 MRI Analysis

For the magnetic resonance imaging neonatal animals were deeply anesthetized with a Ketamin (100 mg/ml) and Xylazin (20 mg/ml) solution and perfused with 7 ml PBS and 4 % paraformaldehyde (PFA) in PBS, both solutions contained 3 % gadolinium as MRI contrast agent. The total head was fixated overnight in the above mention PFA gadolinium solution and stored in 3 % gadolinium in PBS until the measurement. The MR imaging was performed in a 3.0 T small animal scanner in a 3D measurement (ClinScan, Bruker). Neonatal animals were analyzed with turbo spin echo (repetition time (TR) 200 ms, echo time (TE) 8.5 s, turbo factor 8, matrix 144 x 192 pixel, field of view (FOV) 11 x 14 mm, slice thickness 80 µm). 3 week old animals were measured alive under 1 - 2 % Isofluran anesthesia (500 ml/min in air). The breathing rate and body temperature of the head fixed animals was monitored. The juvenile animals were MR imaged by a constructive interference in steady state (CISS) sequence (TR 8.14 ms, TE 4.07 s, matrix 192 x 192 pixel, FOV 16 x 16 mm, slice thickness 90 µm). All further analyses were performed with Osirix v.3.9.4. software 32 bit version.

3.4 Quantitative real time PCR

To analyze the expression levels of the different HCN subtypes during the murine development of the brain the TissueScan Developmental Mouse Tissue qPCR Array from Origin was performed. The detailed description of the method can be found in (Schlusche, 2011). In short, the TaqMan probes of the HCN1 to HCN4 subtypes are labeled with the VIC™ fluorophore while the GAPDH is marked with FAM™ fluorochrome, to enable the execution of a duplex PCR. All primers and probes were obtained from Applied Biosystems (HCN1: Mm00468832m1; HCN2: Mm00468538m1; HCN3: Mm01212852m1; HCN4: Mm01176086m1). To amplify the PCR-products a standard protocol shown in Table 3-1Table 3-8 by utilizing a 7900HT Fast Real-Time PCR System from Applied Biosystems was performed.

	Temperature [°C]	**Time**	**Cycle**
Enzyme activation	50	2 min	1
Initial denaturation	95	10 min	2-40
Denaturation	95	15 s	
Synthesis	60	1 min	

Table 3-8 qPCR protocol used to investigate the expression level of the different HCN subtypes during development

Analysis was performed using the SDS 2.3 program to calculate the cycle threshold (CT) values. All further analyses were processed by the RQ Manager 1.2 and Data Assist v2.0 software.

3.5 Next generation sequencing including sample preparation

The next generation sequencing (NGS) results were obtained and kindly provided by Dr. Marta Florio of the laboratory of Prof. Huttner at the Max-Planck-Institute in Dresden, Germany. For the detailed protocol see Florio et al., 2015.

In short, cells were sorted using fluorescence-activated cell sorting (FACS) in following groups:

for the mouse embryo:
apical radial glia cells (aRG): TUBB3-GFP-/DiI+/Prom1+;
basal radial glia cells (bRG): TUBB3-GFP–/DiI+/Prom1–;
basal intermediated progenitor cells (bIP): TUBB3-GFP–/DiI–/Prom1–;
neurons (N): TUBB3-GFP+/DiI+/Prom1–.

For the human data set:
aRG: DiI+/Prom1+/S-G2-M
bRG: DiI+/Prom1– /S-G2-M
neurons, Nb: DiI+/Prom1–/G1-G0.

The mRNA extraction, transcription, amplification and library preparation were performed using commercially available kits. For the transcription in cDNA poly-dT primer and template switching oligos were used. For these exact and further kits see Florio et al., 2015.

To identify the genes in the transcriptome the reads were aligned to the mouse reference genome (mm10) and the human genome (hg19). The data is expressed in fragments per kilo base per million reads (FPKM) with a threshold bigger than 1.

3.6 Histology

3.6.1 Tissue preparation

For the histological analysis of the brain, the tissue was fixated with different protocols.

To analyze the embryos at different time points the mother was anesthetized with 2-3 % Isofluran, the embryos were exposed and decapitated. The mother was sacrificed by cervical dislocation. The whole embryonic head was immersion fixed in 4 % of PFA overnight.

The animals analyzed at time points older than P0 were sacrificed by cardiac perfusion. Here animals were anesthetized with intra peritoneal (i.p.) injections of Ketamin (100 mg/ml) and Xylazin (20 mg/ml) solution. The thorax was carefully opened and the heart was exposed. PBS and 4 % PFA were washed by a 25 gauge cannula through the left ventricle to clear the mouse body of blood and fixate the tissue. 7 ml or 50 ml solution was used for neonatal or juvenile/adult animals respectively. The brain was carefully removed and immersion fixated in 4 % PFA overnight.

For cryoprotection the tissue was stored in 15 % sucrose in phosphate buffered saline (PBS) until it sank, thereafter the samples were stored in 30 % sucrose in PBS for at least 24 h until the tissue sank again.

For HCN staining 15 % saturated picrinic acid was added to 4 % PFA and PBS was replaced by phosphate buffer (PB) (see materials). The cryoprotection was performed with 10 % and 30 % sucrose in PB, until the brains stopped floating.

All brains were promptly frozen in optimal cutting temperature compound (OCT) in peel-away embedding molds and stored at -80 °C until further treatment.

The samples were sliced at a cryostat CM 3050S (Leica) in 14 µm thick sections and subsequently stored at -80 °C until further staining.

3.6.2 Fluorescent Nissl Stain

For NeuroTrace® staining the sections were treated according to the manufactures manual. NeuroTrace® 530/615 Red Fluorescent Nissl Stain (Molecular Probes) was diluted 1:25 and NeuroTrace® 500/525 Green Fluorescent Nissl Stain (Molecular Probes) 1:600 in PBS. After the staining procedure the sections were mounted in DAPI Fluormount-G (Southern Biotech).

3.6.3 Immunohistochemistry

For immunohistochemistry different protocols were applied to yield the best possible staining.

To stain for cleaved Caspase 3, CNPase, Ki67 and neuron-specific class III β-tubulin (TuJ1), sections were washed in PBS to remove the OCT. Detection of cleaved Caspase 3 and CNPase needed an antigen retrieval, therefor the section were incubated at 70 °C in 10 mM sodium citrate buffer with pH 9 for 30 min. After heating, the sections were cooled down in the buffer. Unspecific binding of the antibodies was reduced by blocking with 5 % normal goat serum and 0.2 % TritonX-100 in PBS for 1 hour at room temperature. The primary antibody was diluted in PBS in different concentrations (cleaved Caspase 3: 1:2000; CNPase: 1:1000; Ki67: 1:250; TuJ1: 1:100) and 100 µl / slide were incubated overnight at 4 °C in a humid chamber. For the detection of cleaved Caspase 3 the primary antibody was added for 2 days. Thereafter, the slides were washed three times for 15 min in PBS on a shaker. To detect the cleaved Caspase 3 and Ki67 antibodies anti-rabbit secondary antibody diluted 1:200 in PBS was used. Antibodies against TuJ1 and CNPase were detected by incubation with anti-mouse antibody (1:200) in PBS. All secondary antibodies were applied for 2 hours at room temperature in a humid chamber in the dark, followed by three times 15 min washing with PBS on a shaker.

To detect GFP in brain sections a primary antibody directly coupled with an Alexa Fluor® 488 fluorophore was used. This staining was performed as described for Ki67 and TuJ1, with a primary antibody dilution of 1:200. After this incubation the sections were washed and mounted.

Staining for neuronal nucleus antigen (NeuN) required antigen retrieval in 10 mM sodium citrate buffer with pH 9 for 30 min at 70 °C. Sections for NeuN and glial fibrillary acidic protein (GFAP) staining were further blocked by 10 % horse serum, 0.2 % bovine serum albumin (BSA) and 1 % TritonX-100 in PBS, followed by the primary antibody diluted (NeuN: 1:250; GFAP: 1:500) in carrier solution (see material section) and incubated overnight at 4 °C in a humid chamber. After four times 5 min washing in PBS, the secondary antibody, anti-mouse diluted 1:500, was applied in 0.5 % TritonX-100 in PBS for two hours at room temperature in a humid chamber in the dark. The sections were washed again four times 5 min in PBS and mounted.

To detect the HCN subunits in brain sections the slides were washed three times for 5 min in PB, followed by blocking for 1 hour in HCN-IHC solution (see material section). The primary antibody was diluted 1:5 for HCN4 in HCN-IHC solution and incubated overnight at 4 °C in a humid chamber. Sections were washed four times for 5 min in

PB and the secondary anti-rat antibody was diluted 1:500 in HCN-IHC solution and incubated for 1 hour at room temperature in a humid chamber in the dark. The sections were washed again four times 5 min in PB and mounted. For double staining with TuJ1 antibody the protocol described for HCN subunits was applied with TuJ1 antibody diluted 1:100 and secondary anti-mouse antibody 1:200. HCN4 Antibody was a kind gift from PD Dr. Wachten.

After the staining procedure all sections were mounted in DAPI Fluormount-G (Southern Biotech).

3.6.4 Microscopy

Overview images of the total brain or brain sections were performed with the Olympus SZX16 Binocular with Olympus DP7Z camera with the corresponding software cellSense Entry 1.4.1. Other total brain pictures were taken with USB Digital Microscope V2.0 and its software MicroscopeCapture V2.0 from Dyntronic.

Furthermore microscopic images were captured with an AxioImager from Zeiss with AxioCam MRc or AxioCam MRm cameras using the Zen 2 lite software.

Images using a confocal microscope were captured using a Olympus FluoView™ FV1000 with Fluoview FV1000 camera and Fluoview 10 software version 4.0 or by using a ZEISS LSM 880 with Airyscan with Zen Black software version 2.1 SP1.

3.6.5 Stereology

Stereological analyses were performed with the Stereo Investigator software Version 10.01 from MicroBrightField at a Nikon eclipse 90i microscope. For the proliferation and apoptosis studies four sections 84 µm apart were counted for the SVZ/VZ, while the sensorimotor cortex was represented by eight slices. The sections for the analysis of VZ/SVZ were approximately at 2.31 mm from bregma (Franklin and Paxinos, 2007). For the investigation of the sensorimotor cortex the regions of interest (ROIs) were at approximately 2.31 mm and 3.75 mm from bregma. For example ROIs see Figure 6-1. The optical disector principle was used to estimate cell densities as described previously (Schmalbach et al., 2015). The parameters for the analysis were: guard space depth 2 µm, base and height of the disector 3600 μm^2 and 10 µm, respectively, distance between the optical disectors 60 µm, objective 40 x Plan-Neofluar® 40 x / 0.75 (Zeiss).

In the migratory analysis five sections 56 µm apart were analyzed. The electroporated patch was divided in layer II/III layer IV to VI with intermediated zone (IZ) and cortical plate as migratory zone and VZ/SVZ region. See Figure 4-8 for example ROIs. All GFP expressing cells in this ROI were counted.

To calculate the cell number the following equation was used:

$$\text{Cells/mm}^3 = \frac{\text{Number of counted cells}}{\text{Counting frame area} * \text{section height} * \text{sampling sites}} * 10^9$$

3.7 Western Blot

For detection of different proteins, Western Blot analysis was performed.

Proteins were extracted from the whole head of the embryos, from postnatal day 0 on the forebrain was carefully dissected. For this purpose, the mother was anesthetized with 2-3 % of Isofluran and the uterus and embryos were exposed. The mother was sacrificed by cervical dislocation. For the adult protein analysis the forebrain was removed shortly before sacrificing the animal by cervical dislocation. All tissue samples were immediately frozen in liquid nitrogen and stored by - 80 °C until further treatment.

To inhibit the degradation of the proteins, all following steps were performed on ice. The samples were homogenized using a 1.5 ml pistil and 200–400 µl sucrose buffer (see materials). The samples were centrifuged with 5000 g for 10 min at 4 °C the pellet was re-suspended and centrifuged a second time under the same conditions, to remove cell debris and the nucleus. To extract only the membrane proteins the reunited supernatant was centrifuged at ~ 100,000 g for 45 min at 4 °C. The supernatant contains the cytosolic proteins, while the membrane proteins in the pellet are re-suspended in 50–100 µl sucrose buffer depending on the pellet size.

To validate the protein concentration of the samples a bicinchoninic acid assay (BCA) assay from Thermo Fisher was used in accordance to the manufacturer protocol. Samples were diluted 1:100 and 1:50 and measured in an Epoch reader from BioTek and its according software Gen 5 2.07.

The separation of the proteins by size was performed with a NuPAGE® Bis-Tris gel electrophoreses (Invitrogen) with a polyacrylamide gradient of 4-12 %.

Gels with 10 wells were used. Approximately 20 µg of total protein per well were applied. The samples were treated accordance to manufacturer protocol and were loaded in a XCell SureLock™ electrophoreses chamber (Invitrogen). In NuPAGE® MOPS SDS running buffer the gels were run for approximately 30 min at 150 mV. As marker 6.5 µl of Spectra™ Multicolor broad range protein ladder from Fermentas was used.

To detect the protein of interest via antibodies the proteins have to be blotted to a nitrocellulose membrane. For this purpose a Mini-Protean® chamber from Bio-Rad containing NuPAGE® transfer buffer with 10 % methanol was used. Proteins are negatively charged so the membrane has to be directed to the anode of the chamber. Blotting is performed for 2 hours at 80 V and 30 min at 88 V or overnight at 6 V followed by 30 min 85 V.

To detect the protein of interest on the nitrocellulose membrane, different antibodies were used. To detect the transgene, which is coupled to hemagglutinin (HA) tag, an anti-HA antibody (Roche) was used. The different HCN subunits are detected via anti-HCN1, anti-HCN2, anti-HCN3, and anti-HCN4 (all mouse, neuromab).

To block unspecific reactions of the antibodies the membrane was blocked with 5 % milk powder and 0.05 % Tween20 in TBS for 1 hour at room temperature on a shaker. Subsequently 6 ml of anti-HA 1:500 and anti-HCN1-4 1:2000 diluted in 1 % milk powder and 0.01% Tween20 in TBS was added. The membrane was incubated for 1 hour at room temperature or overnight at 4 °C on a shaker. To remove unbound antibodies the membrane was washed four times 5 min in 0.05 % Tween20 in TBS at room temperature. The secondary antibody is conjugated with horse radish peroxidase (HRP) and was diluted 1:500 in 1 % milk powder and 0.01 % Tween20 in TBS. The nitrocellulose membrane was incubated in 6 ml of the secondary antibody solution for 1 hour at room temperature. Afterwards the membrane was washed four times 5 min in 0.05 % Tween20 in TBS. To detect the specifically bound antibodies 2 ml of Luminata™ Crescendo Western HRP Substrate (Millipore) was added for 5 min. The protein bands are detected in the Advanced Fluorescent Imager from Intas and analyzed with the according software ChemoStar Imager.

3.8 *In utero* electroporation

For the *in utero* electroporation (IUE) plasmids were prepared with an EndoFree Plasmid Maxi Kit from Quiagen according to manufacturer protocol. The used constructs in the proliferation and migration experiments were pCAGig-GFP, pCAGig-HCN-wt-GFP and pCAGig-HCN-DN-GFP. Constructs were cloned by Kathrin Sauter using the pCAGig-GFP vector (addgene) cut with EcoRV and ligated with HCN4-WT (wtHCN4-pBUD_EGFP; AseI and XbaI) or HCN-DN (HCN4-AYApcDNA1; HindIII/Xba1). See supplement 6.2 for vector charts.

The IUE for the migration experiments were performed in C57Bl/6J dams bred with male C57Bl/6J at E15.

For the IUE the dam was injected i.p. with 0.05 mg/kg of body weight buprenorphine 0.5 hours precedent of the procedure. During the surgery the dam was anesthetized with 1.5-2 % Isofluran (1000 ml/min in air). The body temperature is controlled by a rectal probe. To avoid the dehydration of the eye, the mouse is treated with Vidisic. After shaving and disinfecting the abdomen with Betaisodona, the uterus was exposed by small incisions of the skin and peritoneum. 1-2 µl DNA (0.5-5 µg/µl) were injected into the ventricle of the embryo, by following the midline of the embryo scalp and perforating the uterus, skin and bone right next to it with a capillary. Capillaries were pulled with a Sutter Puller Model P-1000 from borosilicate capillaries with filament (GB100TF-10, 0.78 x 1.00 x 100 mm; Science Products) aiming for a long and thin tip, which is shortened right before the injection, to sharpen the edges of the glass. For visibility of the DNA solution in the ventricle 0.05 % Fast Green was added. Five pulses of 35 V were applied by the 5 mm tweezertrodes (BTX, Harvard Apparatus) targeting the cortex of the E15 embryos. After carefully suturing the peritoneum with an absorbable suture and the abdominal skin with a silk suture, the mother was injected with 5 mg/kg body weight of Caprofen, a long lasting pain killer and anti-inflammatory. The wound was disinfected with Betaisodona and the dam was placed back in her home cage and monitored until total recovery from the anesthesia.

The embryos were immunohistochemically analyzed at E19.

3.9 Cell Culture

All cell culture experiments were performed by Dr. Sabine Vay from the Department for Neurology at the University hospital Cologne. For primary neural stem cell culture (NSC) fetal rat cortices were derived from embryonic day 13.5 as described previously (Rueger et al., 2010). To DMEM/F-12 medium (Gibco), supplemented with L-glutamine, N2-supplement, Penicillin/Streptomycin and sodium pyruvate (Gibco), human recombinant fibroblast growth factor (human FGF2; 10ng/ml, Invitrogen) was added. After two passages, 2 x 10^4 cells were re-plated in chamber slides as monolayers in the presence of FGF2 for further experimental procedures. To assess the proliferation potential, NSC were treated with the I_h blocker ZD7288 (Sigma-Aldrich) in 10 µM and 30 µM concentrations and RNA-extraction or BrdU-assay was performed after 18 hours. Differentiation was initiated by withdrawal of FGF2 and ZD7288 (30 µM) was added every 24 hours. After 3, 5, 7, and 10 days of differentiation, NSC were fixed and immunocytochemically stained.

3.9.1 In *vitro* proliferation assays

For 5-Bromo-2'-deoxyuridine (BrdU) experiments 10 µM BrdU (Fluka) was added for 6 hours to the cell culture medium before fixation with 4 % PFA for 10 min. As antigen retrieval 2 M HCl for 30 min was used. Anti-BrdU antibody was diluted 1:100. Pursuing with the protocol described in 3.9.2.

3.9.2 Immunocytochemistry

To analyze the differentiation in cell culture Sox2 was used as neuronal stem cell marker (1:100), TuJ1 (1:100), as marker for early neurons, GFAP (1:1000) indicating astrocytes and CNPase (1:5000) to mark oligodendrocytic precursor cells, additionally cells were stained with HCN4 antibody (1:5). For the immunocytochemical staining cells were washed with PBS and fixated with 4 % PFA for 10 min. After washing three times for 5 min each with PBS, cells were permeabilized and blocked in 0.1 % TritonX-100 and 10 % goat serum in PBS. Primary antibody was applied overnight in 3 % goat serum at 4 °C in respective concentrations. Thrice repeated washing with PBS for 5 min each were followed by secondary antibody incubation (1 hour at room temperature) with fluoresceine-labeled anti-mouse immunoglobulin G (IgG) or anti-rabbit IgG (1:200, Invitrogen) in 3 % goat serum in PBS. Cells were additionally counterstained with Hoechst 33342 (Invitrogen) diluted 1:500 and incubated for 5 min. Slides are mounted with Fluoromount (Southern Biotech). All microscopic investigations were performed with an inverted fluorescent phase-contrast microscope (Keyence BZ-9000E). Cell numbers in each experiment were analyzed by 10 images per condition and staining.

3.9.3 Transwell migration assay

For migratory analysis a transwell migration assay was performed using a Boyden chamber system (CytoSelect™ 24-Well Cell Migration Assay, pore size 8 µm, Cell Biolabs, Inc., San Diego, USA). Neural stem cells were seeded in the top of the insert (4 x 10^4 cells) with or without ZD7288. After 24 hours, the non-migratory cells were removed and migratory cells were stained with the cell stain solution for 10 minutes. Cells were gently washed and air dried. Then, stained cells were dissolved by the Extraction solution and optical density (OD) was measured at 560 nm in a microplate reader (FLUOstar Omega, BMG Labtech)

3.9.4 Viability Assays

LDH release, in the medium of the cultured cells was measured using the LDH Cytotoxicity Assay Kit (Thermo Scientific). Briefly, the medium (50 µl) was mixed with 50 µl of reaction mixture. After 30 min, 50 µl of stop solution was added and the

absorbance was read at 490 nm and 680 nm. To determine the LDH release, the 680 nm absorbance value was subtracted from the 490 nm absorbance.

The LIVE/DEAD® Cell-Mediated Cytotoxicity Kit (life technologies) was used to analyze the number of apoptotic cells. NSC were stained, with propidium iodide (1:500) as non-permeable dye and simultaneously stained with Hoechst 33342 (1:500). After 5 minutes at 37 °C, cells were counted using the inverted fluorescent phase-contrast microscope (Keyence BZ-9000E). Cell numbers in each experiment were analyzed by 10 images per condition and staining.

3.9.5 Electrophysiology

Neuronal stem cells were grown on glass cover slips, which were transferred into the bath solution shortly before the start of the recordings. Pipettes with filament (GB150F-10, 0.86 x 150 x 100 mm; Science Products) were pulled with a Sutter Puller Model P-1000 with a resistance between 2-6 Ω and were filled with electrode solution. The measurements were performed with an EPC-9 amplifier form HEKA and the Pulse + Pulse Fit v8.79 software v 8.79. All measured cells had an uncompensated series resistance from < 15 MΩ.

4 Results

To the best of my knowledge, this is the first study to reveal a role of HCN channels in early embryonic development. Due to the novelty of this subject, the endogenous HCN-subtype expression in the embryonic forebrain first had to be established together with a mouse line with an early embryonic expression of a forebrain-restricted dominant-negative HCN subunit. This dominant-negative approach was specifically designed to functionally ablate the I_h in a subunit-unspecific manner as early as during embryonic brain development. Using MRI measurements, the morphological alterations were characterized and quantified and showed a pronounced microcephaly phenotype. This phenotype was further investigated *in vivo* and i*n vitro*, where the different developmental processes of the cortical development were dissected and analyzed, namely the proliferation, differentiation, and migration of neural stem cells, progenitor cells, and young neurons. To investigate the mechanism(s) underlying the microcephaly, patch-clamp recordings of primary cortical stem cells were conducted and showed the electrophysiological profile of the analyzed cells.

4.1 Endogenous HCN expression during embryonic development

The expression of HCN subtypes in the postnatal brain of rodents has been previously analyzed (see 1.3.2). However, no data were available with respect to HCN-subtype expression in the embryonic brain. To investigate the impact of I_h on prenatal cortical development, the expression pattern of the different HCN subtypes was analyzed at the mRNA and protein levels.

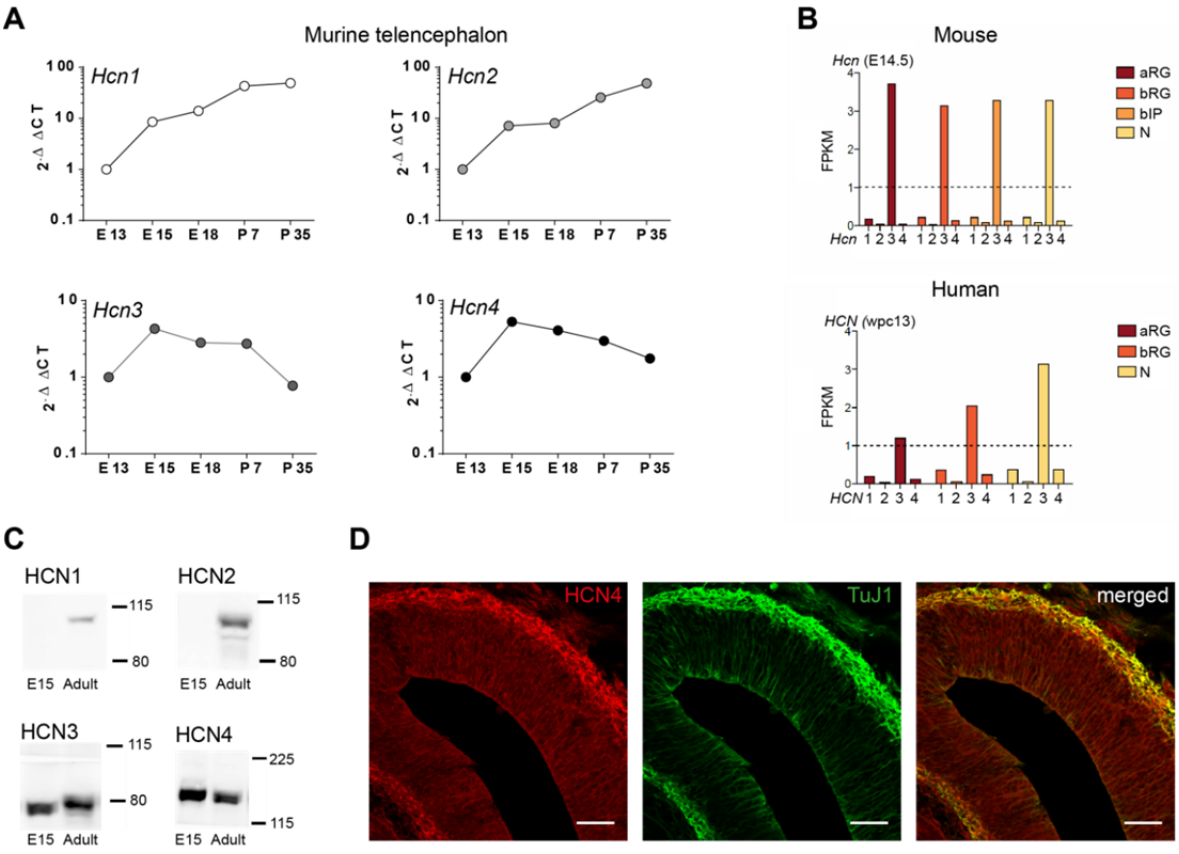

Figure 4-1 Expression of HCN subtypes during development

A, Pooled mRNA from the telencephalon was analyzed in a qPCR assay at different developmental time points, namely at embryonic days (E) 13, 15, 18, and postnatal days (P) 7 and 35. HCN1 and HCN2 expression levels increase throughout development, reaching their highest levels at adult stages (upper panel), while HCN3 and HCN4 expression peaks at E15 (lower panel). Data were normalized to GAPDH and normalized to the value at E13. **B,** RNA sequencing of apical radial glial cells (aRG), basal radial glia cells (bRG), basal intermediate progenitors (bIP) and neurons (N) of the E14.5 mouse cortex (upper panel) and aRG and bRG as well as of neurons in the human embryo 13 weeks post conception (wpc13; lower panel) was performed. In all cell types, HCN3 exhibits the highest expression (FPKM: fragments per kilobase per million reads, dotted line: noise threshold; performed by Dr. Florio). **C,** Western blot analysis in E15 whole-head membrane protein extractions, shows HCN3 and HCN4 as the main subtypes in the embryonal brain. **D,** Immunohistochemistry of E13 murine cortex reveals co-expression of HCN4 and TuJ1, an early neuronal marker.
Scale bars, 50 µm

To first assess the mRNA expression of the different subtypes a qPCR assay was performed to analyze the total mRNA of the mouse telencephalon at various developmental time points in the embryonic brain (E13, 15, and 18) and postnatal tissue (P7 and P35) (data reanalyzed from Schlusche, 2011). HCN1 and HCN2 expression increased during development, reaching the highest levels at adult stages and representing the main HCN subtypes in the adult forebrain (Figure 4-1 A; upper panel), as reported in previous literature (see 1.3.2). Notably, and in contrast to HCN1

and HCN2, the relative expression of HCN3 and HCN4 peaked at E15 and subsequently decreased again, reaching low levels in the adult telencephalon (Figure 4-1 A; lower panel). This expression pattern suggests an alteration in the expression of the major HCN subtypes during development. The data is supported by an mRNA next-generation sequencing study, performed and reanalyzed by Dr. Marta Florio from the laboratory of Prof. Huttner. In the developing murine cortex different cell types were dissected, namely aRG, bRG, bIP and neurons (Florio et al., 2015). In this experiment, HCN3 was the dominating subtype in all cell types analyzed (Figure 4-1 B; upper panel). In the human embryo, 13 weeks post conception (wpc), aRG, bRG and neurons were distinguished (Florio et al., 2015). In accordance with the rodent brain, HCN3 was the subtype with the highest expression, increasing from apical to basal RG until it reached the highest expression level in neurons (Figure 4-1 B; lower panel).

At the protein level, these data were confirmed with respect to the finding that HCN3 and HCN4 were the most highly expressed subtypes. In western blot analysis, the membrane proteins from the whole head of E15 embryos were extracted and compared to adult preparations, detecting only HCN3 and HCN4 (Figure 4-1 C). These data confirm the change in dominant HCN subtypes, which was also suggested by the mRNA levels of the telencephalon. To localize the HCN channel at this early time point in the evolving cortical structures, immunofluorescence experiments were performed. The HCN4 subtype was detected at the outer surface of the cortical plate in the murine forebrain at E13 (Figure 4-1 D; left image). This expression co-localized with β tubulin type III (further called TuJ1) expression, a marker for young neurons (Figure 4-1 D; center image). The HCN3 antibody did not yield specific staining results.

In summary, these experiments show the expression of HCN channels in the embryonic brain, with a switch between the dominant subtypes from HCN3 and/or HCN4 in early prenatal development to HCN1 and HCN2 in the postnatal and adult brain.

4.2 Generation of an embryonic HCN-DN mouse line

To investigate the role of HCN channels and of I_h in early prenatal cortical development, the EMX1-promoter mouse line was used. EMX1 is expressed from as early as E9.5 in a forebrain-specific manner (Iwasato et al., 2000; Gorski et al., 2002). By this forebrain restriction other unwanted phenotypes such as embryonic lethality of the cardiac expression was avoided (see 1.3.4).

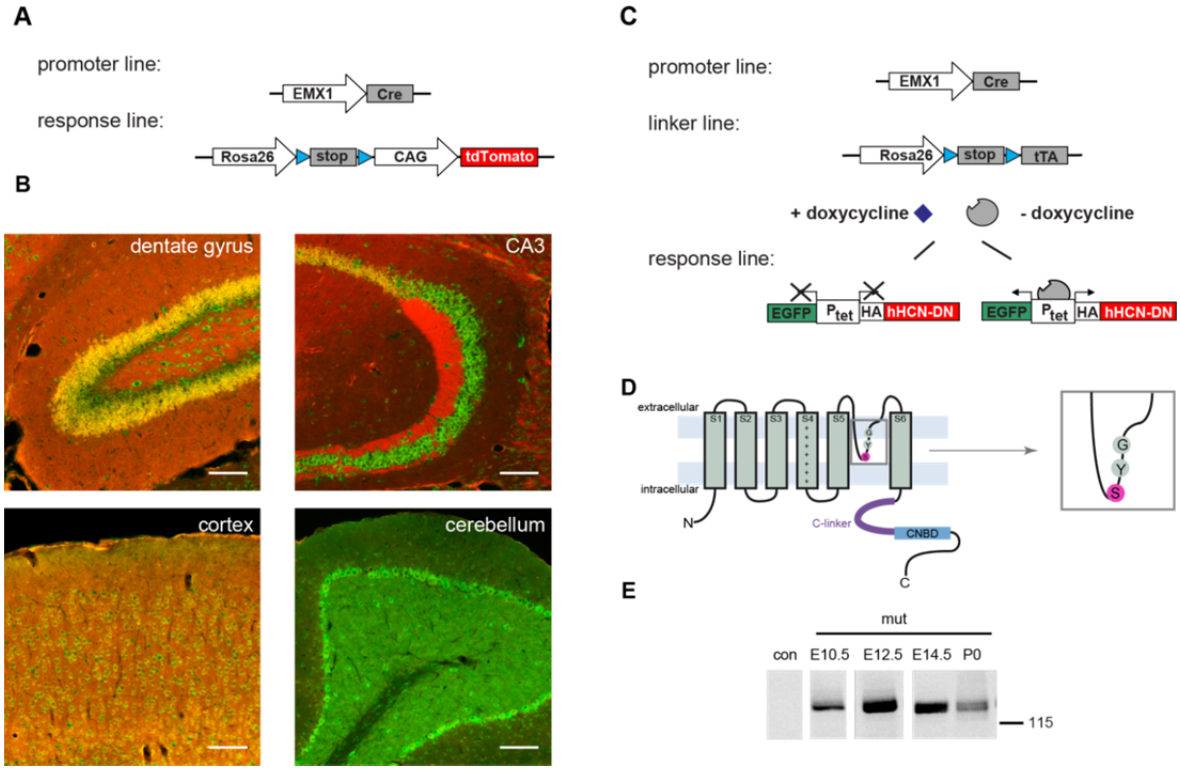

Figure 4-2 EMX1 driven mouse line

A, To validate the EMX1-promoter expression, the EMX1-Cre line was crossed with the Ai9 mouse line, expressing the reporter tandem dimer (td)Tomato under the control of the highly transcribed CAG - promoter (cytomegalovirus enhancer combined with chicken beta actin promoter) in the Rosa26 locus. **B,** Images show fluorescent Nissl staining (green) in sagittal brain sections of the EMX-Ai9 mouse (tdTomato in red); the overlay is depicted in yellow. The expression was forebrain restricted, only visible in dentate gyrus (upper left), CA3 (upper right) and cortex (lower left) but absent in cerebellum (lower right). **C,** In the experimental mouse line EMX-HCN-DN, expression is driven by the EMX1-promoter resulting in the expression of the cre recombinase, which excise the stop sequence in the Rosa26 locus leading to the expression of the tetracycline transactivator (tTA). In the absence of doxycycline, the tTA binds to the responsive element (P_{tet}), a bidirectional promoter, inducing the expression of the human dominant negative HCN subunit (hHCN-DN) and EGFP. **D,** The HCN-DN subtype exhibited the G480S mutation in the GYG motif of the pore region. **E,** Western blot analysis showed the expression of the transgene from E10.5 onward, detected with an antibody against the hemagglutinin - tag coupled to the transgene.
Scale bars, 100 µm

To validate the known expression pattern of the EMX1-Cre mouse line (Iwasato et al., 2000), these mice were bred with the Ai9 line, expressing a floxed stop sequence followed by the CAG promoter (cytomegalovirus enhancer combined with chicken beta actin promoter) and the tandem dimer (td) Tomato red reporter gene (Figure 4-2 A). Cre expression results in the transcription of the reporter gene by excision of the prepending stop sequence in the Rosa26 locus. The forebrain restriction of the EMX1 promoter was demonstrated in sagittal sections of the mouse brain,

counterstained with fluorescent Nissl in green (Figure 4-2 B). TdTomato was detected in the granular cells of the dentate gyrus, excluding the subgranular cell layer. In the cornus ammonis region 1 (CA1) of the hippocampus, the somata of granule cells expressed tdTomato as well as the mossy fibers in CA3 (Figure 4-2 B; upper panel). In the cortex, expression of tdTomato was mainly detected in the neuropil (Figure 4-2 B; lower left). The localization of the tdTomato suggests a preference of the reporter for the processes of the expressing cells. The cerebellum showed no expression, supporting the formerly described forebrain restriction of the promoter line (Figure 4-2 B) (Iwasato et al., 2000).

To evaluate the functional role of HCN channels during development, our lab created a triple transgenic mouse line in which the spatial and temporal expressions of a dominant-negative HCN subunit were controlled (Figure 4-2 C). To achieve an embryonic expression of the transgene, the EMX1-Cre promoter line was crossed with a linker line carrying a floxed stop sequence followed by the tetracycline transactivator (tTA) in the Rosa26 locus. Due to the activation of the cre recombinase, the stop sequence is removed, resulting in the expression of the tTA, which in turn binds to its responsive element (P_{tet}) in the absence of doxycycline. The tTA and P_{tet} resemble the Tet-off system, which gives additional temporal control of the expression pattern by the application of doxycycline. The administration of doxycycline thus leads to the inactivation of the transgene expression. In the absence of doxycycline, P_{tet}, as a bi-directional promoter, is active and leads to the expression of both the human dominant-negative HCN subunit (hHCN-DN) carrying a hemagglutinin tag (HA) and the reporter EGFP. The HCN-DN is a previously described HCN4 subunit with the G480S mutation in the GYG motif of the channel pore resulting in an SYG motif. The mutation leads to a non-conducting channel and to a subunit-independent ablation of I_h (Figure 4-2 D; compare with Figure 1-2) (Sandke, 2006; Merseburg, 2016).

In western blot analysis, the transgene expression was shown to be present as early as E10.5 (Figure 4-2 E). Due to technical limitations, membrane protein from E9.5 embryos could not be extracted in amounts high enough for analysis. Therefore, transgene expression at this early time point could not be proven. The HCN-DN subunit is detected via a hemagglutinin tag (HA-tag)-binding antibody, to distinguish the transgenic subunit from endogenous HCN subtypes.

The spatial restriction and the early expression of the EMX1 - promoter in combination with the subunit-independent suppression of I_h resulted in the first reported approach to the analysis of HCN-channel activity at early embryonic cerebral development. Thus, it was the first *in vivo* investigation of the consequences of alternating HCN - channel function in neural progenitor cells and early neurons in prenatal developmental processes of the murine cortex.

4.3 Morphological characterization of EMX-HCN-DN mice

To analyze the role of HCN channels in embryonic development, the brain structure of HCN-DN mice were first characterized. EMX-HCN-DN mice showed marked and severe morphological abnormalities as early as at P0. The pups were viable until weaning, but then showed increased lethality at approximately three weeks of age. This early lethality did not allow an analysis of adult but only of juvenile (P21) animals to be performed.

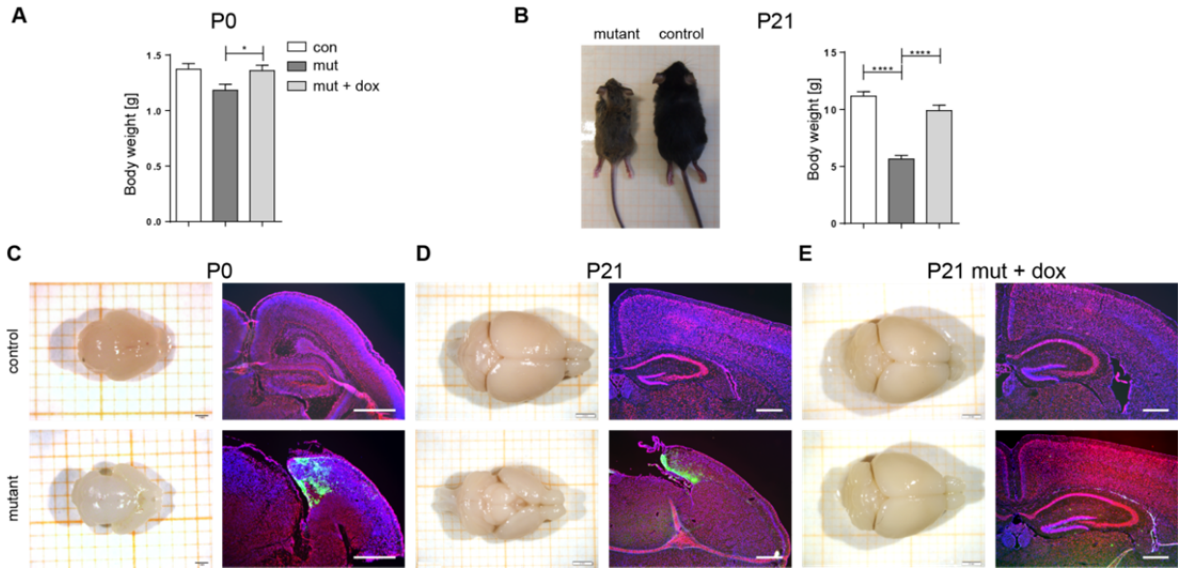

Figure 4-3 Morphological abnormalities in EMX-HCN-DN animals

A, At postnatal day (P) 0, the bodyweight is decreased in mutant mice (mut) compared to control (con) or transgenic animals treated with doxycycline until P0 (mut + dox). **B,** The decrease in body size and weight is more pronounced in mutant animals at P21 compared to control or mut + dox. **C,** Neonatal mutant mice show a decrease in cortex size at macroscopic and microscopic images. The coronal sections stained with red fluorescent Nissl dye reveal the absence of a hippocampal structure. **D,** At P21, the decrease in cortical structures was visible in the total brain (top view). The reduced cortex and the absent hippocampus **are** clearly visible in the overview image of the brain and in the Nissl stained coronal section. **E,** The phenotype was rescued by the application of doxycycline until P0, suppressing the transgene expression until the day of birth, resulting in morphologically normal brains.
Scale bars, **C** left 1 mm, **D** and **E** left 2 mm in; all Nissl staining images 500 µm
* $p < 0.05$, ** $p < 0.01$, *** $p < 0.001$, **** $p < 0.0001$; Data are presented as mean ± S.E.M; one-way ANOVA with post-hoc Tukey´s test; **A**, con: n=14, mut: n=8, mut dox: n=8; **B**, con: n=15, mut: n=10, mut dox: n=8.

As early as at P0, the body weight was decreased in mutant EMX-HCN-DN mice (mut) compared to control animals (con) or mutant mice, which had been fed with doxycycline until P0 (mut + dox) (Figure 4-3 A). At P21, the body size of mutant mice

was drastically reduced in comparison to control mice (Figure 4-3 B; left). This smaller body size of the mutant mice was paralleled by a severe reduction in body weight by approximately 50 % compared to control animals (Figure 4-3 B; right). When administering doxycycline until P0 in mutant + dox mice, this pronounced body weight reduction was prevented (Figure 4-3). There was no detectable difference between the control animals with and without application of doxycycline.

In addition to the overall decrease in body mass and -size, a closer investigation of the brain of neonatal EMX-HCN-DN mice revealed a dramatic decrease in the size of cortical structures (Figure 4-3 C; left). The reduced cortex does not cover the diencephalon or mesencephalon as seen in the control animals. In fluorescent Nissl staining (red) of coronal sections the smaller cortex and the absence of the hippocampal structures were pronounced (Figure 4-3 C; right). This phenotype persisted until P21, leaving the diencephalon and the lateral and third ventricle partially uncovered (Figure 4-3 D). In the neonatal, and in the juvenile animals, GFP-positive transgenic cells accumulated at the basal cortex, lining the apical side of the lateral ventricles (Figure 4-3 C and D). In mice treated with doxycycline during prenatal development, suppressing the expression of the HCN-DN subunit, no morphological abnormalities were observed (Figure 4-3 E). The GFP-positive cells were found in the subgranular zone of the dentate gyrus and the ventricular lining, the areas of postnatal neurogenesis (Figure 4-3 E, lower right).

To quantify the severe loss of forebrain structures, MRI measurements were performed. Preliminary MRI data were published in Schlusche, 2011, but were extended and finalized in the course of this doctoral thesis.

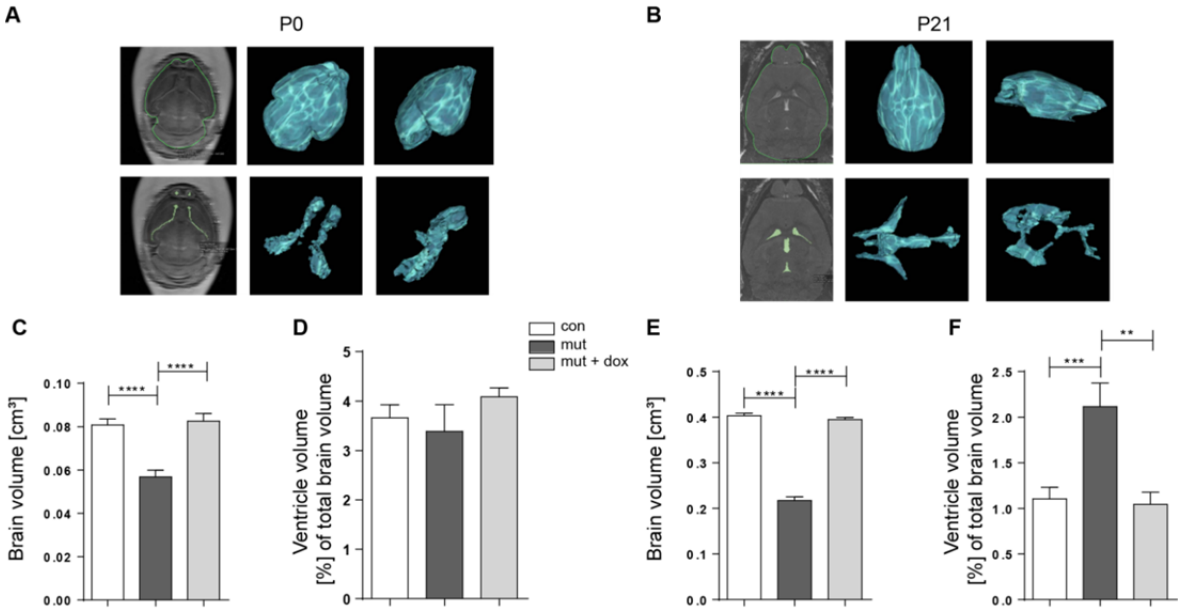

Figure 4-4 Quantification of morphological abnormalities in EMX-HCN-DN animals

A, B, Representative images of MRI data and the 3D rendering of the control brain volume (upper panel) and the ventricle volume (lower panel) were conducted at P0 (**A**) and P21 (**B**). Depicted are the MRI images with two different perspectives on the 3D model. **C,** The brain volume in cm^3 was significantly decreased in mutant (mut) compared to control (con), and was rescued by the administration of dox (mut + dox). **D,** At P0, the ventricle volume in percent of the total brain volume was not affected by I_h ablation. **E,** At P21, the brain volume was severely decreased in mut animals compared with con and mut + dox. **F,** The ventricle volume in juvenile mut mice was increased; no difference between the con and mut + dox was detectable**.**
* $p < 0.05$, ** $p < 0.01$, *** $p < 0.001$, **** $p < 0.0001$; Data is presented as mean ± S.E.M; one-way ANOVA with post-hoc Tukey´s test; **C**, and **D**, brain volume: con: n=14, mut: n=8, mut dox: n=8; ventricle volume: con: n=12, mut: n=4, mut dox: n=7; **E**, and **F**, brain volume: con: n=16, mut: n=10, mut dox: n=8; ventricle volume: con: n=15, mut: n=10, mut dox: n=8.

The reduction was quantified by three-dimensional (3D) volume rendering of the brain and ventricles in neonatal and juvenile animals (Figure 4-4 A and B) (Schlusche, 2011). The brain volume of neonatal mutant mice was significantly decreased by approximately 25 % compared to control and mutant + dox animals (Figure 4-4 C). In contrast, the ventricle volume was not changed between the groups (Figure 4-4 D). In juvenile mutant animals, the brain volume was even further reduced by approximately 50 % compared to control and mutant + dox animals (Figure 4-4 E). Additionally, the relative ventricle size of mutant animals was increased by nearly 50 % in comparison to control and mutant + dox (Figure 4-4 F).

In summary, in P0 and P21 EMX-HCN-DN mice, severe morphological abnormalities were detected along with decreased cortex size and the absence of the hippocampal structures. Upon suppression of HCN-DN expression until birth, this phenotype was rescued, suggesting an important functional role for HCN channels in prenatal developmental processes of the forebrain structures.

4.4 Analysis of developmental processes in the EMX-HCN-DN mouse

To dissect the role of HCN in prenatal development in more detail and to identify the mechanisms affected by the ablation of I_h causing the reduction in brain size, the proliferation, differentiation, and migration of neuronal progenitor cells and cortical neurons were investigated in EMX-HCN-DN mice. Furthermore, apoptosis, a potential mechanism leading to reduced brain size, was analyzed.

4.4.1 Proliferation in EMX-HCN-DN mice

To investigate the overall proliferation in the forebrain of EMX-HCN-DN animals, immunostaining with the Ki67 antibody was performed at P0. Ki67 is a nuclear protein expressed throughout the cell cycle from G1 to M phase, marking proliferating cells (Gerdes et al., 1991).

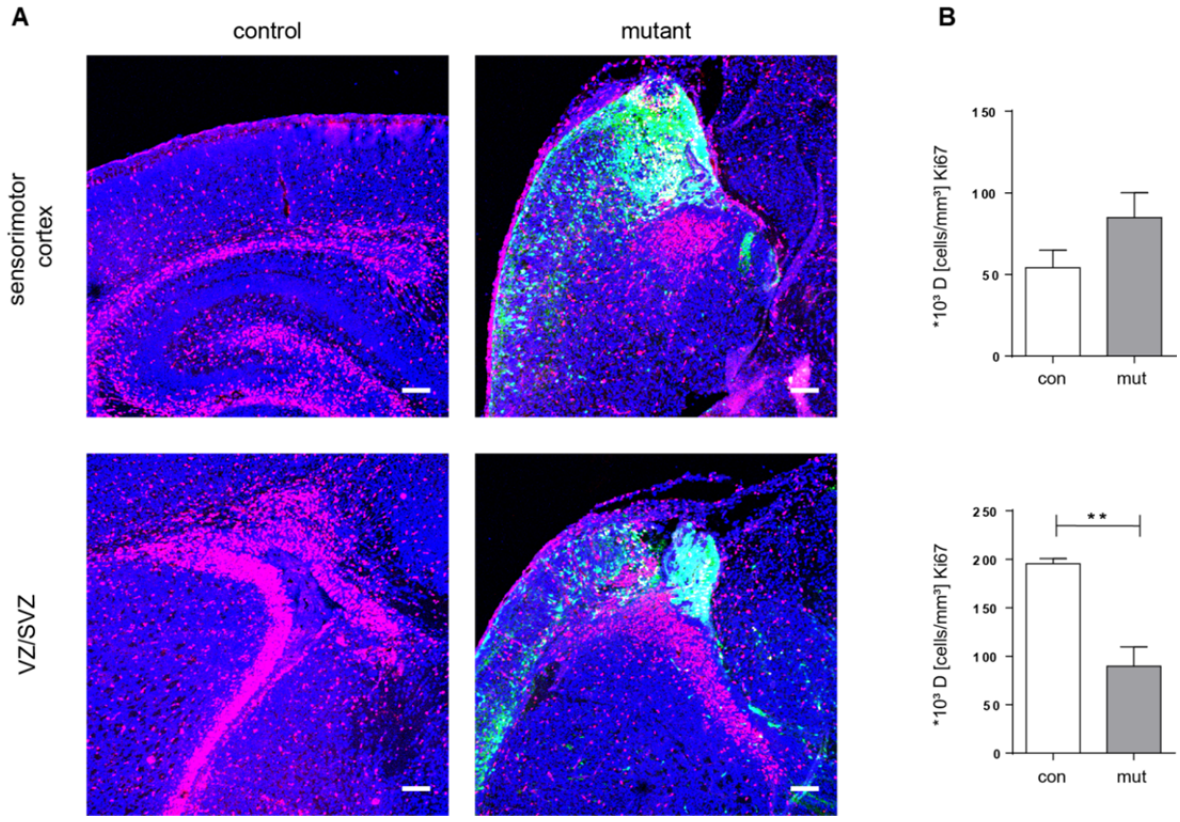

Figure 4-5 Proliferation in EMX-HCN-DN mice at P0

A, Example images show coronal sections of control (con) and mutant (mut) EMX-HCN-DN mice with Ki67 staining (red) in the sensorimotor cortex and ventricular zone/ subventricular zone (VZ/SVZ). Sections were counterstained with DAPI (blue), GFP (green) expression marked the transgenic cells in mut mice. **B,** Stereological quantification of sensorimotor cortex showed no significant difference (upper panel), but in the proliferation zone VZ/SVZ mitotic cells were overall significantly reduced. Data depicted in density (D) in [cells/mm^3].
Scale bars, 100 µm; * $p < 0.05$, ** $p < 0.01$, *** $p < 0.001$, **** $p < 0.0001$; Data is presented as mean ± S.E.M; unpaired t-test, cortex: con: n=6, mut: n=5; VZ/SVZ: con: n=4, mut: n=4.

The proliferation was analyzed in the sensorimotor cortex and the VZ/SVZ (Figure 4-5 A). Coronal sections were stained with Ki67 in red, counterstained with DAPI (blue), and the transgenic cells expressed GFP (green). In the control animals proliferation was detected in both regions of interest and in the dentate gyrus of the hippocampus (Figure 4-5 A; left panel). Elevated Ki67 expression was found in the VZ/SVZ and in the dentate gyrus, regions of proliferation at this postnatal time point, while proliferating cells were also detectable in the cortex, but in smaller numbers. In the mutant sections, Ki67-positive cells were detected in all structures analyzed. The VZ/SVZ was clearly marked with Ki67 staining. Transgenic cells expressing GFP were detected in the remaining cortex, with accumulations proximal to the lateral ventricles (Figure 4-5 A; right panel). Stereological quantification revealed no significant difference in the number of proliferating cells in the sensorimotor cortex between control and mutant EMX-HCN-DN mice, but a decrease in mitotically active cells in the VZ/SVZ (Figure 4-5 B). The reduction in brain size could thus be due to the local decrease in mitotically active cells in the proliferation zone VZ/SVZ.

To verify whether the size reduction in forebrain structures seen in EX-HCN-DN mice was due to decreased stem and progenitor cell proliferation, the NEXCre-HCN-DN mouse line was investigated. NEXCre is expressed from E10.5 onward in post-mitotic neurons, mainly in forebrain structures (Goebbels et al., 2006) and, thus, resembled the expression pattern of EMX1, excluding proliferating precursor cells. This approach allowed the process of proliferation to be dissected from other prenatal developmental processes, such as differentiation and migration, without analyzing the embryos and thereby sacrificing the mother.

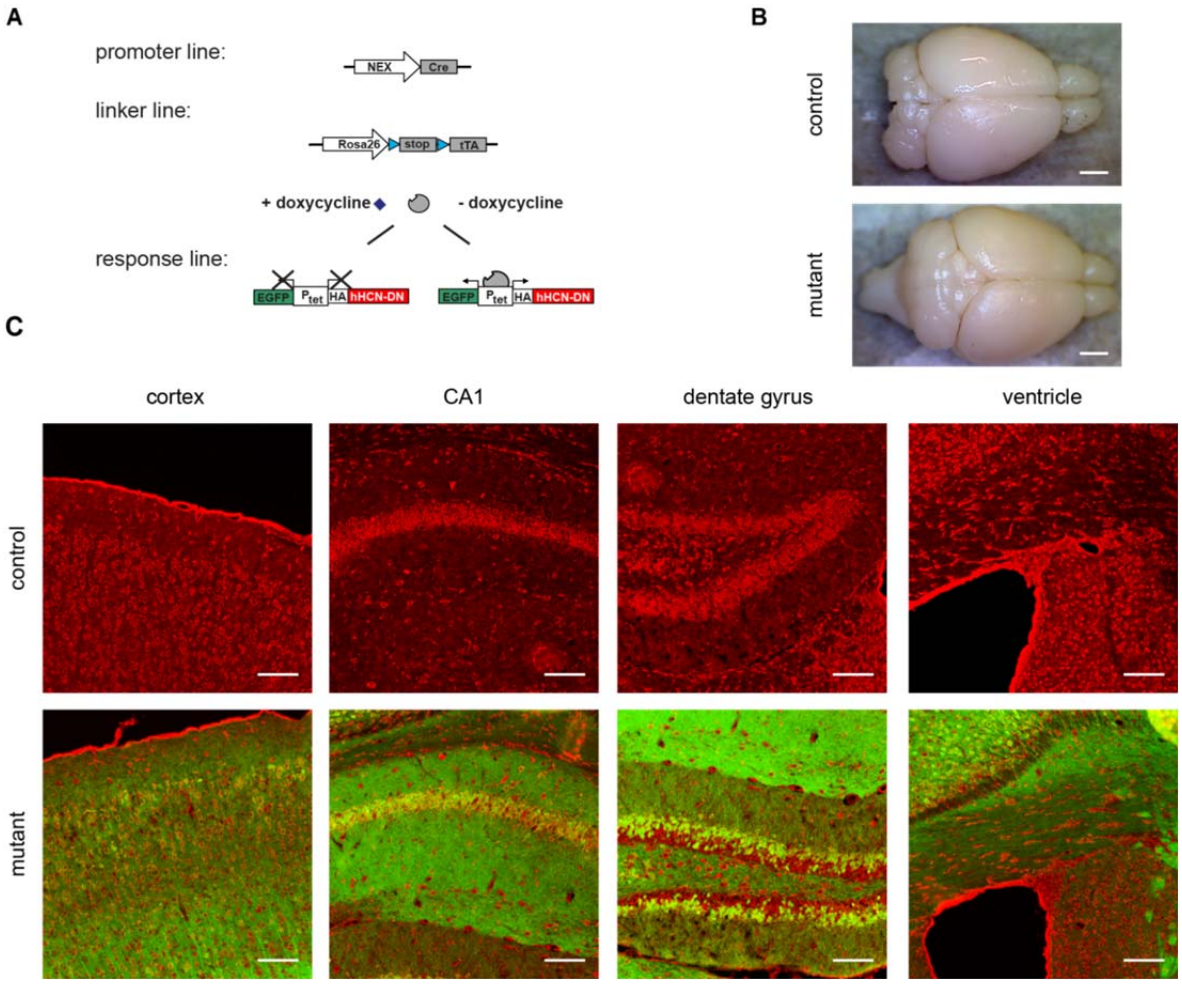

Figure 4-6 Morphological normal brains of NEXCre-HCN-DN mice

A, Cre recombinase was expressed under the NEX promoter, leading to the excision of the floxed stop sequence in the Rosa26 locus, thus allowing the tetracycline transactivator (tTA) to be expressed. In the absence of doxycycline, the dominant-negative HCN-DN subtype and EGFP are expressed through the bidirectional responsive element (P_{tet}) of tTA. **B,** The overall morphology of the adult NEXCre-HCN-DN mice did not differ from controls. **C,** Coronal sections stained with fluorescent Nissl (red) show no alteration in the general structure of the cortex, hippocampus (CA1 and dentate gyrus) or the ventricle. Scale bars, in **B,** 2 mm and in **C,** 100 µm.

To generate NEXCre-HCN-DN mice, a genetic approach similar to that earlier employed for EMX-HCN-DN mice was used (Figure 4-6 A). The expression of the cre recombinase was driven by the Nex promoter using the above-described temporal and spatial expression pattern. Cre recombinase-excised the floxed stop sequence preceding the tTA, located in the Rosa26 locus. The tTA bound in the absence of doxycycline to the bi-directional P_{tet}, allowing the HCN-DN subunit and GFP to be expressed.

In contrast to the microcephaly phenotype of EMX-HCN-DN animals, the NEXCre-HCN-DN mutant animals expressing the HCN-DN subunit from an early prenatal time point onward showed no gross morphological alterations in the brain at the age of six weeks. The visible cortical structures covered the diencephalon and mesencephalon, leaving only the colliculi inferiores and superiores uncovered (Figure 4-6 B). Coronal sections stained with fluorescent Nissl confirmed intact morphologies of the cortex, CA1, and dentate gyrus of the hippocampus and ventricles (Figure 4-6 C). GFP was detected, as reporter for transgenic cells, in the neuropil of the cortex and CA1 and a few cell somata in both regions. In the dentate gyrus, GFP-expressing cells were detected in the granular cells and their dendrites, excluding the subgranular cell layer, the region of neuronal precursor cells potentially undergoing mitosis. Analysis of the sections showing the lateral ventricles revealed GFP in the lower cortical layers and fiber bundles of the striatum and corpus callosum, but not in the VZ/SVZ. This observation is in line with the expression pattern of the NEX promoter, which is active in post-mitotic neurons, but not in proliferating cells (Goebbels et al., 2006).

In summary, observations of a decreased proliferation in P0 EMX-HCN-DN mice in the VZ/SVZ, together with the morphologically normal forebrain of NEXCre-HCN-DN adult mice, suggest an impaired proliferation of neural progenitor cells, due to the ablated I_h in early prenatal development of the murine forebrain.

4.4.2 Differentiation in the EMX-HCN-DN mouse line

The differentiation of neural progenitor cells into neurons, astrocytes, and oligodendrocytes is another important mechanism of cortical development. To analyze the differentiation of HCN-DN-expressing cells in the forebrain, brains of P0 animals were sectioned and stained for markers of each cell type. TuJ1, was used as a marker of early neurons, astrocytes were detected with an antibody against glial fibrillary acidic protein (GFAP) and 2',3'-cyclic-nucleotide 3'-phosphodiesterase (CNPAse) was used for the staining of oligodendrocytes (Eng et al., 1971; Verrier et al., 2013).

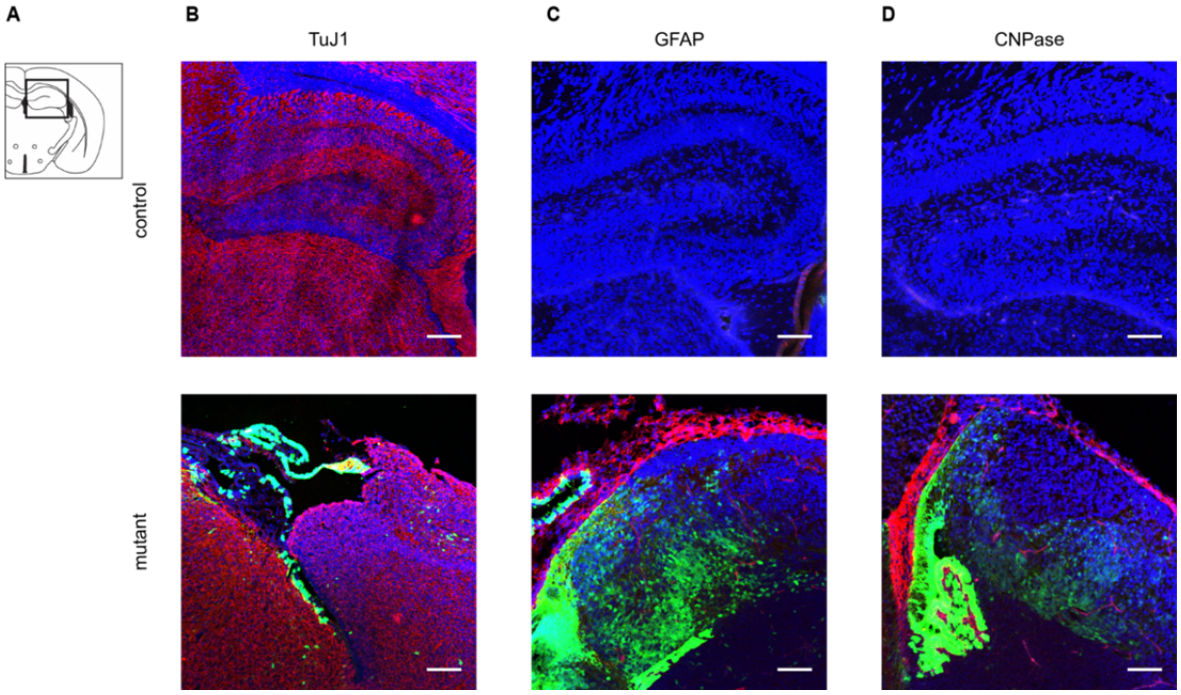

Figure 4-7 Differentiation in P0 EMX-HCN-DN mice

A, The cartoon of a coronal section shows the sectional plane of the control and mutant analyzed brain slides, from (Franklin and Paxinos, 2007). **B,** TuJ1 (red) as a marker for early neurons was expressed in control as well as EMX-HCN-DN mutant mice, showing a partial overlay with the GFP expressing transgenic cells (yellow). **C,** Astrocytes were stained with GFAP (red), a marker was only expressed in P0 EMX-HCN-DN animals, but not in controls. **C,** CNPase as a marker for oligodendrocytes (red) is only detectable in mutant but not in control mice. Both glial markers are present on the surface of the remaining cortical structures. All coronal sections were counterstained with DAPI (blue).
Scale bars, 100 µm.

The hippocampus was used as a landmark in the P0 brains of control animals, and the same brain regions were matched in the EMX-HCN-DN mice (Figure 4-7 A). TuJ1, indicating early neurons, was expressed throughout the brain in control and in mutant EMX-HCN-DN mice. A partial overlay with the transgenic, I_h - ablated, GFP-positive cells was detected, and is shown in yellow (Figure 4-7 B). GFAP, a marker for astrocytes (Figure 4-7 C) and CNPase, expressed in oligodendrocytes (Figure 4-7 D) was not detected in the control animals (Figure 4-7 C and D, upper panel). In contrast, both glial markers were expressed in EMX-HCN-DN mice at P0 (Figure 4-7 C and D). GFAP and CNPase were expressed on the surface of the remaining cortical structure, suggesting the formation of a glial scar-like structure. In control animals, the existence of the neuronal marker and the absence of both glial markers are in

agreement with the temporal pattern of cortical development, with the neurogenesis at earlier time periods, followed by the gliogenesis around birth (see 1.1).

The expression of glial markers in P0 mutants suggests an alteration in the temporal sequence of the differentiation pattern in the I_h-deficient forebrains of EMX-HCN-DN mice.

4.4.3 Migration of cells with I_h ablation

It was not possible to directly investigate the migration of neurons in the EMX-HCN-DN mouse line, due to intermingled processes of proliferation, differentiation, and migration in embryonic development. To study the migration of early neurons, *in utero* electroporation (IUE) was used (see method section for detailed description). At E15, cells lining the ventricle were electroporated with different constructs, all expressed under the control of the CAG promoter and with an internal ribosomal entry site (IRES) coupled GFP as a reporter protein. An HCN-DN subunit with two mutations (G480A/G482A) introduced into the GYG motif of the pore region of the channel was used to ablate I_h (Mesirca et al., 2014). As control constructs, either a wild-type HCN subunit or a vector expressing only GFP was applied. With this approach, neurons from the VZ/SVZ at E15 were marked, which migrated into cortical layers II/III. They reached their destination at E19, the time point chosen to analyze this migration assay.

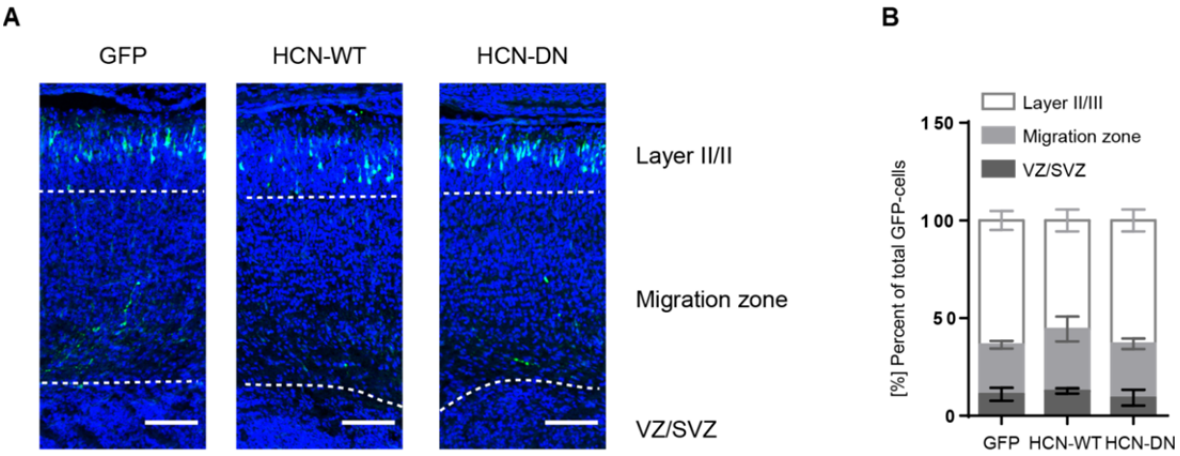

Figure 4-8 Migration analysis of I_h ablated cells *in vivo*

A, Representative images show E19 murine cortices, that were *in utero* electroporated (IUE) at E15 with GFP, wild-type HCN (HCN-WT) with GFP, or dominant-negative HCN (HCN-DN) also with GFP as reporter gene. All constructs were expressed under the control of the CAG promoter. Most cells are able to migrate from the VZ/SVZ through the migration zone consisting of the intermediate zone, subplate, and lower cortical layers into cortical layers II/III. **B,** Stereological quantification of the IUE analysis shows no significant difference between the groups. Numbers are given as percentage of total GFP-expressing cells.
Scale bars, 100 µm; Data is presented as mean ± S.E.M; One-way ANOVA. n=4.

By electroporation at E15, the cells in the VZ/SVZ were transfected with different constructs (GFP, HCN-WT and HCN-DN), and mostly migrated through the intermediate zone, subplate, and lower cortical layers, here referred to as migration zone, reaching cortical layers II/III at E19, without differences between the groups (Figure 4-8 A). Only minor populations were detected in the migration zone and the VZ/SVZ. Quantification did not show significant alterations between the groups (Figure 4-8 B).

In summary, functionally I_h - ablated cells showed no difference in their temporal pattern of migration into cortical layers II/III.

4.4.4 Apoptosis in neonatal EMX-HCN-DN mice

In addition to the impaired proliferation and differentiation, an increase in cell death due to the ablated I_h and the altered biophysical properties of the transgene-expressing cells could also contribute to the severe the EMX-HCN-DN phenotype. To investigate this possibility, neonatal EMX-HCN-DN mice were analyzed for apoptotic processes. A staining for cleaved caspase 3, an enzyme whose activation induces apoptosis upon cleavage, was performed.

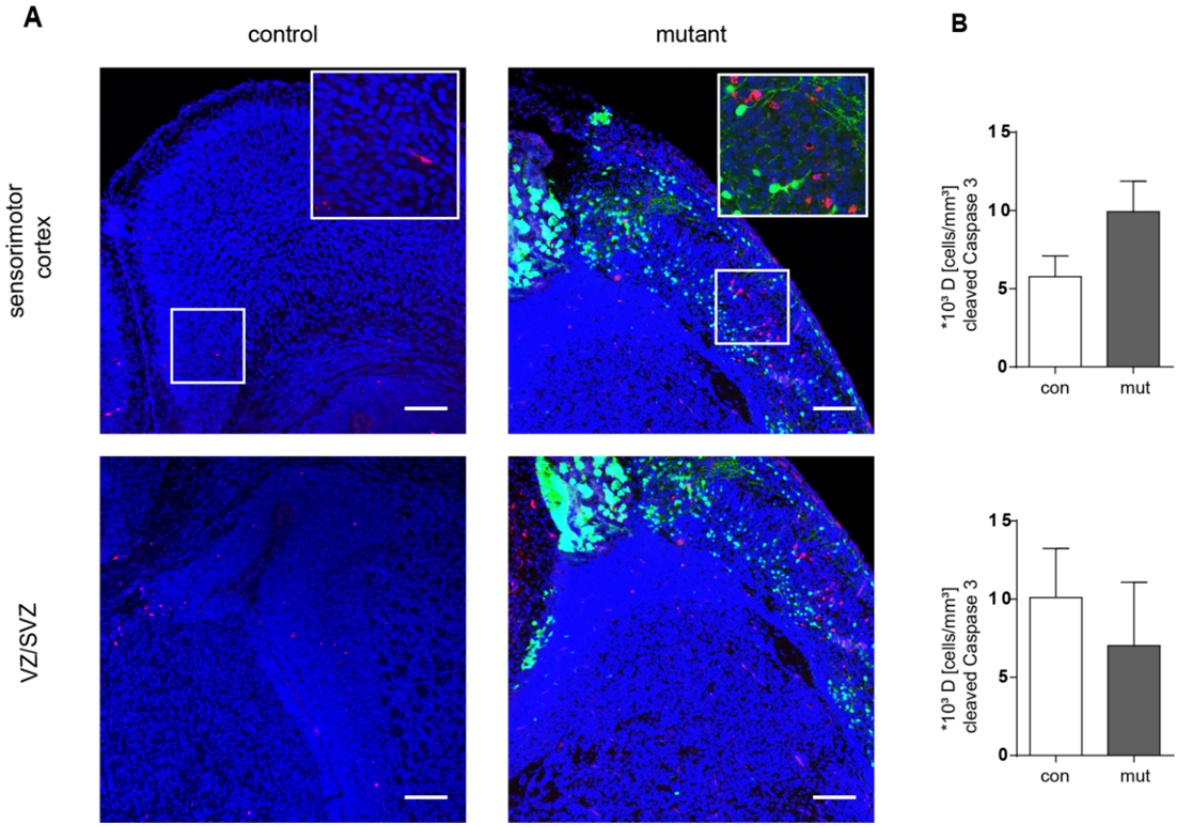

Figure 4-9 Apoptosis in neonatal EMX-HCN-DN mice

A, Representative images of cleaved caspase 3 staining (red) in coronal sections of the sensorimotor cortex and ventricular/subventricular zones (VZ/SVZ) counterstained with DAPI (blue) of control (con) and mutant (mut) EMX-HCN-DN mice. In mutant EMX-HCN-DN mice, GFP expression is visible. Insets show higher magnification of the boxed areas with single cells positive for cleaved caspase 3. **B,** Stereological quantification did not reveal any significant differences in the amount of apoptotic cells in the regions analyzed. Data depicted in density (D) in [cell /mm^3].
Scale bars, 100 µm; Data is presented as mean ± S.E.M; unpaired t-test; cortex: con: n=7, mut: n=5; VZ/SVZ: n=6, mut: n=4.

Apoptosis is a process needed for the refinement of neural connections and cell numbers in the cerebral structures that occur physiologically in the developing brain. In the regions analyzed, the sensorimotor cortex and the VZ/SVZ of control and mutant EMX-HCN-DN mice, only a small number of apoptotic cells, positive for the cleaved caspase 3 protein, were detected (Figure 4-9 A). The stereological quantification did not show a significant difference between apoptotic cell numbers of control and mutant EMX-HCN-DN animals (Figure 4-9 B).

In the sensorimotor cortex and the VZ/SVZ of the murine forebrain, no impact of I_h ablation on apoptosis was detected.

The *in vivo* phenotype of I_h-deficient EMX-HCN-DN mice exhibiting a severe reduction in the volume of the forebrain structures due to impaired cortical development can be ascribed to a reduction in proliferation and altered differentiation of the neural precursor cells. However, no effect of I_h deficiency on the migration or apoptosis was detected.

To confirm these results, and to dissect individual developmental processes from each other, cell culture experiments with primary cortical stem cells from the rat were conducted.

4.5 *In vitro* experiments using primary cortical stem cells with pharmacological blocked I_h

Cell culture experiments with primary cortical stem cells were designed in collaboration with the research group stem cells of the Department of Neurology of the University Hospital and were conducted by Dr. S. Vay.

The *in vitro* experiments allowed the different developmental processes to be discriminated from each other and to apply a different approach to the ablation of I_h by the pharmacological blocker ZD7288. This chemical compound blocks HCN channels without discriminating between the different subunits, causing I_h deficiency in the treated cells.

The proliferation and differentiation of primary cortical stem cells as the first developmental processes in the cortex were investigated in different assays.

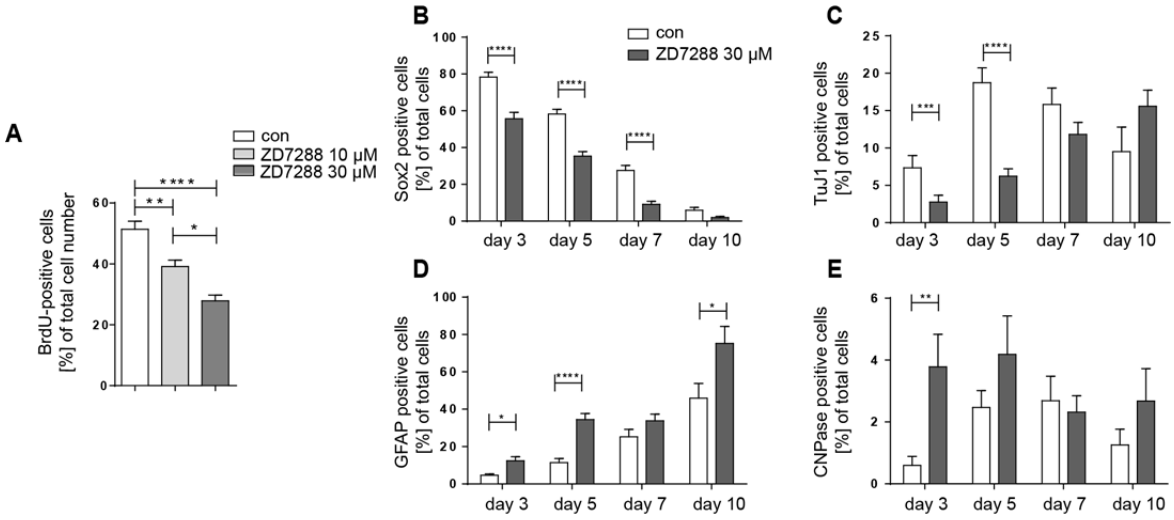

Figure 4-10 *In vitro* analysis of proliferation and differentiation in I_h deficient cortical stem cells

A, Quantification of BrdU positive cells in relation to total cell number of control (con) and ZD7288 (10 µM and 30 µM) cells reveals a dose-dependent decrease in proliferation. **B, C, D, E,** Differentiation was analyzed 3, 5, 7 and 10 days after the withdrawal of FGF2. **B,** Sox2, a stem cell marker, shows a significant decrease of proliferating cells on day 3, 5 and 7 of ZD7288 treated cells compared with controls. **C,** Early neurons, marked with TuJ1 are significantly reduced in cell numbers on day 3 and 5 between control and ZD7288 treated cells. **D,** Upon treatment with ZD7288, astrocytes, stained with GFAP, appeared significantly earlier and in higher cell numbers compared to control cells. **E,** CNPase marked oligodendrocytes emerged earlier at day 3 when treated with ZD7288.
* $p < 0.05$, ** $p < 0.01$, *** $p < 0.001$, **** $p < 0.0001$; Data is presented as mean ± S.E.M; **A,** one-way ANOVA with post-hoc Tukey's test; n > 200 cells per condition from one representative experiment out of three independent experiments with the same outcome. **B, C**, **D**, **E**, Mann-Whitney test; **B, C,** n > 500 cells per condition and day in 2 – 6 independent experiments. **D, E,** n > 300 cells per condition and day in 2 – 5 independent experiments. (Experiments were performed by Dr. S. Vay.)

The proliferation of the cortical stem cells was investigated by analyzing the uridine analog 5-bromo-2'-deoxyuridine (BrdU) incorporation, indicating cells situated in the S phase of the cell cycle (Figure 4-10 A). In accordance with the *in vivo* experiments, the *in vitro* method revealed a decrease in proliferation when the cells were treated with ZD7288 in a dose-dependent manner (10 µM and 30 µM). This result was reflected in the analyses of differentiation, where the amount of Sox2 positive stem cells treated with 30 µM ZD7288 was significantly decreased at day 3, 5 and 7 after FGF2 withdrawal, compared to control cells (Figure 4-10 B). Withdrawal of FGF2 resulted in the differentiation of the pluripotent stem cells. At day 10, the amount of Sox2 positive cells also substantially decreased in the control culture. Thus, there was no longer any difference between these groups (Figure 4-10 B). In control cultures, the number of early neurons, marked with TuJ1, increased between days 3 and 5, with a subsequent decrease in early neurons due to the culture conditions that supported stem cells but not neurons (Figure 4-10 C). At days 3 and 5 the ZD7288-

treated cells showed significantly reduced numbers in TuJ1 positive neurons, which increased at days 7 and 10 with no significant difference left between control cells and treated cells (Figure 4-10 C). Glial cells were marked with GFAP for astrocytes and CNPase stained oligodendrocytes. In the control group, the amount of GFAP positive cells increased over time, reaching their highest expression level at day 10 (Figure 4-10 D). In I_h blocked cells, GFAP positive astrocytes showed significantly higher cell numbers almost throughout the whole time points analyzed (Figure 4-10 D). The untreated control cells exhibited an increase in CNPase positive oligodendrocytes until day 7, followed by a decrease in CNPase positive cell numbers at day 10 (Figure 4-10 E). The ZD7288 - treated cells showed significantly higher numbers of oligodendrocytes at day 3 and remained increased during the following time points except for day 7, but without significance compared to control cells (Figure 4-10 E).

Both glial markers showed an early expression peak in ZD7288 - treated cells compared to control cells, while TuJ1, a marker for young neurons was decreased.

The *in vitro* experiments resembled the results obtained from the *in vivo* work and showed a decrease in proliferation in I_h - ablated cells and an altered differentiation pattern, as seen by the early expression of glial markers.

Furthermore, migration and cell death in primary cortical stem cells with pharmacologically blocked I_h were investigated.

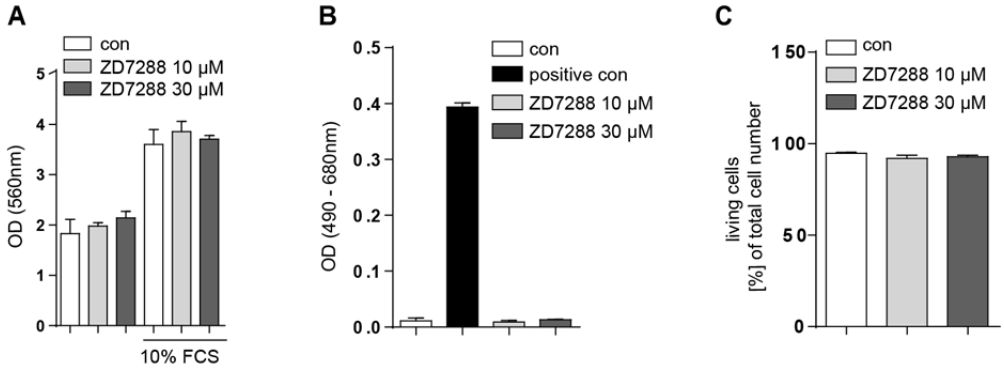

Figure 4-11 Migration and cell death in I_h - ablated primary cortical stem cells

A, A Transwell migration assay was performed with primary stem cells. No difference was observed between control (con) and ZD7288 treated cells (10 µM and 30 µM (left) in the optical density (OD) of the cell lysate, representing the cells migrated through the Boyden chamber. Upon stimulation of migration with 10 % FCS, the cellular behavior did not alter between the groups. **B,** Lactate dehydrogenase (LDH) release was measured as a marker for cell death, lysis of cells (positive control) yielded high amounts of LDH but no difference between control and ZD7288-treated cells was detected. **C,** Propidium iodid (PI) incorporation, a marker for a disrupted membrane, was measured for dead cells and showed no difference between the groups.
Data is presented as mean ± S.E.M; **A**, n= 2, one representative experiment out of two independent ones with the same outcome; **B,** one representative experiment; n = 4; **C,** n> 1000 cells per condition in one experiment. (Experiments were performed by Dr. S. Vay.)

To investigate the migration behavior of primary cortical stem cells, a Transwell migration assay was performed using a Boyden chamber. In this assay, cells had to migrate through a porous membrane in order to reach the lower part of the chamber. Successfully migrated cells were lysed and the optical density (OD) of the lysate was measured. No difference was detectable between control and ZD7288 - treated cells (10 µm and 30 µm) (Figure 4-11 A; left). Next, the migration was stimulated by the application of 10 % FCS to the target well. This stimulus resulted in an overall higher migratory behavior, but did not show a significant difference between the groups (Figure 4-11 A; right).

To exclude a toxic effect of the chemical compound ZD7288, which may cause necrosis or apoptosis, two different assays designed to analyze cell death were performed. Both methods were based on the detection of disruptions of the membrane, which mainly happens during necrosis, but also in late apoptosis (Darzynkiewicz et al., 1992; Chan et al., 2013). In the lactate dehydrogenase (LDH) assay, the release of LDH, a cytosolic enzyme upon membrane leakage, was measured. As a positive control, the supernatant of lysed cells was measured, showing a high LDH level (Figure 4-11 B). Treatment with 10 µM or 30 µM ZD7288 did not result in a

difference in LDH release, compared to control cells (Figure 4-11 B). Propidium iodide (PI) is a membrane - impermeable dye, therefore intercalating only with DNA of cells with a disrupted membrane. No difference in the number of PI – negative and, thereby, living cells was detected between the groups (Figure 4-11 C right). These results exclude a cytotoxic effect of ZD7288 and, with it, I_h ablation in primary cortical stem cells.

Despite the small number of experimental repetitions, the *in vitro* analysis does not suggest an effect of the migratory behavior and cell death due to ZD7288 application. To validate these results the experiments have to be repeated more often.

The *in vitro* experiments confirmed the results obtained by the *in vivo* methods, suggesting an impaired proliferation and differentiation of cells with attenuated I_h activity. However, the migratory behavior and cell death were not affected by the pharmacological inhibition of I_h.

4.6 Identification of HCN-dependent mechanism in proliferation and differentiation of neural progenitor cells

This work is the first report of HCN-channel expression in the embryonic forebrain and of the impact of HCN-channel function in neural development. However, the exact mechanisms of how this channel and its current contributed to early developmental processes are not yet known.

To address the question of whether the observed phenotype was due to the non-conducting channel and, thereby, to the ablated I_h, or whether it was due to an altered interaction of the HCN protein with other proteins, a mouse line with a shortened intracellular HCN4 C-terminus, resulting in the deletion of the cyclic nucleotide-binding domain (CNBD), was investigated (Alig et al., 2009). From the literature, it is known that most proteins interacting with the HCN channel bind to the lower end of the C-terminus, where the CNBD region is located (see 1.3.1) (Wahl-Schott and Biel, 2009). As the name implies, cAMP binds to the CNBD, which means that the mutant channel is insensitive to cAMP, potentially causing a hyperpolarized shift in the activation curve.

In the mouse line analyzed, a genetic approach equivalent to the EMX-HCN-DN mouse line was used (see Figure 4-2 C). In the EMX-HCN-573X mouse model, the spatially restricted of expression was achieved by the EMX1 promoter-driven cre recombinase, and additional temporal control was achieved using the Tet-off system with the prepending floxed stop sequence. Expression of the HCN-573X subunit and the reporter EGFP was achieved using the bi-directional promoter P_{tet}.

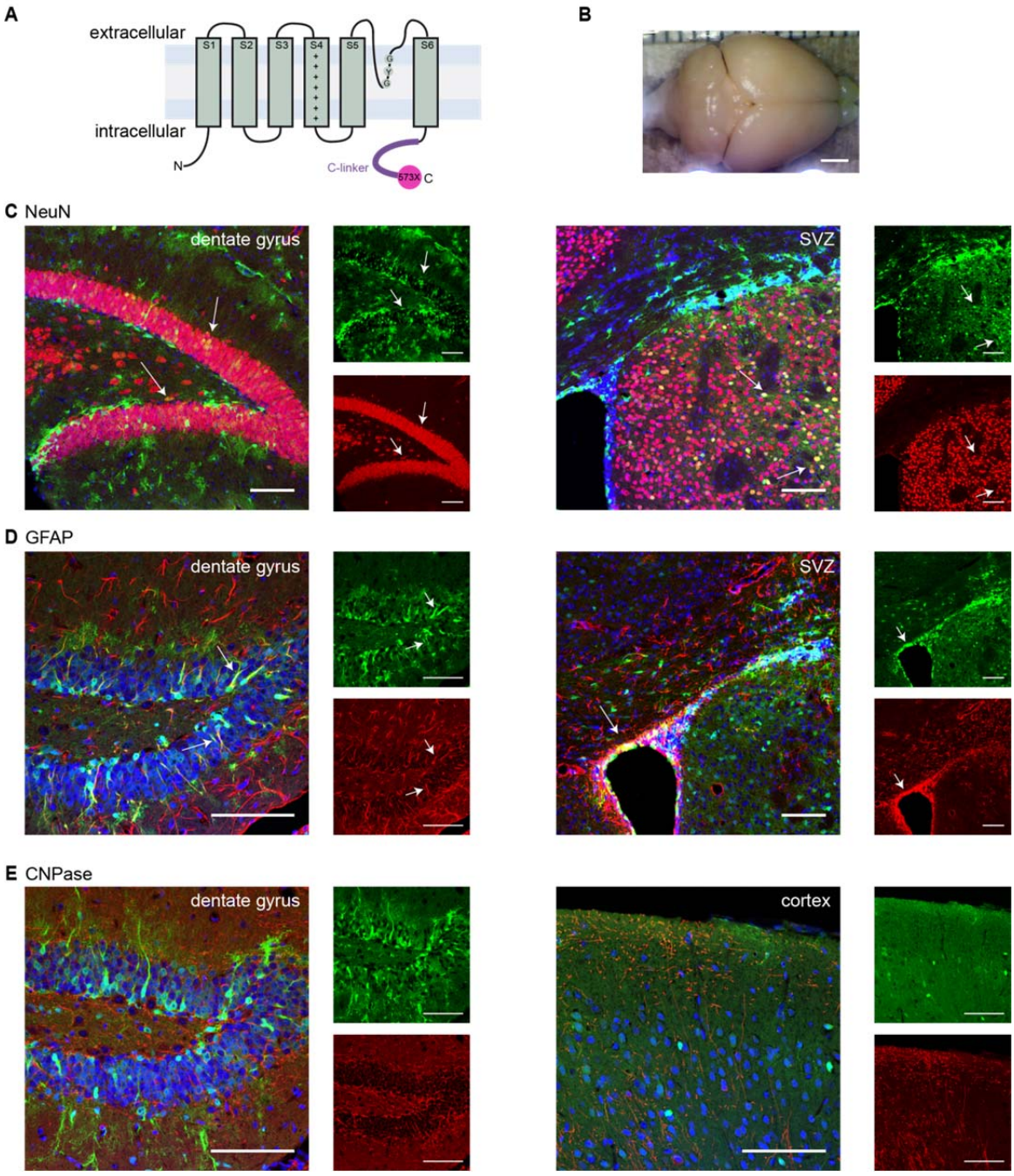
A
extracellular
intracellular
S1
S2
S3
S4
S5
S6
N
C-linker
573X
C
B
C NeuN
dentate gyrus
SVZ
D GFAP
dentate gyrus
SVZ
E CNPase
dentate gyrus
cortex

Figure 4-12 EMX-HCN-573X showed no gross morphological alterations in the forebrain

A, The HCN-572X mutation resulted in a deletion of the C-terminus at the end of the C-linker, causing the loss of the CNBD (for comparison see Figure 1-2). **B,** The brain of EMX-HCN-573X mutant mice showed no gross morphological alterations. **C,** Staining of coronal sections with the neuronal marker NeuN (red) showed an intact dentate gyrus (left panel) and SVZ with parts of the corpus callosum and striatum. A partial overlap with GFP positive transgenic cells in the dentate gyrus and the striatum was detected (white arrows). **D,** For GFAP staining (astrocytes; red), the same regions were analyzed and resulted in a partial overlay with GFP positive cells in the dentate gyrus and the SVZ (white arrows). **D,** CNPase staining, a marker for oligodendrocytes (red), showed in addition to the intact dentate gyrus (left panel), no gross morphological changes in the upper cortical layers (right panel). No overlay of CNPase and GFP positive cells was detected in adult EMX-HCN-573X mice. Small images show single channel pictures of GFP and the respective staining in red. All sections were counterstained with DAPI (blue).
Note the different scale bars; Scale bars, 100 μm.

In EMX-HCN-573X mice, a mutation leading to a C-terminal deletion was introduced in the transgenic HCN subunit, resulting in a loss of the CNBD, the main region for interactions with other intracellular proteins and other molecules (see 1.3.3) (Figure 4-12 A; for comparison see Figure 1-2). Due to the absence of CNBD and impaired cAMP binding, the mutation is thought to result in a hyperpolarized shift of the activation curve at physiological conditions. Ion flux through the channel, however, is not affected (Schulze-Bahr et al., 2003; Alig et al., 2009). In the adult forebrain, no gross morphological alterations were detected. The cortex developed normally, leaving only the colliculi superiores and inferiores of the mesencephalon uncovered (Figure 4-12 B). Coronal sections of the brain of EMX-HCN-573X mice were stained against NeuN (red), a marker for mature neurons, revealing a partial overlay of NeuN with GFP positive transgenic cells in the dentate gyrus (Figure 4-12 C; left panel; white arrows) and the striatum (Figure 4-12 B; right panel; white arrows), which demonstrated the neuronal identity of a major population of HCN-573X expressing cells. Staining with GFAP, an astrocytic marker (red), showed also a partial overlay with GFP-expressing cells, mainly in the dentate gyrus (Figure 4-12 D; left panel; white arrows) and the SVZ (Figure 4-1 D; right panel; white arrows), the regions of neurogenesis in the adult brain. The identity of these GFAP/GFP positive cells is unclear. One possibility is that these cells are proliferative stem cells in the adult brain located in the proliferative zones of the postnatal brain, the SVZ and subgranular zone of the dentate gyrus (Doetsch et al., 1999; Doetsch, 2003). The oligodendrocytic marker CNPase showed no overlap with GFP, in either the dentate gyrus (Figure 4-12 E; left panel) or in cortex (Figure 4-12 E; right panel). All sections analyzed showed normal morphology with respect to the dentate gyrus of the hippocampus, the SVZ with adjacent striatum, corpus callosum, and lower cortical layers, as well as upper cortical layers.

Partial deletion of the C-terminus, the most important domain concerning HCN - channel interactions with other molecules and proteins, did not cause a morphological phenotype comparable to that seen in EMX-HCN-DN mice. The normal morphology found in these mice suggested that the interaction with most other proteins or molecules is not needed for the normal proliferation of neural stem cells. Furthermore, the impaired development of HCN-DN - expressing cells was not dependent on cAMP binding to HCN, and thereby independent of the resulting depolarized shift of the channel activation.

To validate the hypothesis that impaired proliferation of the neural progenitors is due to the ablated I_h, electrophysiological voltage-clamp recordings of the primary cortical stem cells were conducted.

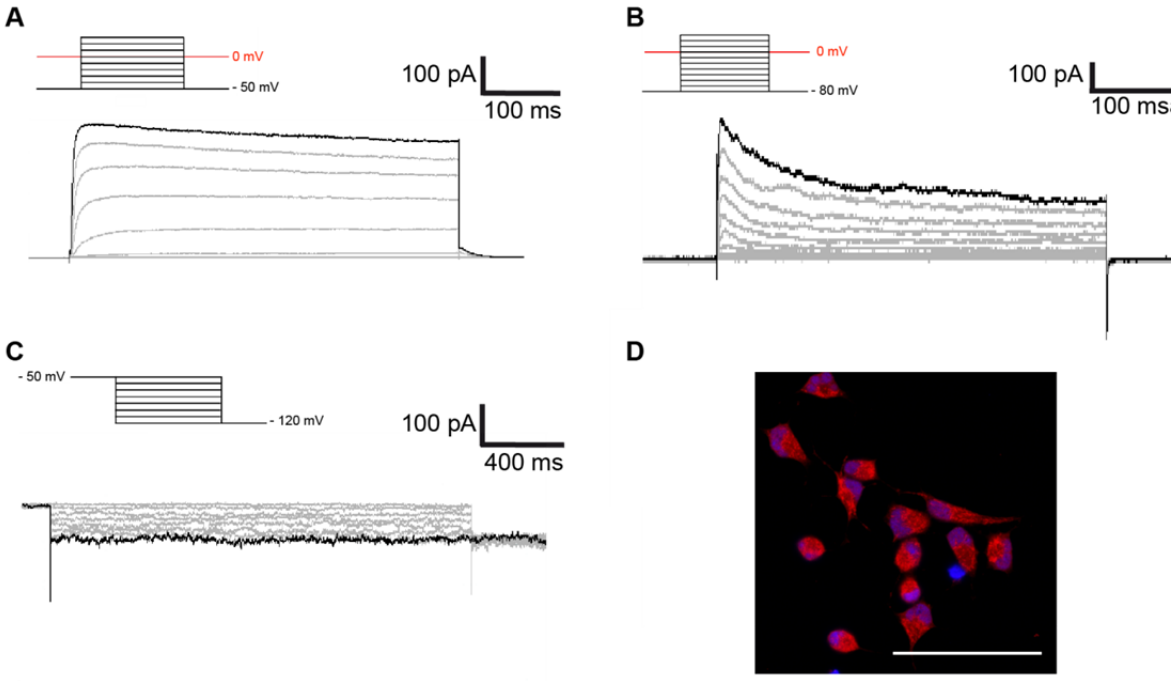

Figure 4-13 Voltage-clamp recordings of primary cortical stem cells

A, Sample traces of a voltage-clamp recording show an outward current in response to nine 500 – ms - long depolarizing steps of 10 mV starting at -50 mV. The inset depicts the protocol used with a potential of 0 mV marked in red. **B,** Sample traces of a voltage-clamp recording show a fast inactivating outward current in response to eleven 500 – ms - long depolarizing steps of 10 mV starting at -80 mV. The inset shows the protocol used with the 0 mV potential marked in red. **C,** Sample traces of a voltage-clamp experiment recorded at a holding potential of -50 mV with 2000 – ms - long hyperpolarizing steps to a test potential of -120 mV shows no hyperpolarization - activated current. The inset represented the hyperpolarizing protocol used. **D,** HCN4 staining (red) of stem cells depicted the HCN channel in intracellular compartments. Counterstain with DAPI is shown in blue.
Scale bar, 50 µm.

An electrophysiological investigation of the murine primary cortical stem cells showed different outward currents using two depolarizing protocols (Figure 4-13 A and B). A slowly activating, non-inactivating current was detected (Figure 4-13 A). Furthermore, a fast activating and inactivating outward current was measured upon depolarization (Figure 4-13 B). According to the ionic components and concentrations of the bath and electrode solutions used (see material section) and the known literature (see 1.2.1) (Picken Bahrey and Moody, 2002), the outward currents were likely mediated by a potassium efflux. The non-inactivating current potentially resembles a delayed rectifying current, while the inactivating current appeared like an A current. Confirmation of the exact channel population underlying this conductance can only be obtained with pharmacological experiments using channel-specific blockers. Upon hyperpolarization, no current was detected and, consequentially, no I_h was detectable in these primary cortical stem cells. (Figure 4-13). In line with these results, staining of the cells with an HCN4 antibody revealed the internalization of the HCN protein, suggesting a non-functional channel population due to its internal localization (Figure 4-13 D). HCN3 staining was not conducted in primary cortical stem cells due to the known nonspecific staining with the available antibodies.

The results obtained with the EMX-HCN-573X mouse line (Figure 4-13), suggested that the severe morphological phenotype seen in EMX-HCN-DN animals was not due to interacting proteins, or the depolarized shift of the activation curve upon cAMP binding, but rather dependent on the ablation of the current. The HCN4 subtype was detected in primary cortical stem cells, but was found only in intracellular compartments and not in the cell membrane (Figure 4-13 D). In agreement with this finding, a current activated upon hyperpolarization was not detected in primary cortical stem cells (Figure 4-13 C). Nevertheless, outward currents were detected, probably carried by potassium ions, which included a delayed, non-inactivating and a fast, inactivating current (Figure 4-13 A and B).

4.7 Summary

This work presents the first analysis of the impact of the HCN channel on early prenatal development of the rodent forebrain. In the embryonic brain of the mouse, HCN3 and HCN4 are the major subtypes found in different precursor cells and neurons mediating the I_h (Figure 4-1). Even in human cortical stem cells and neurons, the HCN3 subtype was detected at the mRNA level. In line with this early expression, the ablation of the current by a genetic approach showed a severe reduction in cortical and hippocampal structures in a development-dependent manner (Figure 4-3, Figure 4-4). The I_h ablation *in vivo* and the pharmacological block *in vitro* showed

a reduction in proliferation (Figure 4-5, Figure 4-6, Figure 4-10) and altered temporal patterns of differentiation (Figure 4-7, Figure 4-10), without affecting the migration or apoptosis of young neurons (Figure 4-8, Figure 4-9, Figure 4-11). Mechanistically, the physiological proliferation was not influenced by the deletion of the C-terminus of the HCN subunit, which resulted in an impaired interaction with other interacting proteins or molecules (Figure 4-12). The exact role of the HCN channel in proliferation could not be determined due to the absence of I_h in primary cortical stem cells, probably due to internalization of the protein (Figure 4-13). However, this is the first time that the impact of the HCN channels and the mediated current was demonstrated *in vitro* and *in vivo* on the early embryonic development of the mouse forebrain.

5 Discussion

5.1 Expression pattern of HCN subunits

The findings of this study suggest an important role of HCN channels in the proliferation of neural progenitor cells. Specifically the HCN3 mRNA shows a pronounced expression in the telencephalon during embryonic development and in different neural progenitor cells (Figure 4-1 A and B). Moreover, upon analysis of membrane fractions of E15 brain lysates, the HCN3 subtype was also detected on the protein level. In addition to HCN3, a strong expression of HCN4 mRNA and protein was detectable (Figure 4-1 A and D). Antibody staining showed that HCN4 is localized in the upper cortical layers and co-localized with TuJ1, a neuronal marker, suggesting expression in early neurons (Figure 4-1 D) and, thus, an obvious spatial distinction from HCN3 expression in neural progenitor cells. In contrast, the HCN1 and HCN2 proteins were not detected in the embryonic mouse brain (Figure 4-1 D).

As a result of the low abundance of HCN3 in the postnatal brain of rodents (Moosmang et al., 1999; Notomi and Shigemoto, 2004) and difficulties in cloning and expression in heterologous systems (Stieber et al., 2005; Mistrík et al., 2006), little is known about the function and properties of this HCN channel subtype. This study presented here indicates a new function of the HCN3 subtype in the proliferation and differentiation of neural stem and progenitor cells.

To validate the observed expression pattern of the four HCN subtypes, publicly available databases were analyzed for HCN gene expression.

Consistent with the results in the present study, the Allen brain atlas of the developing mouse brain showed *in situ* hybridization of the HCN1 mRNA and revealed no expression at E11.5, E13.5, and E15.5 (www.developingmouse.brain-map.org; Sep 25, 2016). In this data set, the other subtypes were not analyzed at early time points.

Additionally, the GENSAT organization analyzed the expression of HCN2 and HCN4 subtypes (www.gensat.org; Sep 25, 2016). HCN1 and HCN3 expression patterns were not investigated. The GENSAT organization generated mice with the expression of EGFP under the control of different promoters on a bacterial artificial chromosome (BAC) integrated multiple times in the genome.

According to the GENSAT data, the *Hcn2* promoter is mainly active in the hypothalamus, midbrain, medulla, and pons. Within the cortical structures, HCN2 is only sparsely expressed in the subplate and marginal zone. This expression pattern suggests the localization of HCN2 in migrating interneurons. This inhibitory cell type

migrates tangentially between E15 and E16 from the medial ganglionic eminence (MGE) into the neocortex, guided by the marginal zone and the subplate (Lavdas et al., 1999; Liodis et al., 2007). In the adult brain, several subpopulations of interneurons (e.g. somatostatin-expressing neurons in the neocortex) express functional I_h (Lupica et al., 2001; Aponte et al., 2006; Ma et al., 2006). Furthermore, the Cajal-Retzius cells are localized in the marginal zone of the embryonic cortex and, thus, could potentially express HCN2. This transient cell population has a great impact on radial migration (Gil et al., 2014). Additionally, Cajal-Retzius cells are known to express I_h in the postnatal cortex (Kilb and Luhmann, 2000). The weak expression pattern shown by the GENSAT organization supports the present findings of HCN2 expression. The HCN2 mRNA shows increasing amounts in the development of the telencephalon, with expression starting in the embryo, while the HCN2 protein, cannot be detected in the membrane fraction of E15 embryos (Figure 4-1A and C). Furthermore, and again in line with the GENSAT data showing the *Hcn2* promoter activity in differentiated cells, the HCN2 subtype was not detected in the mRNA sequencing study restricted to neural progenitor cells.

The *Hcn4* promoter-driven EGFP expression, investigated by the GENSAT organization, depicts localization in the midbrain, medulla and pons as well as in the developing cortical structures at E15.5. A more detailed view on the cortex reveals *Hcn4* promoter activity in the intermediate zone and cortical plate with higher expression in the subplate and marginal zone. This expression pattern suggests HCN4 localization in pyramidal neurons migrating through the intermediate zone and cortical plate (see 1.1). Additionally, the higher expression in the subplate and intermediated zone can be explained by the localization of the thalamocortical projections, at this early time point. Thalamocortical neurons are known to express I_h in the adult mouse brain (Ludwig et al., 2003; Kanyshkova et al., 2012). The subplate is needed to form these correct projections (Ghosh et al., 1990; Hoerder-Suabedissen and Molnár, 2015). This expression pattern differs from the expression of the HCN4 subunit in the cortical plate which was found in the immunohistochemical analysis of this study. A potential explanation for this discrepancy might reside in the transgenic BAC approach underlying the GENSAT data, which could be misleading as to the expression strength of individual HCN subunits. The multiple integrations of the BAC transgene could lead to a much higher expression of EGFP compared to the endogenous expression of the respective promoter (Chandler et al., 2007). This would explain the broad EGFP staining in the GENSAT analysis, while the expression was restricted to the marginal zone/layer I cells in the immunohistochemical analysis (Figure 4-1 D). Additionally, the I_h was not detected in electrophysiological investigations of migrating neurons in the embryonic cortical structures (Picken Bahrey and Moody, 2002). Furthermore, the absence of *Hcn4* promoter activity in the ventricular and subventricular zone (VZ/SVZ) is in agreement with the results

presented here, suggesting the absence of HCN4 mRNA in progenitor cells, mainly localized in the VZ/SVZ.

On the protein level, Seo et al. showed very weak expressions of the HCN1, 2 and 4 subtypes in the intermediate zone of the emerging hippocampal anlage at E14.5, while suggesting the highest expression for HCN4 (Seo et al., 2015). Upon broadening of the analysis to the postnatal brain, the overall expression of the different HCN subtypes in the hippocampus and cortical plate revealed a developmental increase in HCN1 and HCN2 proteins and a decrease in HCN3 and HCN4; however, HCN3 was only partially analyzed (Surges et al., 2006; Kanyshkova et al., 2009; Battefeld et al., 2012).

In accordance with the cortical expression patterns, analysis of different mouse embryonic stem cell lines showed the presence of the HCN3 subtype, supporting its role in the proliferation of cells. In contrast, much lower levels of HCN2 mRNA were observed (Wang et al., 2005; Lau et al., 2011).

The exclusive expression of the HCN3 subtype in early neurons of the developing cortex (Figure 4-1B) differs from previously experimental data and the literature, which collectively suggested an expression of the HCN4 and, to a lesser degree, HCN2 subtypes in early neurons during development. HCN4 could be difficult to detect due to the guanine-cytosine (GC)-rich sequences (*Hcn4* GC content: 60 %; NCBI Reference Sequence: NM_001081192.1). The difficulty to amplify the HCN4 transcript by PCR using polyA-primer (personal communication with K. Sauter) suggests long stretches of GC-rich sequences. To amplify the mRNA for the next generation sequencing performed by our collaborators, the same method was applied. This could result in an underrepresentation of the HCN4 mRNA. Moreover, the higher expression of GFP in the GENSAT data set due to possible multiple integrations of the BAC-GFP system and thereby an artificial overactivity of the *Hcn4* promoter could lead to an overrepresentation of the actual expression of the endogenous subunit. Moreover, the thalamocortical projections, possibly also expressing HCN4, can mimic the expression in the subplate/intermediate zone due to the close localization and the low resolution of the analyzed images by the GENSAT organization. Altogether this can result in a non-physiological representation of the HCN4 subtype expression pattern, which needs further investigation.

Analysis of the human cell types investigated by mRNA next-generation sequencing showed a gradual increase of the HCN3 expression when comparing aRGs to bRGs to neurons (Figure 4-1B lower panel), suggesting a differential impact of the channel on these distinct cell types. In the course of the evolution, the impact of the basal progenitors on the brain has been increasing, contributing to a more complex and bigger cortex (Molnár, 2011); while no basal progenitors exist in the reptile brain, the

above-described development of the murine brain showed evolving populations of the basal cell types, while the primate cerebral cortex is even more so characterized by a proliferative and large basal progenitor pool (Molnár, 2011). This in turn suggests an important role of the HCN channels during brain growth in humans.

In summary, the findings presented here suggest a developmental switch in cortical expression of the specific HCN subtypes, with HCN3 and HCN4 being mainly expressed during embryonic phases, while HCN1 and HCN2 being expressed later in the postnatal and adult stages. Furthermore, the HCN3 subtype is expressed in the proliferative population of neural stem and progenitor cells, while HCN4 is expressed in young neurons.

5.2 EMX-HCN-DN mouse line as model for HCN channel dysfunction during embryonic brain development

To investigate the prenatal role of HCN channels and I_h *in vivo*, the EMX1 promoter was selected for spatial and temporal restriction of the HCN-DN expression. EMX1 is expressed from E9.5 on, in a forebrain-restricted manner in excitatory neurons and partially in glia cells, corresponding to the cell types generated in the VZ/SVZ (See 1.1; Figure 4-2) (Iwasato et al., 2000; Gorski et al., 2002). To verify the reported forebrain restriction, EMX1-Cre mice were bred the with the Ai9 reporter line expressing the red fluorescent tandem dimer (td) Tomato (Figure 4-2 B). TdTomato is a large cytosolic protein. This mouse line showed the expected forebrain restriction and the reporter was not expressed in regions like the cerebellum (Figure 4-2-B). In the dentate gyrus, tdTomato was not detected in the subgranular zone or the soma of CA3 pyramidal neurons, while the CA3 pyramidal cell axons showed a red fluorescence (Figure 4-2-B). This distribution of tdTomato was also seen in mouse lines using different promoters with similar expression patterns (like CaMKIIα) shown in the Allen brain atlas (mouse connectivity studies; www.connectivity.brain-map.org/transgenic; Sep 25, 2016), suggesting the localization mainly in dendrites and axons.

The dominant-negative HCN subunit, expressed as a transgene in the mouse lines further analyzed in this study, interacts with endogenous HCN subunits and results in a functional ablation of I_h in a subunit-unspecific manner. The dominant-negative effect of HCN subunits with current-inhibiting mutations, mainly in the GYG motif of the pore region, was shown before (Xue et al., 2002; Er et al., 2003), while the functionality of the HCN-DN mutation used in this work was initially established in our laboratory (Sandke, 2006; Merseburg, 2016). The subunit-unspecific ablation of I_h can prevent the compensatory mechanism leading to up-regulation of unaffected HCN

subunits in single knockout studies. Analyzing mouse lines with individual HCN subtype knockouts showed morphologically normal brains, suggesting these compensatory mechanisms (see 1.3.4).

The genetic approach used in the EMX-HCN-DN mouse line additionally took advantage of the Tet-off system. Upon cre recombinase activation of the tetracycline transactivator (tTA) and in the absence of doxycycline the tTA binds to its responsive element (P_{tet}) enabling the transgene expression (Figure 4-2 C). The administration of doxycycline thus leads to the inactivation of the transgene expression, which is a control to exclude positional effects by the manipulated genome of the transgenic mice (Eszterhas et al., 2002). While the transgenic animals that are not exposed to doxycycline exhibit severe reductions of body size and brain volume, doxycycline-treated animals show a normal body weight and size as well as normal forebrain morphology (Figure 4-3). These findings exclude a phenotype-causing positional effect of the randomly inserted transgenic HCN-DN construct.

In the transgenic EMX-HCN-DN mice, the reduction of body size and weight together with the reduction in forebrain structures (Figure 4-3) led to an increased lethality around weaning precluding analyses in adult animals. Therefore, juvenile (3-week-old) mice were characterized instead. It was beyond the scope of this study to investigate the mechanisms underlying this phenotype.

Neonatal and juvenile EMX-HCN-DN mice showed a significantly decreased brain volume compared to control animals and compared to mutant mice exposed to doxycycline (Figure 4-4 C). Additionally, mutant mice at P21 showed a significantly increased ventricle volume compared to the control and doxycycline-treated group (Figure 4-4 F). This severe volume increase is due to the small remaining cortex incompletely covering diencephalon and mesencephalon, and leaving the lateral ventricles open to the subarachnoid space.

Next, the mechanisms underlying the severely reduced forebrain structure were examined, focusing on key developmental processes such as neuronal proliferation, differentiation, and migration. While the differentiation is postnatally detectable due to the late expression of glial markers (see control animals in Figure 4-7) and the migration was analyzed at embryonic ages (Figure 4-8), the proliferation, mainly taking part at embryonic time periods (E11 -E16, (Kwan et al., 2012)), was also analyzed postnatally (Figure 4-5). The proliferation zones VZ/SVZ were clearly distinguishable by immunohistochemistry with a Ki67 antibody in the mutant mice (Figure 4-5). With this clear identification of the remaining area of proliferation in the neonatal brain, this process could be analyzed. For a more detailed prenatal investigation of the proliferation of I_h ablated cells, earlier embryonic time points should be analyzed in the future.

In summary, the morphological alterations seen in the EMX-HCN-DN mice are very likely attributable to the dominant-negative HCN subunit, i.e. due to the I_h ablation. The mouse line gave the opportunity to target and investigate the proliferation and differentiation of I_h ablated neural stem and progenitor cells during cortical development *in vivo.*

5.3 The effect of I_h blockade on proliferation

The key findings of this work revealed the impact of genetic or pharmacological inhibition of I_h on the proliferation of neural stem and progenitor cells. In neonatal EMX-HCN-DN animals, the proliferation in the VZ/SVZ was significantly reduced *in vivo* (Figure 4-5). In agreement with this result, the *in vitro* experiments in primary rat cortical stem cells showed a decrease in BrdU incorporation upon ZD7288 treatment (Figure 4-10). Furthermore, the link between HCN-DN expression, impaired proliferation and the reduced forebrain size of the transgenic EMX-HCN-DN animals was corroborated by the absence of structural changes in the forebrain of NEXCre-HCN-DN animals (Figure 4-6), in which the onset of HCN-DN expression is delayed to post-mitotic neurons.

Inhibition of I_h leads to a hyperpolarization of the membrane potential in the HCN-DN expressing transgenic cells as well as in ZD7288 treated cells (Aponte et al., 2006; Merseburg, 2016). Hyperpolarization of the membrane potential of neural stem cells may interfere with their proliferation. Two distinct mechanisms could account for this effect: on the one hand the influence of the average resting membrane potential of neural stem cells, and on the other hand membrane potential fluctuations during cell cycle progression could be dependent on the I_h.

5.3.1 Resting membrane potential in neural stem cells and the contribution of I_h

The membrane potential, determined by the concentration gradient of extra- and intracellular ions and set by the activity of diverse ion channels and pumps, is long known to influence crucial cellular processes. The average resting membrane potential possibly has an influence on the proliferation of cells. The membrane potential progressively hyperpolarizes during cell differentiation. While the fertilized egg and embryonic stem cells are in a depolarized state, differentiated, non-proliferative cells are hyperpolarized (Binggeli and Weinstein, 1986; Yang and Brackenbury, 2013). However, depending on the proliferative state of the cell, one specific cell type can exhibit different membrane potentials. For example, the Chinese hamster ovary (CHO) cells have a membrane potential of approximately -60 mV when they are in a quiescent, confluent state (Cone and Tongier, 1973). Upon dissociation

the membrane potential depolarizes by about 50 mV to a potential of approximately -10 mV, resulting in the proliferation of CHO cells (Cone and Tongier, 1973). Furthermore, the depolarization of the membrane of proliferative cells was shown in pulmonary smooth muscle cells (Platoshyn et al., 2000). A hyperpolarizing shift of the membrane potential in human mesenchymal stem cells during adipogenic or osteogenic differentiation was detected (Sundelacruz et al., 2008). Upon artificial depolarization by increased extracellular potassium concentration or ouabain, the differentiation arrested as seen in the suppression of the expression of genes marking both differentiation processes (Sundelacruz et al., 2008). Interestingly, the attempt to reverse the differentiation of osteoblasts and adipocytes, upon depolarization resulted in a downregulation of the expression of differentiation marker genes, while the upregulation of stem cell markers was not detected (Sundelacruz et al., 2013). Furthermore, neurons show the most hyperpolarized membrane potential in the mammalian system hence lack the ability to proliferate. Interestingly, cultured neurons regain their mitotic activity upon long lasting pharmacological depolarization, yet lacking the final cytokinesis (Cone and Cone, 1976). In this study the harsh treatment of the mature neurons with ouabain, a sodium/potassium pump inhibitor (Laursen et al., 2013), veratridine as non-specific sodium channel activator (Yoshinaka-Niitsu et al., 2012), or the cation-selective pore forming protein gramicidine (Hicks et al., 2008) can have a variety of secondary effects, one being the misguided mitotic ability of the neurons. Nevertheless, consistent with this result, the optogenetic depolarization of young migrating neurons in acute embryonic cortical slices led to the re-entry in the cell cycle and to cell division (Calderon de Anda et al., 2016). In contrast to the different embryonic stem and progenitor cells, the resting membrane potential of adult murine neural progenitor cells was hyperpolarized at approximately –80 mV, but the enhanced proliferation seen upon barium chloride application was associated with the depolarization of the membrane (Yasuda et al., 2008). The hyperpolarization in the proliferative state was also observed in postnatal astrocytic progenitors (MacFarlane and Sontheimer, 2000).

As mentioned above, the HCN channels contribute via hyperpolarization-activated depolarization, to the establishment of the membrane potential and are thereby crucial for the determination of the biophysical properties of the cell. In mature neurons, the expression of the HCN-DN subunit leads to a hyperpolarized membrane potential compared to control cells (Merseburg, 2016) due to the loss of sodium influx through HCN channels close to the neuronal resting potential. The reversal potential of the ion flux through different HCN channels is around -25 to -40 mV (Mistrik et al., 2005; Rodrigues and Oertel, 2005; Stieber et al., 2005), which is still more depolarized than the membrane potential of neural stem cells, being around -40 to -70 mV (Aprea and Calegari, 2012). The I_h is thereby potentially driving the depolarization of the membrane.

Based on the known properties of I_h, the channel presumably does not exhibit a high open probability at the membrane potential of resting neural stem cells. According to the literature, HCN3 and HCN4 channels start to activate at around -70 mV and -80 mV, respectively, and the voltages of half maximal activations of the HCN3 and HCN4 subtypes in HEK cells are -95 +/-1 mV and –109 +/-1 mV, respectively (Ludwig et al., 1999; Mistrik et al., 2005). However, the human HCN3 and HCN4 channels show already a small channel open probability starting at a membrane potential around -50 mV (Stieber et al., 2005; Biel et al., 2009), which may result in a small current at the resting membrane potential of neural stem cells and, thus, might act depolarizing on these cells. These properties are highly dependent on the experimental setup and can vary in the physiological setting of the stem cells. Furthermore, I_h can stabilize the membrane potential at this depolarized state due to the previously reported voltage-independent current I_{ins} (Proenza et al., 2002; Aponte et al., 2006). Moreover, the co-expression and interaction of accessory subunits or modulating molecules are able to shift the activation threshold to more depolarized potentials and could contribute to a higher current density at the neural stem cells' resting membrane potential (Zolles et al., 2006; Li et al., 2009; Santoro et al., 2011).

The results presented here are supported by experiments regarding the impact of I_h inhibition on the proliferation in a mouse embryonic stem cell line (Lau et al., 2011). The electrophysiological investigation showed a hyperpolarization-activated current but did not unambiguously identify this current as I_h given that the application of ZD7288 resulted only in a partial inhibition (Lau et al., 2011). Nevertheless, in accordance with Wang et al. the expression of the HCN2 and HCN3 subunits were verified by PCR, while only the HCN3 protein was detected in the plasma membrane of the stem cells, explaining the cAMP insensitivity of the I_h measured by Wang et al. (Wang et al., 2005; Lau et al., 2011). Upon current inhibition by cesium chloride or ZD7288 the proliferation was decreased in a dose-dependent manner, showing the same effect as that detected in *in vivo* and *in vitro* experiments presented here.

Together, the data obtained by genetic or pharmacological inhibition of I_h strongly support the hypothesis of hyperpolarization of the membrane following attenuation of HCN channel function, which resulted in the inability of progenitor cells to proliferate (Figure 4-5 and Figure 4-10).

5.3.2 Membrane potential fluctuations during cell cycle progression and the potential contribution of the I_h

In addition to the overall depolarized membrane potential, the literature suggests a slow oscillation of the membrane potential during cell cycle progression (Blackiston et al., 2009; Urrego et al., 2014). The S-phase of the cell cycle is associated with a relative hyperpolarization of the membrane potential, while the membrane of cells in

M and G1 phases is more depolarized (Sachs et al., 1974; Boonstra et al., 1981; Wonderlin et al., 1995; Ng et al., 2010; Lau et al., 2011; Urrego et al., 2014). The exact time course of the rise and fall of the potential seems to differ between cell types and experimental settings (Sachs et al., 1974; Boonstra et al., 1981). Additionally, the fluctuation appears to differ within postnatal astrocytes, resulting in a depolarization upon S-phase entrance (MacFarlane and Sontheimer, 2000). Taken together these fluctuations are well established in cancer cells and other highly proliferative cells. Although these findings have not been investigated in neural stem cells so far, their universal validity is widely assumed and there are studies suggesting a similar mechanism of cell cycle regulation in neural progenitor cells. In embryonic rat oligodendrocyte progenitors, the membrane potential of the G0/G1 phase was more depolarized compared to the hyperpolarized S phase (Ghiani et al., 1999). Interestingly the inhibition of potassium channels or the activation of sodium channels, both causing depolarization, inhibit the cell cycle in the G1 phase (Ghiani et al., 1999). The application of both substances only led to the inhibition of proliferation when applied during the G1 phase, showing the necessity of the hyperpolarization for the cell cycle progression into the S phase (Ghiani et al., 1999). Furthermore, the depolarization during the M phase was shown in glioma cells and proliferating astrocytes (Habela et al., 2008). Collectively, these results suggest the presence of the membrane potential oscillations also in neural progenitor cells.

In murine embryonic stem cells, these cell cycle fluctuations were also detected (Ng et al., 2010; Lau et al., 2011). Interestingly, closer investigation of the cell cycle upon HCN channel inhibition with ZD7288 revealed a decrease in the number of cells in the G1 phase, while the cell number in the S phase of the cell cycle was increased (Lau et al., 2011). In another murine embryonic stem cell line, these results were reproduced, and a further analysis of the cell cycle in ZD7288-treated cells was conducted (Omelyanenko et al., 2016). The entire cell cycle was prolonged by approximately 30 %. Contrary to Lau et al., they have shown, that the number of cells in the S phase was increased ZD7288 treatment, but the cell number in G2/M phase was decreased, with no difference in the G1 phase (Lau et al., 2011; Omelyanenko et al., 2016). Omelyanenko et al. calculated the length of the different cell cycle phases considering the doubling time and cell cycle fraction. Their calculation indicated that ZD7288 treatment had increased G1 and S phases duration, while only the S phase lengthened in the study conducted by Lau et al. (Omelyanenko et al., 2016). This difference in the length of cell cycle phases could be due to the different cell lines and/or introduced by the different culture conditions (Jovic et al., 2013; Tamm et al., 2013).

Furthermore, detailed analysis of the S phase revealed a slower progression through this cell cycle phase upon I_h inhibition, by the slower incorporation of modified nucleotides into the DNA (Omelyanenko et al., 2016).

Preliminary data from this study indicate an increase in the length of the cell cycle and S phase in the rat primary neural stem cells of treated with ZD7288 by investigation of BrdU incorporation over time (data not shown) (Nowakowski et al., 1989).

According to these results, one might speculte that the I_h is activated upon the hyperpolarization at the S phase and slowly depolarizes the membrane potential, which is needed for the entry into the G2 phase. Upon I_h inhibition the S phase length increases, until the cell cycle progression stops at the end of the S phase and proliferation is blocked.

In summary, the reduced proliferation in the I_h-ablated cells *in vivo* and *in vitro* is likely caused by the altered biophysical properties of the neural stem and progenitor cells, leading to a hyperpolarization of the membrane potential. In neural stem cells, the resting membrane potential is between -40 mV and -70 mV (Aprea and Calegari, 2012). The cells exit the cell cycle by shifting to more hyperpolarized potentials. A more detailed investigation of the membrane potential shows oscillations during cell cycle progression, which are slow and assumed to be still in a more depolarized state than the resting membrane potential of the corresponding non-proliferative cells (Yang and Brackenbury, 2013). The hyperpolarization is needed to enter the S phase while a slow and progressive depolarization is suggested until the depolarized membrane potential in the M phase is reached. Upon I_h ablation, it is likely that cells progress more slowly through the S phase and are not able to enter the G2 phase, resulting in a cell cycle exit and a decrease in proliferation.

5.4 Impact of the membrane potential on proliferation

The abovementioned assumptions suggest a role of the I_h in the proliferation of neural stem and progenitor cells mainly due to its influence on their biophysical properties, i.e. by modulating their membrane potential. It has long been known, that the membrane potential is closely connected to the proliferation of different cell types (Cone and Cone, 1976). Even though, the direct connection is not clear yet. The following chapter, therefore, is about to speculate on the influence of the membrane potential on proliferation, its connection to neural stem cells and the possible impact of the I_h on these processes.

5.4.1 Calcium signaling

Calcium is one of the most important second messengers in cells and contributes fundamentally to the cell cycle progression and thereby to the proliferation of a variety of cells (see 1.2.1) (Capiod, 2011). The expression of different types of

voltage-gated calcium channels (VGCC) was shown in embryonic stem cells and different cancer cells (Rodriguez-Gomez et al., 2012; Gray et al., 2013). On the contrary, the influx of calcium through VGCCs is of minor importance in neural stem cells. Most studies suggested a role of the VGCCs in the differentiation of neural progenitor cells (D'Ascenzo et al., 2006; Lepski et al., 2013; Toth et al., 2016). However, there are reports about calcium currents in the embryonic neural progenitor cells, although they do not account for the possible presence of cells that undergo differentiation (LoTurco et al., 1995; Cai et al., 2003; Picken Bahrey and Moody, 2003).

This suggests that the cytosolic calcium increase observed in proliferating neural stem cells is mediated by internal calcium stores or ligand-gated channels and thereby independent of the depolarizing action of the HCN channels and the mediated current (see 1.2.1).

5.4.2 Direct activation of cell signaling upon changes in membrane potential

The activation of various proteins can be directly linked to the depolarization of the plasma membrane.

The nano-clustering of K-Ras was shown upon membrane depolarization by increasing extracellular potassium concentration (Zhou et al., 2015). The nano-clustering leads to the activation of the extracellular signal-regulated kinase/mitogen-activated protein kinase (ERK/MAPK) pathway (Zhou et al., 2015). The MAP kinase activation can be directly linked to the proliferation of different cell types (Dhillon et al., 2007).

Furthermore, the nuclear respiratory factor (Nrf) 2 is a transcription factor regulating gene expression associated with DNA replication, mitosis, and cytokinesis (Scarpulla, 2008). Interestingly, its activation by the translocation to the nucleus can be provoked by depolarization of the plasma membrane (Yang et al., 2004), leaving Nrf2 as a perfect candidate to directly connect the membrane potential and proliferation.

Additionally, there are a number of immediate early genes that are induced upon membrane depolarization and thought to be involved in neural plasticity (Herschman et al., 2000). The kinase induced upon depolarization (KID) 1 is one such example. KID1 is found in the brain and conducts auto-phosphorylation and histone phosphorylation, thereby regulating gene expression (Feldman et al., 1998).

The potassium channel ether-à-go-go (EAG), which can be found in a variety of different cancer types, promotes proliferation (Pardo et al., 1999; Pardo and Stuhmer, 2008). Interestingly, the current itself only partially leads to the increase in

proliferation. Additionally, the conformational change upon voltage sensing, even without current flow, elevates proliferation activity in the affected cells (Hegle et al., 2006). Hegle et al. used a mutation in the selectivity filter of the EAG1 channel to show the current-independent function of the channel (Hegle et al., 2006). The EMX-HCN-DN mice also have a mutation in the selectivity filter. This mutation blocks the current but does not change the conformation upon voltage sensing, arguing against the current-independent function seen in the EAG channel.

In summary, the depolarizing action and/or membrane potential stabilization of the HCN channels and the mediated I_h can function as an indirect regulator of protein or transcription activation.

5.4.3 Cell volume regulation

The alterations of the cell volume can influence important processes like proliferation or apoptosis (Lang et al., 2007). Because of the tight coupling of the volume to the intracellular ion concentrations, it is difficult to distinguish their respective impacts on membrane potential regulation and cell volume. It is known that the volume alternates during cell cycle progression, being increased at the beginning of the M phase but shrinking toward its end, accompanied by chloride and potassium flux (Lang et al., 2007; Hoffmann et al., 2009). The smallest volume is measured during the G1/S phase, when intracellular calcium and sodium concentrations are potentially higher, and in turn can lead to the subsequent volume increase (Lang et al., 2007; Hoffmann et al., 2009).

Due to the sodium conductance of the HCN channels, these channels could contribute to the sodium influx, and thereby to the volume increase.

Taken together the HCN channels and their mediated I_h can have dual functions in the proliferation activity of neural stem and progenitor cells, by influencing the membrane potential and by its sodium inward current.

5.5 The inhibition of HCN channels and its influence on differentiation

The data obtained in this study revealed that the genetic or pharmacological inhibition of HCN channels altered the differentiation of neural stem and progenitor cells. Both *in vivo* and *in vitro* findings showed an early appearance of glial markers suggesting a temporal change in the differentiation (Figure 4-7 and Figure 4-10 B, C, D, E). A preliminary experiment investigating the ratio of primary cortical stem cells

which incorporated BrdU indicated that the primary neural stem cells have an increase in cell cycle length (data not shown) (Nowakowski et al., 1989).

In agreement with this work, inhibition of I_h with ZD7288 in murine embryonic stem cells led to a decrease in pluripotency and an increase of differentiation markers in spontaneous differentiating conditions (Omelyanenko et al., 2016). Together with the decrease in proliferation, this was accompanied by a lengthening of the cell cycle (Lau et al., 2011; Omelyanenko et al., 2016). Omelyanenko et al. showed that the lengthening was due to an increase in G1 and S phase length (Omelyanenko et al., 2016). From general stem cell research, it is known, that the length of the G1 phase is an important parameter for the differentiation of a cell (Chen et al., 2015). During the G1 phase, the cell is susceptible to differentiating factors. Thus, G1 phase in pluripotent cells is fast, and a longer during differentiation divisions resulting in a fast phase in pluripotent cells and longer phase during differentiational divisions (Chen et al., 2015). This was also shown in neural stem cells (Calegari et al., 2005; Lukaszewicz et al., 2005; Roccio et al., 2013). Furthermore, experiments in neural stem cells revealed that this is not only consequence, but also cause for the differentiation. The artificial lengthening of the G1 phase induced and increased neurogenesis and gliogenesis, while proliferative divisions were decreased (Lukaszewicz et al., 2002; Calegari and Huttner, 2003; Roccio et al., 2013). Furthermore, the cell cycle length increased during cortical development as a function of time, independent of the increased neurogenic divisions (Takahashi et al., 1995; Calegari et al., 2005).

The lengthening of the cell cycle, and in particular the longer G1 phase in the ZD7288-treated cells, would lead to an earlier differentiation of the neural stem cells. In agreement with this assumption, the *in vitro* differentiation assay showed a decrease in Sox2 positive stem cells upon I_h inhibition (Figure 4-10 B). However, the major finding of the *in vivo* and *in vitro* differentiation experiments was that the ZD7288-treated cell cultures exhibited the glial cell fate much earlier, as evident by the early expression of glial markers. This finding would be explained by the lengthening of the cell cycle during the cortical development leading to a much longer cell cycle in the later gliogenesis compared to the earlier neurogenesis (Takahashi et al., 1995; Calegari et al., 2005). In summary, the lengthening of the cell cycle would lead to a decrease in proliferative divisions and an increase in differentiation potentially towards the glial cell fate.

A further explanation for the temporal alterations in the differentiation of the neural stem cells *in vivo* and *in vitro* can be related to voltage-gated calcium channels. In murine neural stem and progenitor cells, small L-type calcium currents were detected with a differentiation–dependent increase in current density (D'Ascenzo et al., 2006). Inhibition of the L-type calcium channels led to a decrease of the neuronal outcome (D'Ascenzo et al., 2006; Lepski et al., 2013). On the contrary, its activation increased

the cell numbers with neuronal fate. Both treatments had no effect on the proliferation or amount of analyzed cells (D'Ascenzo et al., 2006). Increased levels of cAMP and the subsequent activation of the L-type calcium current showed the same effects on the neuronal outcome of the neural progenitor cells (Lepski et al., 2013). In both studies, it was not investigated if the decreased neuronal cell fate due to inhibition of the L-type calcium current was accompanied by an increase in glial cells.

Furthermore, in HEK cells and hippocampal neurons Lin et al. were able to show an inhibition of the L-type calcium channels by the interaction with the N-terminus of the closed HCN2 subunit (Lin et al., 2010). This suggests that the altered differentiation in the EMX-HCN-DN mice would be due to the overexpression of the HCN protein and thereby an increased interaction between the HCN N-terminus and the L-type channels. Furthermore, the altered differentiation would be seen also in the EMX-HCN-573X mice, with the deleted C-terminus, and in the IUE experiments upon electroporation and thereby overexpression of the pore mutant and the wild-type HCN channel, but were not further investigated. However, it does not explain the altered differentiation outcome of the neural stem cell culture treated with I_h inhibitor and expressing only endogenous levels of HCN protein. Together with the diverging sequences of the N-terminus of the different HCN channel subtypes this interaction is not very likely but cannot be excluded.

Taken together, the altered differentiation pattern of the I_h -blocked cells *in vivo* and *in vitro* is likely due to the cell cycle lengthening, resulting in an early differentiation of the neural stem and progenitor cells. Furthermore, the hyperpolarizing shift of the resting membrane potential upon I_h inhibition shifts the membrane potential further away from the L-type calcium channel activation. The shift would, in turn, reduce the calcium influx trough L-type VGCC into the differentiating cell, inhibiting the neuronal cell fate and potentially increasing glial cell numbers.

5.6 HCN channels interactions with other proteins and small molecules

HCN subunits can interact with a variety of different proteins and small molecules which modulate I_h (see 1.3.3). By investigating the EMX-HCN-573X mouse line, these interactions were partially analyzed. The expression of the HCN-573X subunit, which lacked the CNBD, resulted in a normal morphology of the analyzed forebrains (Figure 4-12). The overexpression led to the heteromerization of the endogenous subunits with the mutated HCN-573X, resulting in a dominant-negative effect on the modulation of the channel (Alig et al., 2009). Furthermore, the CNBD is needed for the interaction of the HCN channels with cAMP, TRIP8b, MiRP1, KCTD3, filamin A, tamlin,

S-SCAM and Mint2 (see 1.3.3) (Gravante et al., 2004; Kimura et al., 2004; Michels et al., 2008; Brandt et al., 2009; Santoro et al., 2009; Ying et al., 2012; Cao-Ehlker et al., 2013; Noam et al., 2014). These modulations seemed to be irrelevant for the physiological proliferation of neural stem cells seen in the EMX-HCN-573X mice. In agreement with this, the HCN3 subtype is less or not at all cAMP responsive, and it is the major channel subtype expressed at these early prenatal time points (Figure 4-1). As a result, cAMP binding would induce only a minor depolarization shift of the activation curve. Nevertheless, there are two further molecules, Src kinase, and PIP_2, which modulate HCN channels independently of the CNBD. Although the HCN3 subtype is not well investigated so far, these two sites are well conserved in the HCN subtypes and are supposed to interact with all four HCN subtypes, including HCN3. The Src kinase leads to a depolarizing shift of the activation curve upon HCN phosphorylation (Zong et al., 2005; Arinsburg et al., 2006; Li et al., 2009). Additionally, the effect of PIP_2 on HCN3 channels was investigated in intergeniculate leaflet neurons, where a depolarizing shift of the activation curve of approximately 17 mV was observed (Ying et al., 2011). This shift can vary in neural stem and progenitor cells but probably results in a half-maximal activation of approximately -60 mV for human HCN3 (Stieber et al., 2005) and -78 mV for mouse HCN3 (Mistrik et al., 2005), suggesting at least a small current density in the range of the known membrane potentials of neural stem cells (-40 to -70mV) (Aprea and Calegari, 2012).

Using the HCN-573X mutation, does not exclude that the decreased proliferation seen in EMX-HCN-DN mice is due to the increased interaction of the overexpressed subunit with other interacting proteins. Nevertheless, in the primary cortical stem cell culture, the same reduction in the ability to proliferate is seen upon I_h inhibition using a pharmacological blocker. In the *in vitro* experiments, no protein was overexpressed, thus excluding the possibility of an altered protein interactions due to the increased HCN protein content as the single cause for the reduced proliferation.

In summary, the severely reduced forebrain size resulting from a decrease in proliferation in the EMX-HCN-DN animals are most likely due to the functional ablation of I_h and not caused by an off-target effect produced by the overexpression of the transgene. This phenotype is potentially dependent on the Src kinase and/or PIP_2 modulation of the HCN channel protein, but is most likely not dependent on other interacting proteins or cAMP.

5.7 Electrophysiological characterization of neural stem cells

To analyze the exact role of the I_h during the proliferation of neural stem cells, the electrophysiological profile of the primary cortical stem cells were investigated *in vitro* (Figure 4-13). Two different macroscopic outward currents were detected, probably both potassium conducting. The current trace characteristics suggest a delayed rectifying current (I_{DR}) and transient, inactivating current (I_A) (Figure 4-13 A and B).

There is a variety of studies reporting different voltage-gated potassium channels expressed in proliferative cells. By determining the membrane potential in excitable and non-excitable cells the super-family of potassium channels has an important function for the proliferation of these cells. Here, the focus will be on neural stem and progenitor cells. In congruence with the presented findings, the further analyzed human and murine neural stem cells exhibit two populations of outward directed potassium channels, namely the I_{DR} and the I_A (Cai et al., 2003; Li et al., 2008; Lim et al., 2008; Schaarschmidt et al., 2009). There are contradictory results as to other voltage-gated ion channels: additional inward sodium channels in different current densities, a small voltage-gated calcium current and a hyperpolarization-activated inward current of unknown origin have been described (Cai et al., 2003; Lim et al., 2008). This inward current could be assigned to the HCN channels based on its reversal potential and cesium-dependent inhibition, yet it was also blocked upon barium application, which is an indicator for the inwardly rectifying potassium current (I_{IR}) (Lim et al., 2008). In the electrophysiological recordings conducted in this project, no hyperpolarization-activated or the above mentioned sodium currents were detected, calcium currents, however, were not measurable in this experimental set up due to the addition of the calcium chelator EGTA to the pipet solution (see material section).

Previous studies suggest an important role of the potassium channels on the proliferative activity of the neural stem and progenitor cells. In long-term cultures of mesencephalic progenitor cells, the specific blockade of the I_{DR} was able to enhance proliferation shown by an increase in BrdU incorporation (Liebau et al., 2006). The increase in proliferation was also seen in experiments blocking specifically the I_{IR} with barium chloride, in astrocytes and adult neural progenitors in the SVZ (MacFarlane and Sontheimer, 2000; Yasuda et al., 2008). In these and other studies proliferation was arrested upon the general inhibition of voltage-gated potassium currents in different systems such as human neural progenitor cells, astrocytes, oligodendrocytic progenitors and even in murine embryonal stem cells (Ghiani et al., 1999; MacFarlane and Sontheimer, 2000; Yasuda et al., 2008; Schaarschmidt et al., 2009; Ng et al., 2010).

In embryonic slices at E12 or E14 I_{DR}, calcium-activated potassium currents, voltage-gated calcium currents, and in some cells sodium currents were detected (Mienville and Barker, 1997; Picken Bahrey and Moody, 2003). The differentiation status of the analyzed cells was not established in these studies, leaving the possibility that channel expression starts with differentiation, like the VGCC or sodium channels as marker for excitable cells (see 5.5).

The difference in the electrophysiological profiles seen in the different experimental setups can be due to the variety of neural progenitor cells like aRG, bRG, aIP and bIP (see 1.1). The experiments were conducted at different time points during the development, and therefore with varying contributions of the different neural progenitors.

Besides I_{DR}, electrophysiological recordings of embryonic stem cells of the mouse detected I_h in a minority of investigated cells (Wang et al., 2005). The I_h was inhibited by cesium, a known HCN channel blocker. No effect of elevated cytosolic cAMP levels due to isoproterenol, a beta-adrenoceptor agonist were detected, suggesting the contribution of HCN3 subtype, as it is non-responsive to cAMP (Mistrik et al., 2005; Wang et al., 2005). In accordance with this, the mRNAs for HCN3 and, at much lower levels, HCN2 were detected (Wang et al., 2005). In contrast, neither I_h nor the mRNA of any subtype were detected in human embryonic stem cells, while I_{DR} was present (Wang et al., 2005). Consistent with the experiments conducted in neural stem and progenitor cells, Wang et al. showed a decrease in proliferation upon the inhibition of voltage- and calcium-dependent potassium currents (Wang et al., 2005). Unfortunately, in this study, the inhibition of the murine I_h and its impact on proliferation were not investigated (Wang et al., 2005).

It must be mentioned though, that these experiments were performed in mouse and human stem cell lines, which could alter the electrophysiological profile of the analyzed cells, due to the artificial treatment and the possible changes in the cells upon long-term propagation in culture (Pan et al., 2009).

These results suggest a major impact of the ion channel composition on the proliferation of neural progenitor cells in different regions and at different time points during development. Manipulation of the conductance of potassium channels as one of the major determinants of the membrane potential underlined the importance of the biophysical properties of these early cells. However, these results did not show a detectable current mediated by the HCN channels in neural stem or progenitor cells and are thereby contrary to the severe phenotype of the EMX-HCN-DN mice and the impaired proliferation in the *in vivo* and *in vitro* experiments upon I_h inhibition.

The surprising result of the severe effect of the genetic and pharmacological inhibition of the I_h (Figure 4-3, Figure 4-4, Figure 4-5, Figure 4-7, Figure 4-10) together with the absence of a detectable I_h in the electrophysiological recordings (Figure 4-13), led to several hypotheses regarding the contribution of HCN channels to the proliferation and differentiation in the *in vivo* and *in vitro* experiments. There are only a few reports suggesting the presence of I_h in proliferative cells. In embryonic stem cells, Lau et al. showed a current trace, claiming to have identified the I_h, but inhibition with ZD7288 was incomplete, leaving the exact identity of this current open (Lau et al., 2011). However, Wang et al. measured the I_h in an embryonic stem cell line (Wang et al., 2005).

One possible reason for this discrepancy could be the experimental environment and its change during the electrophysiological experiment. In here presented experiments, the primary neural stem cells were cultured in DMEM/F-12 medium including supplements (see method sections for details), with a bicarbonate pH buffer system, while an HEPES buffered bath solution was used in the electrophysiological recordings (see method section for details). This change in the medium could be a potential stress factor for the neural stem cells, which could lead to an altered protein surface expression and thereby to the absence of the I_h (Cheng et al., 2016). To analyze and potentially avoid this problem, the primary neural stem cells could be patched in HEPES-buffered DMEM to assure the same environment to the cells.

Furthermore, there are more physiological explanations for the absence of the current which could also be valid for other experiments conducted in acute slices of embryonic brains (Picken Bahrey and Moody, 2002, 2003). Such possibilities would be a small current amplitude of the instantaneous component of the I_h, or varying localizations of the HCN subunits.

5.7.1 The instantaneous I_h component

The I_h consists of two different components: the I_{ins}, a voltage-independent current and the steady-state current I_{ss}, the slowly activating current upon hyperpolarization (see 1.3.1) (Macri et al., 2002; Proenza et al., 2002; Rodrigues and Oertel, 2005; Aponte et al., 2006). In heterologous systems, the HCN3 exhibits a relatively large I_{ins} with 13 % of the total current (Mistrik et al., 2005). In a physiological system like the stellate cells of the mammalian ventral cochlear nucleus, the I_{ins} exhibits small current densities (Rodrigues and Oertel, 2005). This small current can contribute to the membrane potential of the neural stem cells, which can be difficult to measure in a physiological system, without artificial channel overexpression, if the current amplitudes are low. It is known, that the I_{ins} can be regulated independently of the I_{ss}, for example by intracellular chloride concentrations, or MiRP1 co-expression (see 1.3.3) (Proenza et al., 2002; Mistrík et al., 2006). The intracellular chloride

concentration has an inverse effect on the I_{ins} (Mistrík et al., 2006). However, in neural stem cells, the chloride concentration is relatively high, due to the absence of the potassium/chloride co-transporter 2 (KCC2) (Rivera et al., 1999), which would lead to a potential suppression of the I_{ins}, arguing against the contribution of I_{ins} in neural stem cells. The other regulatory mechanism, which could contribute to the demonstrated effect of HCN channels on the proliferation of neural stem cells, is the interaction with MiRP1. In CHO cells MiRP1 interaction with the HCN2 channel protein led to an increase of I_{ins} and a decrease in the steady state component (Proenza et al., 2002). In contrast, the EMX-HCN-573x animals, which omit parts of the C-terminus responsible for these interactions, showed normal brain morphology. This result suggests that proliferation is independent of C-terminus interacting proteins. Nevertheless, the independent regulation of I_{ins} and I_{ss} supports the idea of the possible presence of single current component. Assuming a small amplitude of the voltage-independent I_{ins}, this can be difficult to detect in the cells, but due to a higher open probability it would stabilize the membrane potential of the neural stem cells close to the HCN reversal potential (-20 mV to -40 mV) (Mistrik et al., 2005; Rodrigues and Oertel, 2005; Stieber et al., 2005) being relatively depolarized. The inhibition of the I_{ins} would then lead to the hyperpolarizing shift, reducing the ability of the cells to proliferate (Binggeli and Weinstein, 1986; Yang and Brackenbury, 2013).

5.7.2 Subcellular localization of HCN channel subunits

In the immunohistochemical investigations of our primary cortical stem cells, the HCN4 protein was localized intracellularly (Figure 4-13 D). This localization suggested a short time span of the membrane integration of the HCN subunit, with a subsequent rapid internalization.

From cancer cell lines it is known, that the membrane potential hyperpolarizes at the entry in the S phase, and a slow depolarization is suggested at the end of the S phase resulting in a depolarized potential in the M phase (Urrego et al., 2014). According to this scenario, the I_h could play a major role in depolarizing the plasma membrane and thereby facilitating the transition from S to G2/M phase. This specific role of the channel would require a short membrane integration of the HCN channel, followed by a fast internalization. The fast internalization of the HCN protein was shown for HCN1 in hippocampal pyramidal neurons following status epilepticus after one hour (Jung et al., 2011). This can explain the lack of measurable current in our heterogeneous neural stem cell population, containing cells in all phases of the cell cycle. Nevertheless, a short expression of the HCN channel and its I_h leading to the depolarization of the membrane potential appears to be essential for the cell cycle progression. The current inhibition led to the decreased proliferation seen in the *in vivo* and *in vitro* experiments.

Furthermore, the immunohistochemical analysis of the primary cortical stem cells (Figure 4-13 D) implies localization of the HCN4 protein in the nuclear membrane.

Different ion channels are expressed in the different intracellular membranes with a variety of functions (Checchetto et al., 2016). The nucleus is surrounded by the nuclear envelope, a bi-layered membrane system consisting of the inner and the outer nuclear membrane (Mazzanti et al., 2001). The outer nuclear membrane belongs to the endoplasmic reticulum (ER) (Mazzanti et al., 2001). The perinuclear space is therefore connected to the lumen of the ER. The whole nuclear envelope is spanned by the nuclear pore complexes, which are highly permeable to small molecules and ions as well as macromolecules (Mazzanti et al., 2001). This results in a relatively balanced ion flux between the nucleoplasm and the cytoplasm. However, the perinuclear space contains high calcium and low potassium concentrations compared to the nucleoplasm or cytoplasm (Checchetto et al., 2016). In the inner membrane of the nuclear envelope, different ion channels are located, e.g. ATP and calcium-gated, as well as voltage-gated potassium channels (Checchetto et al., 2016). The I_{IR} channels were detected in cancer cell lines and rat neuronal cells. The function of these channels at the nuclear location was not established so far (Stonehouse et al., 2003; Olsen and Sontheimer, 2004). Furthermore, the Kv1.3 channel was detected in the nuclear membrane (Jang et al., 2015); its inhibition is associated with the phosphorylation and activation of cAMP response element-binding protein (CREB) and c-fos, two important transcription factors (Jang et al., 2015). Additionally, the EAG1 or Kv10.1 channel was detected in the nuclear membrane, and its physiological functionality was determined by electrophysiological investigation of the channel (Chen et al., 2011). The exact function of the channels was not established, but the channel protein was associated with heterochromatin (Chen et al., 2011). Cations like sodium, potassium, magnesium and calcium are linked to the more compact existence of DNA associated with lower transcription rates, suggesting one possible function of the ion channels (Strick et al., 2001).

The localization in the nuclear membrane can explain the absence of the detectable I_h in primary neural stem cells and the intracellular location of the HCN4 channel protein (Figure 4-13 C and D). Furthermore, the membrane permeability of ZD7288 still allows inhibition of HCN channels localized in the nuclear membrane (Harris and Constanti, 1995). In contrary, the western blot analysis of the 15 days old embryos showed protein expression of HCN3 and HCN4 in the plasma membrane fraction of the brain tissue (Figure 4-1 C). Furthermore, the resting membrane potential of the inner nuclear membrane is depolarized at approximately -30 mV (Checchetto et al., 2016). At this depolarized potential HCN channels would not be active (Stieber et al., 2005; Biel et al., 2009).

In summary, the data presented here do not explain the exact mechanism as to how loss of I_h affects the proliferation of neural stem cells. The abovementioned hypotheses of a small I_h current density and/or the short expression of the channel protein in the plasma membrane are not mutually exclusive with the nuclear localization of HCN subunits. Chen et al. showed that the Kv10.1 channel is expressed at the cell surface before it can be found in the inner nuclear membrane, suggesting a role in a cell signaling pathway (Chen et al., 2011). This could also be true for the HCN channels.

5.8 Known limitations of ZD7288

In the conducted cell culture experiments with primary cortical stem cells from the rat, I_h was pharmacologically blocked by application of the inhibitor ZD7288. This inhibitor was long thought to interact specifically with HCN channels and was used in a variety of electrophysiological experiments using concentrations from 1 µM to 100 µM (Surges et al., 2003; Bender et al., 2005; Momin et al., 2008; Li et al., 2009; Huang et al., 2011). In heterologous expressing HEK cells, the half maximal inhibitory concentration (IC_{50}) of all four different HCN subtypes varied from approximately 20 to 40 µM (Stieber et al., 2005).

However, recent studies showed unspecific interactions with other ion channels. With an IC_{50} of about 40 µM, ZD7288 blocked T-type calcium channels in hippocampal neurons from the rat (Sánchez-Alonso et al., 2008). This effect was also shown in other cell types and HEK cells, with heterologous expression of the Cav3.1, 3.2 and 3.3, the calcium channel subtypes underlying the T-type current (Felix et al., 2003). Furthermore, Wu et al. showed the inhibition of voltage-dependent sodium currents upon ZD7288 application with an IC_{50} of about 1.17 µM, suggesting that ZD7288 blocks sodium currents more efficiently than HCN channels (Wu et al., 2012).

In this work, 10 µM or 30 µM ZD7288 were used in all experiments, except the assay investigating the differentiation of primary neural stem cells, where only 30 µM were applied. These concentrations are in the range of the previously used ZD7288 concentrations and around the half maximal inhibitory concentration (~20 - 40 µM) (Stieber et al., 2005).

In neural stem or progenitor cell, most investigators were unable to detect voltage-gated-calcium channels (Piper et al., 2000; Li et al., 2008; Lim et al., 2008), and even when they did,, these currents were associated with the differentiation of the analyzed cells (D'Ascenzo et al., 2006; Lepski et al., 2013; Toth et al., 2016). In other experiments, using murine embryonic slices, small calcium currents were measured upon depolarization. Nevertheless, the onset of differentiation in these cells could not

be excluded (LoTurco et al., 1995; Cai et al., 2003; Picken Bahrey and Moody, 2003). The closer investigation of the molecular substrate of these voltage-gated calcium channels revealed proteins belonging to the L-type family of calcium channels which were not affected by the ZD7288 application (Cai et al., 2003; D'Ascenzo et al., 2006; Lepski et al., 2013).

Furthermore, the detection of sodium currents was inconsistent in the literature about neural stem or progenitor cells, suggesting that the onset of sodium current is also connected to the cell cycle exit, and thus to differentiation of these cells (Piper et al., 2000; Picken Bahrey and Moody, 2003; Li et al., 2008; Lim et al., 2008). This suggests a possible role of sodium currents in the altered differentiation seen in the *in vitro* experiments, but not in the decreased proliferation (Figure 4-10).

Moreover, a ZD7288 induced inhibition of exocytosis was shown in neurons and pituitary lactotrophs (Chevaleyre and Castillo, 2002; Gonzalez-Iglesias et al., 2006). The effect on the proliferation and differentiation which was observed in the primary cortical stem cells upon application of ZD7288 presumably did not result from inhibited exocytosis, given the fact that stem cells are not especially active in exocytosis.

In the presented investigation of the electrophysiological profile of the used primary cortical stem cells of the rat, calcium current could not be detected due to a calcium chelator in the pipette solution. Additionally, fast sodium current were not detect in these cells.

In summary, it is unlikely that a known side effect of ZD7288 on calcium or sodium channels inhibited the proliferation of the primary cortical stem cells used in this study. This suggests that the decrease in proliferation is indeed mediated by the pharmacological blockade of the HCN channels. These results are supported by the *in vivo* data, using a genetic strategy to functionally inactivate I_h. However, it cannot be excluded that the temporal alterations seen in the differentiation of the primary cortical stem cells by the inhibitor ZD7288 resulted exclusively from the inhibition of I_h. It is possible that an undetected inhibition of sodium currents contributed to the observed effect. Calcium currents do not seem to be affected by ZD7288, due to the expression of L-type channels, but as an off-target effect of ZD7288 on T-type calcium channels. However, the genetic ablation of the I_h in the EMX-HCN-DN mouse showed a temporal alteration of differentiation as well, supporting the role of the ZD7288 inhibition of the HCN channels as a specific mechanism of its effect on differentiation.

5.9 Conclusions

This work presents a so far unknown importance of the HCN channels and the conducted I_h for the proliferation and differentiation of neural stem and progenitor cells.

A HCN subtype switch was detected with HCN3 and HCN4 being highly expressed during embryonic development in different cell types, and HCN1 and HCN2 being the main subtypes in the adult forebrain. The early expression of HCN3 was detected in different neural progenitor cells while HCN4 was mainly expressed in early embryonic neurons.

In a transgenic mouse line, the forebrain-restricted genetic ablation of $I_{h,}$ resulted in a microcephaly phenotype that was caused by impaired proliferation of neural progenitor cells. This result was verified by pharmacological I_h ablation in rat primary cortical stem cells. As the depolarized resting membrane potential and the membrane potential oscillations during the cell cycle are essential for the cell cycle progression, the proliferation rate of cortical stem cells could be decreased due to a hyperpolarization of the resting membrane potential in I_h-inhibited cells.

In the *in vivo* as well as the *in vitro* experiments, a temporally altered pattern of differentiation was detected, with the early expression of glial markers upon I_h inhibition. One might hypothesize that this is caused by the lengthening of the cell cycle, supporting the differentiation of neural progenitor cells in combination with an impaired L-type calcium channel signaling in the differentiating cells due to the hyperpolarization of the membrane potential.

The electrophysiological investigation of the primary cortical stem cells detected two different potassium outward currents, the I_{DR} and I_A, whereas no I_h was measurable. This could be explained by a small current amplitude of I_h or its component the I_{ins} and/or a transient presence of the HCN channel in the plasma membrane. Furthermore, the HCN channel can be localized to the nuclear membrane regulating transcription of genes, for example, by ion composition of the nucleoplasm.

Furthermore, the HCN3 expression in human and murine cortical progenitor cells suggests a conserved function across species. Moreover, the results obtained in rat primary cortical stem cells showing the decrease of proliferation upon I_h inhibition, suggest an evolutionarily conserved function of the HCN channels and their corresponding I_h.

In summary, this work suggests a novel role of HCN channels in the early developmental processes of the cortical structures through its function as ion channel.

5.10 Outlook

To support the results of this study concerning the effect of the I_h ablation on proliferation, the *in vivo* analysis of the proliferation should be conducted at embryonic stages. This could be achieved by analyzing the EMX-HCN-DN transgenic embryos at E13 or by *in utero* electroporation of a HCN-DN subunit at E13, and analyzing the pups at E16. This would target the time points of the peak proliferation in the murine cortex, and could add valuable data to the study.

Furthermore, it is still not clear, how I_h influences the proliferation of neural stem cells. Analyses of a whole cell population of neural stem cells instead of individual cells to investigate different cell cycle stages, as well as a larger number of cells in a shorter period, would help explain the effects of I_h inhibition in neural stem cells. This could be achieved by the application of a voltage-sensitive dye and simultaneous imaging of a population of cells. Furthermore, the membrane potential oscillations during the cell cycle progression of neural stem cells could be investigated via this method, which would provide important evidence to the so far unknown mechanism of cell cycle regulation and membrane potential in those cells.

Another way to address the problem of the cell cycle status of the analyzed cells is to visualize the cell cycle state by the fluorescence ubiquitination cell cycle indicator (FUCCI) vector (Sakaue-Sawano et al., 2008). This construct uses the oscillating expression and fast degradation of cell cycle proteins. A truncated version of the Cdt1 protein coupled to a red fluorophore is expressed during the G1 phase and accumulates in G0, while truncated geminin, which is expressed during S, G2 and M phases, is marked with a green fluorophore (Sakaue-Sawano et al., 2008). This construct enables the appreciation of the cell cycle phase of living cells and would be useful to sort the cells prior to the electrophysiological investigation to analyze only cells of one specific cell cycle phase. Primary cortical stem cells transfected with the FUCCI construct should show a higher probability to conduct I_h during the S and/or G2 phase, while the green fluorophore coupled geminin construct is expressed.

To address another hypothesis of the mechanism of the contribution of I_h to the proliferation of neural stem and progenitor cells, the potential localization of the HCN protein in the nuclear membrane should be investigated. This could be analyzed by western blot analysis of the nuclear membrane fraction of the cells, or the immunohistochemical investigation of the exact localization of the HCN channels by

co-staining with nuclear membrane markers. Furthermore, electrophysiological measurements of the nuclear membrane could be conducted.

These further investigations could bring additional insights into the role of I_h in the proliferation of neural stem and progenitor cells.

6 Supplement

6.1 ROIs of Stereology

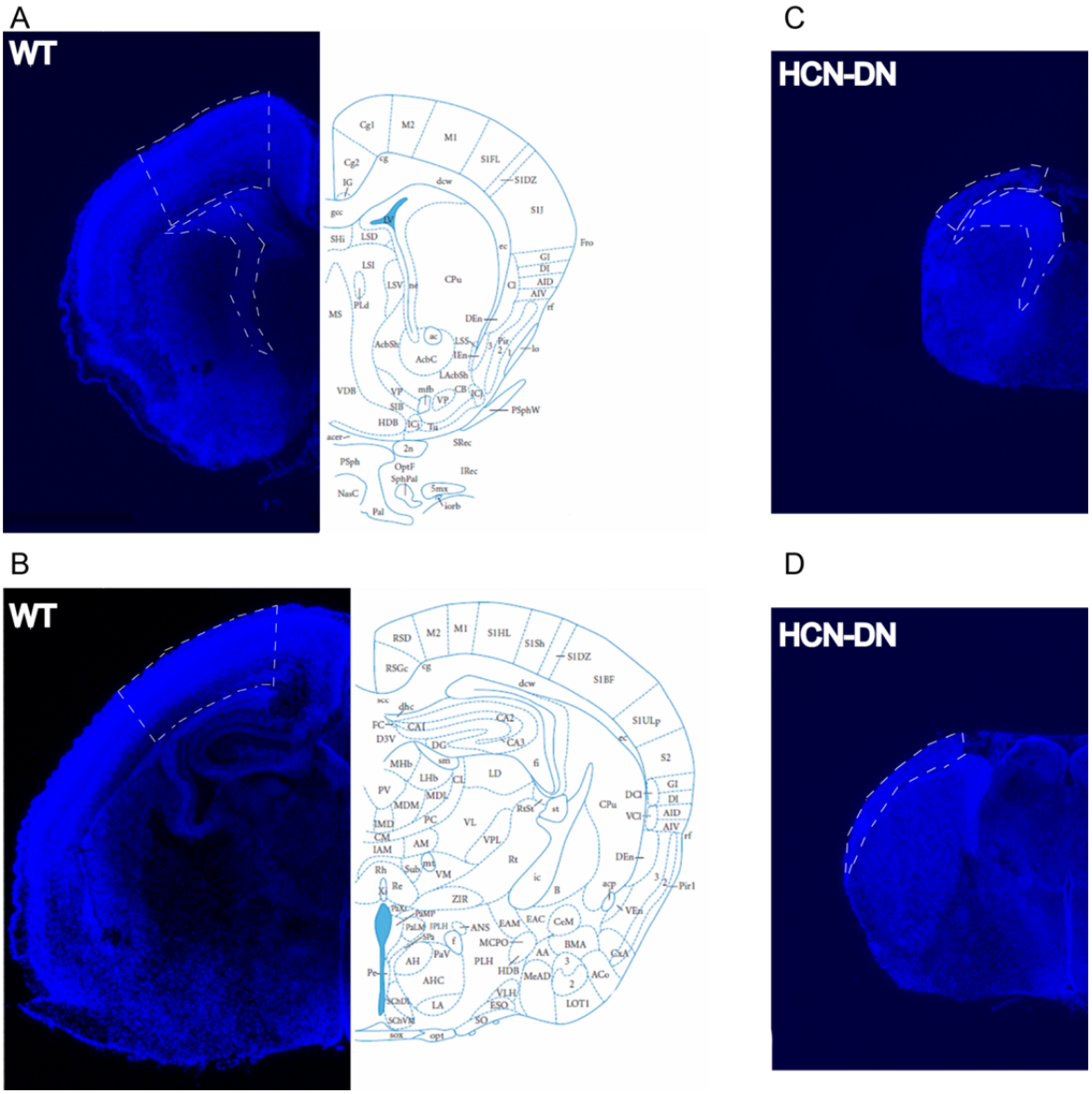

Figure 6-1 Region of Interest (ROI) for stereological investigation of sensorimotor cortex and ventricular and subventricular zone (VZ/SVZ).

A, Wild-type (WT) mouse ROI of the sensorimotor cortex and VZ/SVZ with DAPI staining and corresponding brain map at 2.31 mm from bulbus olfactorius. **B,** Wild-type (WT) mouse ROI for sensorimotor cortex with DAPI staining and corresponding brain map at 3.75 mm from bulbus olfactorius For analysis cortical data from **A** and **B** were pooled. **C**, and **D,** EMX-HCN-DN mouse with ROIs from the investigated areas. Brain maps from (Paxinos et al., 2007).

6.2 Vector charts for IUE

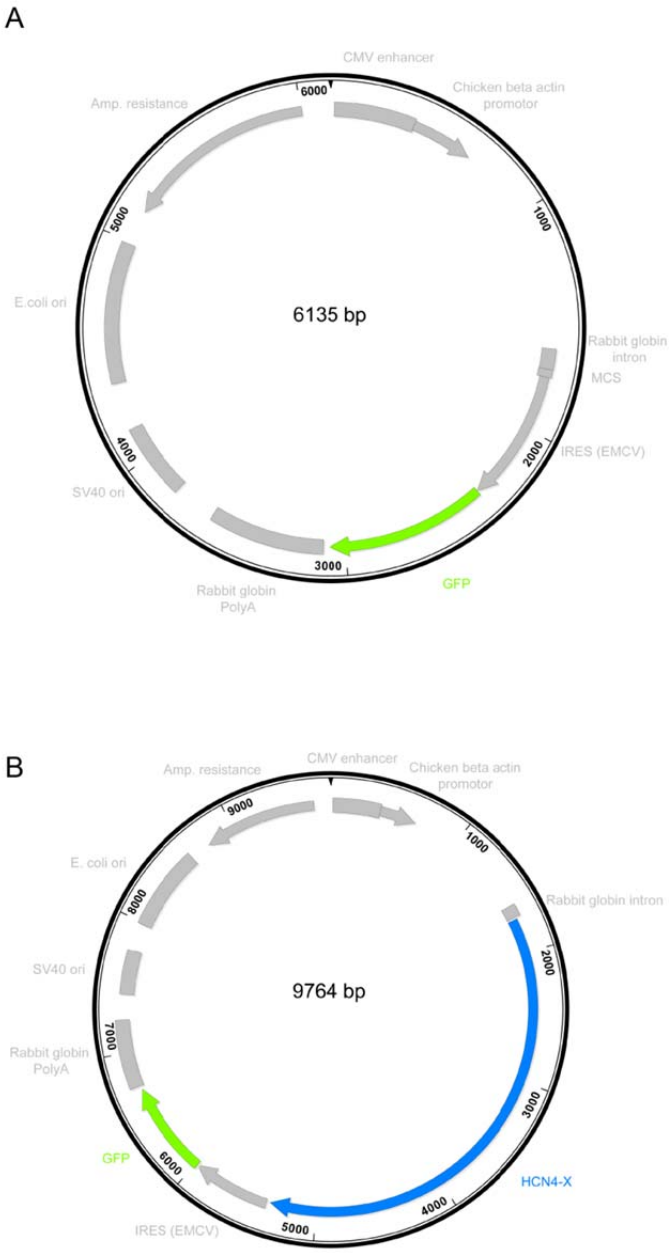

Figure 6-2 Vector charts of the IUE constructs.

A, Addgene vector with ubiquitinous expressed CAG promotor (CMV enhancer combined with chicken beta actin promotor), GFP expression is driven by an internal ribosomal entry site (IRES) from the encephalomyocarditis virus (EMCV). **B,** In the vector backbone shown in **A** human HCN-WT or HCN-DN (HCN-X) was cloned in the multiple cloning site.

7 References

Alig J, Marger L, Mesirca P, Ehmke H, Mangoni ME, Isbrandt D (2009) Control of heart rate by cAMP sensitivity of HCN channels. Proc Natl Acad Sci 106:12189–12194.

Anderson S a, Marín O, Horn C, Jennings K, Rubenstein JL (2001) Distinct cortical migrations from the medial and lateral ganglionic eminences. Development 128:353–363.

Anderson S, Mione M, Yun K, Rubenstein JL (1999) Differential origins of neocortical projection and local circuit neurons: role of Dlx genes in neocortical interneuronogenesis. Cereb Cortex 9:646–654.

Ang ESBC, Haydar TF, Gluncic V, Rakic P (2003) Four-dimensional migratory coordinates of GABAergic interneurons in the developing mouse cortex. J Neurosci 23:5805–5815.

Antonopoulos J, Pappas IS, Parnavelas JG (1997) Activation of the GABA A Receptor Inhibits the Proliferative Effects of bFGF in Cortical Progenitor Cells. Eur J Neurosci 9:291–298.

Aponte Y, Lien C-C, Reisinger E, Jonas P (2006) Hyperpolarization-activated cation channels in fast-spiking interneurons of rat hippocampus. J Physiol 574:229–243.

Aprea J, Calegari F (2012) Bioelectric State and Cell Cycle Control of Mammalian Neural Stem Cells. Stem Cells Int 2012:1–10.

Arinsburg SS, Cohen IS, Yu H-G (2006) Constitutively Active Src Tyrosine Kinase Changes Gating of HCN4 Channels Through Direct Binding to the Channel Proteins. J Cardiovasc Pharmacol 48:1–6.

Bando Y, Hirano T, Tagawa Y (2014) Dysfunction of KCNK Potassium Channels Impairs Neuronal Migration in the Developing Mouse Cerebral Cortex. Cereb Cortex 24:1017–1029.

Barbuti A, Gravante B, Riolfo M, Milanesi R, Terragni B, DiFrancesco D (2004) Localization of pacemaker channels in lipid rafts regulates channel kinetics. Circ Res 94:1325–1331.

Barbuti A, Terragni B, Brioschi C, DiFrancesco D (2007) Localization of f-channels to caveolae mediates specific β2-adrenergic receptor modulation of rate in sinoatrial myocytes. J Mol Cell Cardiol 42:71–78.

Battefeld A, Rocha N, Stadler K, Bräuer AU, Strauss U (2012) Distinct perinatal features of the hyperpolarization-activated non-selective cation current Ih in the rat cortical plate. Neural Dev 7:21.

Behar TN, Li YX, Tran HT, Ma W, Dunlap V, Scott C, Barker JL (1996) GABA stimulates

chemotaxis and chemokinesis of embryonic cortical neurons via calcium-dependent mechanisms. J Neurosci 16:1808–1818.

Behar TN, Schaffner a E, Scott C a, O'Connell C, Barker JL (1998) Differential response of cortical plate and ventricular zone cells to GABA as a migration stimulus. J Neurosci 18:6378–6387.

Behar TN, Schaffner AE, Scott CA, Greene CL, Barker JL (2000) GABA receptor antagonists modulate postmitotic cell migration in slice cultures of embryonic rat cortex. Cereb Cortex 10:899–909.

Behar TN, Scott CA, Greene CL, Wen X, Smith S V., Maric D, Liu Q-YY, Colton CA, Barker JL (1999) Glutamate Acting at NMDA Receptors Stimulates Embryonic Cortical Neuronal Migration. J Neurosci 19:4449–4461.

Ben-Ari Y (2002) Excitatory actions of gaba during development: the nature of the nurture. Nat Rev Neurosci 3:728–739.

Ben-Ari Y (2006) Basic developmental rules and their implications for epilepsy in the immature brain. Epileptic Disord 8:91–102.

Bender RA, Baram TZ (2008) Hyperpolarization activated cyclic-nucleotide gated (HCN) channels in developing neuronal networks. Prog Neurobiol 86:129–140.

Bender RA, Galindo R, Mameli M, Gonzalez-vega R, Valenzuela F, Baram TZ (2005) Synchronized network activity in developing rat hippocampus involves regional hyperpolarization-activated cyclic nucleotide- gated (HCN) channel function. Eur J Neurosci 22:2669–2674.

Bender RA, Soleymani S V, Brewster AL, Nguyen ST, Beck H, Mathern GW, Baram TZ (2003) Enhanced expression of a specific hyperpolarization-activated cyclic nucleotide-gated cation channel (HCN) in surviving dentate gyrus granule cells of human and experimental epileptic hippocampus. J Neurosci 23:6826–6836.

Berridge MJ (1995) Calcium signalling and cell proliferation. BioEssays 17:491–500.

Biel M, Wahl-Schott C, Michalakis S, Zong X (2009) Hyperpolarization-Activated Cation Channels: From Genes to Function. Physiol Rev 89:847–885.

Binggeli R, Weinstein RC (1986) Membrane potentials and sodium channels: Hypotheses for growth regulation and cancer formation based on changes in sodium channels and gap junctions. J Theor Biol 123:377–401.

Bittman K, Owens DF, Kriegstein a R, LoTurco JJ (1997) Cell coupling and uncoupling in the ventricular zone of developing neocortex. J Neurosci 17:7037–7044.

Blackiston DJ, McLaughlin KA, Levin M (2009) Bioelectric controls of cell proliferation: Ion channels, membrane voltage and the cell cycle. Cell Cycle 29:3519–3528.

Boonstra J, Mummery CL, Tertoolen LGJ, Van Der Saag PT, De Laat SW (1981) Cation

transport and growth regulation in neuroblastoma cells. Modulations of K+ transport and electrical membrane properties during the cell cycle. J Cell Physiol 107:75–83.

Bordey A, Sontheimer H (1997) Postnatal development of ionic currents in rat hippocampal astrocytes in situ. J Neurophysiol 78:461–477.

Borodinsky LN, Root CM, Cronin JA, Sann SB, Gu X, Spitzer NC (2004) Activity-dependent homeostatic specification of transmitter expression in embryonic neurons. Nature 429:523–530.

Bortone D, Polleux F (2009) KCC2 Expression Promotes the Termination of Cortical Interneuron Migration in a Voltage-Sensitive Calcium-Dependent Manner. Neuron 62:53–71.

Boyes J, Bolam JP, Shigemoto R, Stanford IM (2007) Functional presynaptic HCN channels in the rat globus pallidus. Eur J Neurosci 25:2081–2092.

Brandt MC, Endres-Becker J, Zagidullin N, Motloch LJ, Er F, Rottlaender D, Michels G, Herzig S, Hoppe UC (2009) Effects of KCNE2 on HCN isoforms: distinct modulation of membrane expression and single channel properties. AJP Hear Circ Physiol 297:H355–H363.

Brewster AL, Chen Y, Bender R a, Yeh A, Shigemoto R, Baram TZ (2006) Quantitative Analysis and Subcellular Distribution of mRNA and Protein Expression of the Hyperpolarization-Activated Cyclic Nucleotide-Gated Channels throughout Development in Rat Hippocampus. Cereb Cortex 17:702–712.

Brosenitsch TA, Katz DM (2002) Expression of Phox2 transcription factors and induction of the dopaminergic phenotype in primary sensory neurons. Mol Cell Neurosci 20:447–457.

Brown H, Difrancesco D (1980) Voltage-clamp investigations of membrane currents underlying pace-maker activity in rabbit sino-atrial node. J Physiol 308:331–351.

Cai J, Cheng A, Luo Y, Lu C, Mattson MP, Rao MS, Furukawa K (2003) Membrane properties of rat embryonic multipotent neural stem cells. J Neurochem 88:212–226.

Calderon de Anda F, Madabhushi R, Rei D, Meng J, Gräff J, Durak O, Meletis K, Richter M, Schwanke B, Mungenast A, Tsai L-H (2016) Cortical neurons gradually attain a post-mitotic state. Cell Res 26:1033–1047.

Calegari F, Haubensak W, Haffner C, Huttner WB (2005) Selective lengthening of the cell cycle in the neurogenic subpopulation of neural progenitor cells during mouse brain development. J Neurosci 25:6533–6538.

Calegari F, Huttner WB (2003) An inhibition of cyclin-dependent kinases that lengthens, but does not arrest, neuroepithelial cell cycle induces premature neurogenesis. J Cell Sci 116:4947–4955.

Cao-Ehlker X, Zong X, Hammelmann V, Gruner C, Fenske S, Michalakis S, Wahl-Schott C, Biel M (2013) Up-regulation of Hyperpolarization-activated Cyclic Nucleotide-gated Channel 3 (HCN3) by Specific Interaction with K+ Channel Tetramerization Domain-containing Protein 3 (KCTD3). J Biol Chem 288:7580–7589.

Capiod T (2011) Cell proliferation, calcium influx and calcium channels. Biochimie 93:2075–2079.

Chan CS, Glajch KE, Gertler TS, Guzman JN, Mercer JN, Lewis AS, Goldberg AB, Tkatch T, Shigemoto R, Fleming SM, Chetkovich DM, Osten P, Kita H, Surmeier DJ (2011) HCN channelopathy in external globus pallidus neurons in models of Parkinson's disease. Nat Neurosci 14:85–92.

Chan FK-M, Moriwaki K, De Rosa MJ (2013) Detection of Necrosis by Release of Lactate Dehydrogenase Activity. In: Methods in molecular biology (Clifton, N.J.), pp 65–70.

Chandler KJ, Chandler RL, Broeckelmann EM, Hou Y, Southard-Smith EM, Mortlock DP (2007) Relevance of BAC transgene copy number in mice: transgene copy number variation across multiple transgenic lines and correlations with transgene integrity and expression. Mamm Genome 18:693–708.

Chattopadhyay N, Espinosa-Jeffrey A, Tfelt-Hansen J, Yano S, Bandyopadhyay S, Brown EM, de Vellis J (2008) Calcium receptor expression and function in oligodendrocyte commitment and lineage progression: Potential impact on reduced myelin basic protein in CaR-null mice. J Neurosci Res 86:2159–2167.

Checchetto V, Teardo E, Carraretto L, Leanza L, Szabo I (2016) Physiology of intracellular potassium channels: A unifying role as mediators of counterion fluxes? Biochim Biophys Acta - Bioenerg 1857:1258–1266.

Chen J, Kriegstein AR (2015) A GABAergic projection from the zona incerta to cortex promotes cortical neuron development. Science (80-) 350:554–558.

Chen S, Wang J, Siegelbaum S a (2001) Properties of Hyperpolarization-Activated Pacemaker Current Defined by Coassembly of Hcn1 and Hcn2 Subunits and Basal Modulation by Cyclic Nucleotide. J Gen Physiol 117:491–504.

Chen X, Hartman A, Guo S (2015) Choosing Cell Fate Through a Dynamic Cell Cycle. Curr Stem Cell Reports 1:129–138.

Chen Y, Sánchez A, Rubio ME, Kohl T, Pardo LA, Stühmer W (2011) Functional KV10.1 Channels Localize to the Inner Nuclear Membrane Meuth SG, ed. PLoS One 6:e19257.

Cheng Z, Teo G, Krueger S, Rock TM, Koh HW, Choi H, Vogel C (2016) Differential dynamics of the mammalian mRNA and protein expression response to misfolding stress. Mol Syst Biol 12:855–855.

Chevaleyre V, Castillo PE (2002) Assessing the role of Ih channels in synaptic

transmission and mossy fiber LTP. Proc Natl Acad Sci 99:9538–9543.

Choi BH, Lapham LW (1978) Radial glia in the human fetal cerebrum: A combined golgi, immunofluorescent and electron microscopic study. Brain Res 148:295–311.

Chow SS, Van Petegem F, Accili EA (2012) Energetics of cyclic AMP binding to HCN channel C terminus reveal negative cooperativity. J Biol Chem 287:600–606.

Chung WK, Shin M, Jaramillo TC, Leibel RL, LeDuc CA, Fischer SG, Tzilianos E, Gheith AA, Lewis AS, Chetkovich DM (2009) Absence epilepsy in apathetic, a spontaneous mutant mouse lacking the h channel subunit, HCN2. Neurobiol Dis 33:499–508.

Chvatal A, Berger T, Vorisek I, Orkand RK, Kettenmann H, Sykova E (1997) Changes in glial K+ currents with decreased extracellular volume in developing rat white matter. J Neurosci Res 49:98–106.

Ciccolini F, Collins TJ, Sudhoelter J, Lipp P, Berridge MJ, Bootman MD (2003) Local and global spontaneous calcium events regulate neurite outgrowth and onset of GABAergic phenotype during neural precursor differentiation. J Neurosci 23:103–111.

Cone C, Cone C (1976) Induction of mitosis in mature neurons in central nervous system by sustained depolarization. Science (80-) 192:155–158.

Cone CD, Tongier M (1973) Contact inhibition of division: Involvement of the electrical transmembrane potential. J Cell Physiol 82:373–386.

D'Ascenzo M, Piacentini R, Casalbore P, Budoni M, Pallini R, Azzena GB, Grassi C (2006) Role of L-type Ca 2+ channels in neural stem/progenitor cell differentiation. Eur J Neurosci 23:935–944.

Darzynkiewicz Z, Bruno S, Del Bino G, Gorczyca W, Hotz MA, Lassota P, Traganos F (1992) Features of apoptotic cells measured by flow cytometry. Cytometry 13:795–808.

De Juan Romero C, Borrell V (2015) Coevolution of radial glial cells and the cerebral cortex. Glia 63:1303–1319.

DeAzevedo LC, Fallet C, Moura-Neto V, Daumas-Duport C, Hedin-Pereira C, Lent R (2003) Cortical radial glial cells in human fetuses: Depth-correlated transformation into astrocytes. J Neurobiol 55:288–298.

DeBerg HA, Bankston JR, Rosenbaum JC, Brzovic PS, Zagotta WN, Stoll S (2015) Structural Mechanism for the Regulation of HCN Ion Channels by the Accessory Protein TRIP8b. Structure 23:734–744.

Demarque M, Represa A, Becq H élène, Khalilov I, Ben-Ari Y, Aniksztejn L (2002) Paracrine Intercellular Communication by a Ca2+- and SNARE-Independent

Release of GABA and Glutamate Prior to Synapse Formation. Neuron 36:1051–1061.

Desai AR, McConnell SK (2000) Progressive restriction in fate potential by neural progenitors during cerebral cortical development. Development 127:2863–2872.

Dhillon AS, Hagan S, Rath O, Kolch W (2007) MAP kinase signalling pathways in cancer. Oncogene 26:3279–3290.

Dibbens LM, Reid CA, Hodgson B, Thomas EA, Phillips AM, Gazina E, Cromer BA, Clarke AL, Baram TZ, Scheffer IE, Berkovic SF, Petrou S (2010) Augmented currents of an HCN2 variant in patients with febrile seizure syndromes. Ann Neurol 67:542–546.

Doetsch F (2003) The glial identity of neural stem cells. Nat Neurosci 6:1127–1134.

Doetsch F, Caillé I, Lim DA, García-Verdugo JM, Alvarez-Buylla A (1999) Subventricular Zone Astrocytes Are Neural Stem Cells in the Adult Mammalian Brain. Cell 97:703–716.

Dyhrfjeld-Johnsen J, Morgan RJ, Soltesz I (2009) Double Trouble? Potential for Hyperexcitability Following Both Channelopathic up- and Downregulation of I(h) in Epilepsy. Front Neurosci 3:25–33.

Emery EC, Young GT, Berrocoso EM, Chen L, McNaughton PA (2011) HCN2 Ion Channels Play a Central Role in Inflammatory and Neuropathic Pain. Science (80-) 333:1462–1467.

Er F, Larbig R, Ludwig A, Biel M, Hofmann F, Beuckelmann DJ, Hoppe UC (2003) Dominant-negative suppression of HCN channels markedly reduces the native pacemaker current I(f) and undermines spontaneous beating of neonatal cardiomyocytes. Circulation 107:485–489.

Eszterhas SK, Bouhassira EE, Martin DIK, Fiering S (2002) Transcriptional interference by independently regulated genes occurs in any relative arrangement of the genes and is influenced by chromosomal integration position. Mol Cell Biol 22:469–479.

Feldman JD, Vician L, Crispino M, Tocco G, Marcheselli VL, Bazan NG, Baudry M, Herschman HR (1998) KID-1, a Protein Kinase Induced by Depolarization in Brain. J Biol Chem 273:16535–16543.

Felix R, Sandoval A, Sánchez D, Gómora JC, Vega-Beltrán JLD la, Treviño CL, Darszon A (2003) ZD7288 inhibits low-threshold Ca2+ channel activity and regulates sperm function. Biochem Biophys Res Commun 311:187–192.

Fenske S, Krause SC, Hassan SIH, Becirovic E, Auer F, Bernard R, Kupatt C, Lange P, Ziegler T, Wotjak CT, Zhang H, Hammelmann V, Paparizos C, Biel M, Wahl-Schott CA (2013) Sick sinus syndrome in HCN1-Deficient mice. Circulation 128:2585–2594.

Fenske S, Mader R, Scharr A, Paparizos C, Cao-Ehlker X, Michalakis S, Shaltiel L, Weidinger M, Stieber J, Feil S, Feil R, Hofmann F, Wahl-Schott C, Biel M (2011) HCN3 Contributes to the Ventricular Action Potential Waveform in the Murine Heart. Circ Res 109:1015–1023.

Ferry S, Traiffort E, Stinnakre J, Ruat M (2000) Developmental and adult expression of rat calcium-sensing receptor transcripts in neurons and oligodendrocytes. Eur J Neurosci 12:872–884.

Fishell G, Rudy B (2011) Mechanisms of Inhibition within the Telencephalon: "Where the Wild Things Are." Annu Rev Neurosci 34:535–567.

Florio M et al. (2015) Human-specific gene ARHGAP11B promotes basal progenitor amplification and neocortex expansion. Science (80-) 347:1465–1470.

Frace AM, Maruoka F, Noma A (1992) Current By External Anions in Rabbit Sino-Atrial Node. J Physiol 453,:307–318.

Francis F, Meyer G, Fallet-Bianco C, Moreno S, Kappeler C, Socorro AC, Tuy FPD, Beldjord C, Chelly J (2006) Human disorders of cortical development: from past to present. Eur J Neurosci 23:877–893.

Franklin KBJ, Paxinos G (2007) The Mouse Brain in Stereotaxic Coordinates, Third Edit.

Gao P, Postiglione MP, Krieger TG, Hernandez L, Wang C, Han Z, Streicher C, Papusheva E, Insolera R, Chugh K, Kodish O, Huang K, Simons BD, Luo L, Hippenmeyer S, Shi S-H (2014) Deterministic Progenitor Behavior and Unitary Production of Neurons in the Neocortex. Cell 159:775–788.

Gauss R, Seifert R, Kaupp UB (1998) Molecular identification of a hyperpolarization-activated channel in sea urchin sperm. Nature 393:583–587.

Ge W-P, Miyawaki A, Gage FH, Jan YN, Jan LY (2012) Local generation of glia is a major astrocyte source in postnatal cortex. Nature 484:376–380.

Gerber AM, Beaman-Hall CM, Mathur A, Vallano M Lou (2010) Reduced blockade by extracellular Mg2+ is permissive to NMDA receptor activation in cerebellar granule neurons that model a migratory phenotype. J Neurochem 114:191–202.

Gerdes J, Li L, Schlueter C, Duchrow M, Wohlenberg C, Gerlach C, Stahmer I, Kloth S, Brandt E, Flad HD (1991) Immunobiochemical and molecular biologic characterization of the cell proliferation-associated nuclear antigen that is defined by monoclonal antibody Ki-67. Am J Pathol 138:867–873.

Ghiani C a, Yuan X, Eisen a M, Knutson PL, DePinho R a, McBain CJ, Gallo V (1999) Voltage-activated K+ channels and membrane depolarization regulate accumulation of the cyclin-dependent kinase inhibitors p27(Kip1) and p21(CIP1) in glial progenitor cells. J Neurosci 19:5380–5392.

Ghosh A, Antonini A, McConnell SK, Shatz CJ (1990) Requirement for subplate neurons in the formation of thalamocortical connections. Nature 347:179–181.

Gil V, Nocentini S, del RÃ-o JA (2014) Historical first descriptions of Cajalâ€“Retzius cells: from pioneer studies to current knowledge. Front Neuroanat 8:32.

Goebbels S, Bormuth I, Bode U, Hermanson O, Schwab MH, Nave K-A (2006) Genetic targeting of principal neurons in neocortex and hippocampus of NEX-Cre mice. genesis 44:611–621.

Gonzalez-Iglesias AE, Kretschmannova K, Tomic M, Stojilkovic SS (2006) ZD7288 inhibits exocytosis in an HCN-independent manner and downstream of voltage-gated calcium influx in pituitary lactotrophs. Biochem Biophys Res Commun 346:845–850.

Gorski J a, Talley T, Qiu M, Puelles L, Rubenstein JLR, Jones KR (2002) Cortical excitatory neurons and glia, but not GABAergic neurons, are produced in the Emx1-expressing lineage. J Neurosci 22:6309–6314.

Gravante B, Barbuti A, Milanesi R, Zappi I, Viscomi C, DiFrancesco D (2004) Interaction of the pacemaker channel HCN1 with filamin A. J Biol Chem 279:43847–43853.

Gray LS, Schiff D, Macdonald TL (2013) A model for the regulation of T-type Ca 2+ channels in proliferation: roles in stem cells and cancer. Expert Rev Anticancer Ther 13:589–595.

Gu X, Spitzer NC (1995) Distinct aspects of neuronal differentiation encoded by frequency of spontaneous Ca2+ transients. Nature 375:784–787.

Habela CW, Olsen ML, Sontheimer H (2008) ClC3 Is a Critical Regulator of the Cell Cycle in Normal and Malignant Glial Cells. J Neurosci 28:9205–9217.

Hallows JL, Tempel BL (1998) Expression of Kv1.1, a Shaker-like potassium channel, is temporally regulated in embryonic neurons and glia. J Neurosci 18:5682–5691.

Hanson MG, Landmesser LT (2004) Normal patterns of spontaneous activity are required for correct motor axon guidance and the expression of specific guidance molecules. Neuron 43:687–701.

Harris NC, Constanti A (1995) Mechanism of block by ZD 7288 of the hyperpolarization-activated inward rectifying current in guinea pig substantia nigra neurons in vitro. J Neurophysiol 74:2366–2378.

Harzheim D, Pfeiffer KH, Fabritz L, Kremmer E, Buch T, Waisman A, Kirchhof P, Kaupp UB, Seifert R (2008) Cardiac pacemaker function of HCN4 channels in mice is confined to embryonic development and requires cyclic AMP. EMBO J 27:692–703.

Haubensak W, Attardo A, Denk W, Huttner WB (2004) Neurons arise in the basal neuroepithelium of the early mammalian telencephalon: a major site of neurogenesis. Pnas 101:3196–3201.

Haydar TF, Wang F, Schwartz ML, Rakic P (2000) Differential Modulation of Proliferation in the Neocortical Ventricular and Subventricular Zones. J Neurosci 125:2621–2629.

Heck N, Kilb W, Reiprich P, Kubota H, Furukawa T, Fukuda A, Luhmann HJ (2007) GABA-A receptors regulate neocortical neuronal migration in vitro and in vivo. Cereb Cortex 17:138–148.

Hegle AP, Marble DD, Wilson GF (2006) A voltage-driven switch for ion-independent signaling by ether-a-go-go K+ channels. Proc Natl Acad Sci 103:2886–2891.

Herrmann S, Schnorr S, Ludwig A (2015) HCN Channels—Modulators of Cardiac and Neuronal Excitability. Int J Mol Sci 16:1429–1447.

Herrmann S, Stieber J, Stöckl G, Hofmann F, Ludwig A (2007) HCN4 provides a "depolarization reserve" and is not required for heart rate acceleration in mice. EMBO J 26:4423–4432.

Herschman HR, Ferguson GD, Feldman JD, Farias-Eisner R, Vician L (2000) Searching for depolarization-induced genes that modulate synaptic plasticity and neurotrophin-induced genes that mediate neuronal differentiation. Neurochem Res 25:591–602.

Heuermann RJ, Jaramillo TC, Ying S-W, Suter B a., Lyman K a., Han Y, Lewis AS, Hampton TG, Shepherd GMG, Goldstein P a., Chetkovich DM (2016) Reduction of thalamic and cortical Ih by deletion of TRIP8b produces a mouse model of human absence epilepsy. Neurobiol Dis 85:81–92.

Hicks MR, Damianoglou A, Rodger A, Dafforn TR (2008) Folding and Membrane Insertion of the Pore-Forming Peptide Gramicidin Occur as a Concerted Process. J Mol Biol 383:358–366.

Higashimori H, Sontheimer H (2007) Role of Kir4.1 channels in growth control of glia. Glia 55:1668–1679.

Hirai K, Yoshioka H, Kihara M, Hasegawa K, Sakamoto T, Sawada T, Fushiki S (1999) Inhibiting neuronal migration by blocking NMDA receptors in the embryonic rat cerebral cortex: A tissue culture study. Dev Brain Res 114:63–67.

Hoerder-Suabedissen A, Molnár Z (2015) Development, evolution and pathology of neocortical subplate neurons. Nat Rev Neurosci 16:133–146.

Hoffmann EK, Lambert IH, Pedersen SF (2009) Physiology of Cell Volume Regulation in Vertebrates. Physiol Rev 89:193–277.

Honarnejad K, Herms J (2012) Presenilins: Role in calcium homeostasis. Int J Biochem

Cell Biol 44:1983–1986.

Hu L, Santoro B, Saponaro A, Liu H, Moroni A, Siegelbaum S (2013) Binding of the auxiliary subunit TRIP8b to HCN channels shifts the mode of action of cAMP. J Gen Physiol 142:599–612.

Huang Z, Lujan R, Kadurin I, Uebele VN, Renger JJ, Dolphin AC, Shah MM (2011) Presynaptic HCN1 channels regulate Cav3.2 activity and neurotransmission at select cortical synapses. Nat Neurosci 14:478–486.

Huang Z, Walker MC, Shah MM (2009) Loss of Dendritic HCN1 Subunits Enhances Cortical Excitability and Epileptogenesis. J Neurosci 29:10979–10988.

Inoue K, Furukawa T, Kumada T, Yamada J, Wang T, Inoue R, Fukuda A (2012) Taurine inhibits K +-Cl - cotransporter KCC2 to regulate embryonic Cl - homeostasis via with-no-lysine (WNK) protein kinase signaling pathway. J Biol Chem 287:20839–20850.

Iwasato T, Datwani a, Wolf a M, Nishiyama H, Taguchi Y, Tonegawa S, Knöpfel T, Erzurumlu RS, Itohara S (2000) Cortex-restricted disruption of NMDAR1 impairs neuronal patterns in the barrel cortex. Nature 406:726–731.

Jang SH, Byun JK, Jeon W, Choi SY, Park J, Lee BH, Yang JE, Park JB, O'Grady SM, Kim D, Ryu PD, Joo S, Lee SY (2015) Nuclear Localization and Functional Characteristics of Voltage-gated Potassium Channel Kv1.3. J Biol Chem 290:12547–12557.

Jovic D, Sakaue-Sawano A, Abe T, Cho C-S, Nagaoka M, Miyawaki A, Akaike T (2013) Direct observation of cell cycle progression in living mouse embryonic stem cells on an extracellular matrix of E-cadherin. Springerplus 2:585.

Jung S, Jones TD, Lugo JN, Sheerin AH, Miller JW, D'Ambrosio R, Anderson AE, Poolos NP (2007) Progressive dendritic HCN channelopathy during epileptogenesis in the rat pilocarpine model of epilepsy. J Neurosci 27:13012–13021.

Jung S, Warner LN, Pitsch J, Becker AJ, Poolos NP (2011) Rapid Loss of Dendritic HCN Channel Expression in Hippocampal Pyramidal Neurons following Status Epilepticus. J Neurosci 31:14291–14295.

Kalil K, Li L, Hutchins BI (2011) Signaling Mechanisms in Cortical Axon Growth, Guidance, and Branching. Front Neuroanat 5:1–15.

Kanyshkova T, Meuth P, Bista P, Liu Z, Ehling P, Doengi M, Chetkovich DM, Pape H (2012) Differential regulation of HCN channel isoform expression in thalamic neurons of epileptic and non-epileptic rat strains. Neurobiol Dis 45:450–461.

Kanyshkova T, Pawlowski M, Meuth P, Dube C, Bender R a, Brewster AL, Baumann A, Baram TZ, Pape H-C, Budde T (2009) Postnatal Expression Pattern of HCN Channel Isoforms in Thalamic Neurons: Relationship to Maturation of Thalamocortical Oscillations. J Neurosci 29:8847–8857.

Katz LC, Shatz CJ (1996) Synaptic Activity and the Construction of Cortical circuits. Science 274:1133–1138.

Kaupp UB, Seifert R (2001) Molecular Diversity of Pacemaker Ion Channels. Annu Rev Physiol 63:235–257.

Kessaris N, Fogarty M, Iannarelli P, Grist M, Wegner M, Richardson WD (2006) Competing waves of oligodendrocytes in the forebrain and postnatal elimination of an embryonic lineage. Nat Neurosci 9:173–179.

Khazipov R, Luhmann HJ (2006) Early patterns of electrical activity in the developing cerebral cortex of humans and rodents. Trends Neurosci 29:414–418.

Kilb W, Luhmann HJ (2000) Characterization of a hyperpolarization-activated inward current in Cajal-Retzius cells in rat neonatal neocortex. J Neurophysiol 84:1681–1691.

Kimura K, Kitano J, Nakajima Y, Nakanishi S (2004) Hyperpolarization-activated, cyclic nucleotide-gated HCN2 cation channel forms a protein assembly with multiple neuronal scaffold proteins in distinct modes of protein-protein interaction. Genes to Cells 9:631–640.

Knop GC, Seeliger MW, Thiel F, Mataruga A, Kaupp UB, Friedburg C, Tanimoto N, Müller F (2008) Light responses in the mouse retina are prolonged upon targeted deletion of the HCN1 channel gene. Eur J Neurosci 28:2221–2230.

Komuro H, Rakic P (1996) Intracellular Ca2+ fluctuations modulate the rate of neuronal migration. Neuron 17:275–285.

Kressin K, Kuprijanova E, Jabs R, Seifert G, Steinhäuser C (1995) Developmental regulation of Na+ and K+ conductances in glial cells of mouse hippocampal brain slices. Glia 15:173–187.

Kriegstein A, Alvarez-Buylla A (2009) The glial nature of embryonic and adult neural stem cells. Annu Rev Neurosci 32:149–184.

Kriegstein AR, Goetz M (2003) Radial glia diversity: A matter of cell fate. Glia 43:37–43.

Kriegstein AR, Noctor SC (2004) Patterns of neuronal migration in the embryonic cortex. Trends Neurosci 27:392–399.

Kwan KY, Sestan N, Anton ES (2012) Transcriptional co-regulation of neuronal migration and laminar identity in the neocortex. Development 139:1535–1546.

Lang F, Föller M, Lang K, Lang P, Ritter M, Vereninov A, Szabo I, Huber SM, Gulbins E (2007) Cell Volume Regulatory Ion Channels in Cell Proliferation and Cell Death. In: Methods in Enzymology, pp 209–225.

Lau Y-T, Wong C-K, Luo J, Leung L-H, Tsang P-F, Bian Z-X, Tsang S-Y (2011) Effects of hyperpolarization-activated cyclic nucleotide-gated (HCN) channel blockers on

the proliferation and cell cycle progression of embryonic stem cells. Pflugers Arch 461:191–202.

Laursen M, Yatime L, Nissen P, Fedosova NU (2013) Crystal structure of the high-affinity Na+,K+-ATPase-ouabain complex with Mg2+ bound in the cation binding site. Proc Natl Acad Sci 110:10958–10963.

Lavdas AA, Grigoriou M, Pachnis V, Parnavelas JG (1999) The medial ganglionic eminence gives rise to a population of early neurons in the developing cerebral cortex. J Neurosci 19:7881–7888.

Leclerc C, Néant I, Moreau M (2012) The calcium: an early signal that initiates the formation of the nervous system during embryogenesis. Front Mol Neurosci 5:3.

Lepski G, Jannes CE, Nikkhah G, Bischofberger J (2013) cAMP promotes the differentiation of neural progenitor cells in vitro via modulation of voltage-gated calcium channels. Front Cell Neurosci 7:155.

Letinic K, Zoncu R, Rakic P (2002) Origin of GABAergic neurons in the human neocortex. Nature 417:645–649.

Levison SW, Goldman JE (1993) Both oligodendrocytes and astrocytes develop from progenitors in the subventricular zone of postnatal rat forebrain. Neuron 10:201–212.

Lewis AS, Chetkovich DM (2011) HCN channels in behavior and neurological disease: Too hyper or not active enough? Mol Cell Neurosci 46:357–367.

Lewis AS, Schwartz E, Chan CS, Noam Y, Shin M, Wadman WJ, Surmeier DJ, Baram TZ, Macdonald RL, Chetkovich DM (2009) Alternatively spliced isoforms of TRIP8b differentially control h channel trafficking and function. J Neurosci 29:6250–6265.

Lewis AS, Vaidya SP, Blaiss C a, Liu Z, Stoub TR, Brager DH, Chen X, Bender R a, Estep CM, Popov AB, Kang CE, Van Veldhoven PP, Bayliss D a, Nicholson D a, Powell CM, Johnston D, Chetkovich DM (2011) Deletion of the hyperpolarization-activated cyclic nucleotide-gated channel auxiliary subunit TRIP8b impairs hippocampal Ih localization and function and promotes antidepressant behavior in mice. J Neurosci 31:7424–7440.

Li C-H, Zhang Q, Teng B, Mustafa SJ, Huang J-Y, Yu H-G (2009) Src Tyrosine Kinase Alters Gating of Hyperpolarization-Activated HCN4 Pacemaker Channel through Tyr531. Am J Physiol 294:1–20.

Li T, Jiang L, Chen H, Zhang X (2008) Characterization of Excitability and Voltage-gated Ion Channels of Neural Progenitor Cells in Rat Hippocampus. J Mol Neurosci 35:289–295.

Liebau S, Pröpper C, Böckers T, Lehmann-Horn F, Storch A, Grissmer S, Wittekindt OH (2006) Selective blockage of K v 1.3 and K v 3.1 channels increases neural

progenitor cell proliferation. J Neurochem 99:426–437.

Lim CG, Kim S-S, Suh-Kim H, Lee Y-D, Ahn SC (2008) Characterization of Ionic Currents in Human Neural Stem Cells. Korean J Physiol Pharmacol 12:131.

Lin JjH-C, Takano T, Arcuino G, Wang X, Hu F, Darzynkiewicz Z, Nunes M, Goldman SA, Nedergaard M (2007) Purinergic signaling regulates neural progenitor cell expansion and neurogenesis. Dev Biol 27:380–392.

Lin YC, Huang J, Zhang Q, Hollander JM, Frisbee JC, Martin KH, Nestor C, Goodman R, Yu HG (2010) Inactivation of L-type calcium channel modulated by HCN2 channel. AJP Cell Physiol 298:C1029–C1037.

Liodis P, Denaxa M, Grigoriou M, Akufo-Addo C, Yanagawa Y, Pachnis V (2007) Lhx6 Activity Is Required for the Normal Migration and Specification of Cortical Interneuron Subtypes. J Neurosci 27:3078–3089.

Lörincz A, Notomi T, Tamás G, Shigemoto R, Nusser Z (2002) Polarized and compartment-dependent distribution of HCN1 in pyramidal cell dendrites. Nat Neurosci 5:1185–1193.

LoTurco JJ, Owens DF, Heath MJS, Davis MBE, Kriegstein AR (1995) GABA and glutamate depolarize cortical progenitor cells and inhibit DNA synthesis. Neuron 15:1287–1298.

Ludwig A, Budde T, Stieber J, Moosmang S, Wahl C, Holthoff K, Langebartels A, Wotjak C, Munsch T, Zong X, Feil S, Feil R, Lancel M, Chien KR, Konnerth A, Pape H-C, Biel M, Hofmann F (2003) Absence epilepsy and sinus dysrhythmia in mice lacking the pacemaker channel HCN2. EMBO J 22:216–224.

Ludwig A, Zong X, Jeglitsch M, Hofmann F, Biel M (1998) A family of hyperpolarization-activated mammalian cation channels. Nature 393:587–591.

Ludwig A, Zong X, Stieber J, Hullin R, Hofmann F, Biel M (1999) Two pacemaker channels from human heart with profoundly different activation kinetics. EMBO J 18:2323–2329.

Luján R, Albasanz JL, Shigemoto R, Juiz JM (2005) Preferential localization of the hyperpolarization-activated cyclic nucleotide-gated cation channel subunit HCN1 in basket cell terminals of the rat cerebellum. Eur J Neurosci 21:2073–2082.

Lukaszewicz A, Savatier P, Cortay V, Giroud P, Huissoud C, Berland M, Kennedy H, Dehay C (2005) G1 Phase Regulation, Area-Specific Cell Cycle Control, and Cytoarchitectonics in the Primate Cortex. Neuron 47:353–364.

Lukaszewicz A, Savatier P, Cortay V, Kennedy H, Dehay C (2002) Contrasting effects of basic fibroblast growth factor and neurotrophin 3 on cell cycle kinetics of mouse cortical stem cells. J Neurosci 22:6610–6622.

Lupica CR, Bell J a, Hoffman a F, Watson PL (2001) Contribution of the

hyperpolarization-activated current (I(h)) to membrane potential and GABA release in hippocampal interneurons. J Neurophysiol 86:261–268.

Ma Y, Hu H, Berrebi AS, Mathers PH, Agmon A (2006) Distinct Subtypes of Somatostatin-Containing Neocortical Interneurons Revealed in Transgenic Mice. J Neurosci 26:5069–5082.

MacFarlane SN, Sontheimer H (2000) Modulation of Kv1.5 currents by Src tyrosine phosphorylation: potential role in the differentiation of astrocytes. J Neurosci 20:5245–5253.

Macri V, Angoli D, Accili E a (2012) Architecture of the HCN selectivity filter and control of cation permeation. Sci Rep 2:894.

Macri V, Proenza C, Agranovich E, Angoli D, Accili EA (2002) Separable gating mechanisms in a mammalian pacemaker channel. J Biol Chem 277:35939–35946.

Magee JC (1999) Dendritic lh normalizes temporal summation in hippocampal CA1 neurons. Nat Neurosci 2:508–514.

Manent J-B, Demarque M, Jorquera I, Pellegrino C, Ben-Ari Y, Aniksztejn L, Represa A (2005) A Noncanonical Release of GABA and Glutamate Modulates Neuronal Migration. J Neurosci 25:4755–4765.

Manent J-B, Represa A (2007) Neurotransmitters and brain maturation: early paracrine actions of GABA and glutamate modulate neuronal migration. Neuroscientist 13:268–279.

Marín O, Valiente M, Ge X, Tsai L-H (2010) Guiding neuronal cell migrations. Cold Spring Harb Perspect Biol 2:a001834.

Mazzanti M, Bustamante JO, Oberleithner H (2001) Electrical dimension of the nuclear envelope. Physiol Rev 81:1–19.

McCormick DA, Pape HC (1990) Properties of a hyperpolarization-activated cation current and its role in rhythmic oscillation in thalamic relay neurones. J Physiol 431:291–318.

Merseburg A (2016) HCN / h-channel deficiency in forebrain neurons impairs early postnatal development and alters neuronal network activity in mice (Mus musculus , Linnaeus 1758). Dissertation, Universität Hamburg.

Mesirca P et al. (2014) Cardiac arrhythmia induced by genetic silencing of “funny” (f) channels is rescued by GIRK4 inactivation. Nat Commun 5:4664.

Michels G, Er F, Khan IF, Endres-Becker J, Brandt MC, Gassanow N, Johns DC, Hoppe UC (2008) K+ channel regulator KCR1 suppresses heart rhythm by modulating the pacemaker current If. PLoS One 3.

Mienville JM, Barker JL (1997) Potassium current expression during prenatal corticogenesis in the rat. Neuroscience 81:163–172.

Mistrik P, Mader R, Michalakis S, Weidinger M, Pfeifer A, Biel M (2005) The Murine HCN3 Gene Encodes a Hyperpolarization-activated Cation Channel with Slow Kinetics and Unique Response to Cyclic Nucleotides. J Biol Chem 280:27056–27061.

Mistrík P, Pfeifer A, Biel M (2006) The enhancement of HCN channel instantaneous current facilitated by slow deactivation is regulated by intracellular chloride concentration. Pflugers Arch Eur J Physiol 452:718–727.

Molnár Z (2011) Evolution of Cerebral Cortical Development. Brain Behav Evol 78:94–107.

Molyneaux BJ, Arlotta P, Menezes JRL, Macklis JD (2007) Neuronal subtype specification in the cerebral cortex. Nat Rev Neurosci 8:427–437.

Momin A, Cadiou H, Mason A, McNaughton P a. (2008) Role of the hyperpolarization-activated current I h in somatosensory neurons. J Physiol 586:5911–5929.

Moody WJ, Bosma MM (2005) Ion Channel Development, Spontaneous Activity, and Activity-Dependent Development in Nerve and Muscle Cells. Physiol Rev 85:883–941.

Moosmang S, Biel M, Hofmann F, Ludwig a (1999) Differential distribution of four hyperpolarization-activated cation channels in mouse brain. Biol Chem 380:975–980.

Much B, Wahl-Schott C, Zong X, Schneider A, Baumann L, Moosmang S, Ludwig A, Biel M (2003) Role of Subunit Heteromerization and N-Linked Glycosylation in the Formation of Functional Hyperpolarization-activated Cyclic Nucleotide-gated Channels. J Biol Chem 278:43781–43786.

Munsch T, Pape HC (1999) Upregulation of the hyperpolarization-activated cation current in rat thalamic relay neurones by acetazolamide. J Physiol 519 Pt 2:505–514.

Nadarajah B, Brunstrom JE, Grutzendler J, Wong RO, Pearlman a L (2001) Two modes of radial migration in early development of the cerebral cortex. Nat Neurosci 4:143–150.

Nadarajah B, Parnavelas JG (2002) Modes of neuronal migration in the developing cerebral cortex. Nat Rev Neurosci 3:423–432.

Nava C et al. (2014) De novo mutations in HCN1 cause early infantile epileptic encephalopathy. Nat Genet.

Ng S-Y, Chin C-H, Lau Y-T, Luo J, Wong C-K, Bian Z-X, Tsang S-Y (2010) Role of voltage-gated potassium channels in the fate determination of embryonic stem cells. J Cell Physiol 224:165–177.

Noam Y, Ehrengruber MU, Koh A, Feyen P, Manders EMM, Abbott GW, Wadman WJ,

Baram TZ (2014) Filamin A promotes dynamin-dependent internalization of hyperpolarization-activated cyclic nucleotide-gated type 1 (HCN1) channels and restricts Ih in hippocampal neurons. J Biol Chem 289:5889–5903.

Noctor SC, Martínez-Cerdeño V, Ivic L, Kriegstein AR (2004) Cortical neurons arise in symmetric and asymmetric division zones and migrate through specific phases. Nat Neurosci 7:136–144.

Nolan MF, Malleret G, Lee KH, Gibbs E, Dudman JT, Santoro B, Yin D, Thompson RF, Siegelbaum S a, Kandel ER, Morozov A (2003) The hyperpolarization-activated HCN1 channel is important for motor learning and neuronal integration by cerebellar Purkinje cells. Cell 115:551–564.

Notomi T, Shigemoto R (2004) Immunohistochemical localization of Ih channel subunits, HCN1-4, in the rat brain. J Comp Neurol 471:241–276.

Nowakowski RS, Lewin SB, Miller MW (1989) Bromodeoxyuridine immunohistochemical determination of the lengths of the cell cycle and the DNA-synthetic phase for an anatomically defined population. J Neurocytol 18:311–318.

Olsen ML, Sontheimer H (2004) Mislocalization of Kir channels in malignant glia. Glia 46:63–73.

Omelyanenko A, Sekyrova P, Andäng M (2016) ZD7288, a blocker of the HCN channel family, increases doubling time of mouse embryonic stem cells and modulates differentiation outcomes in a context-dependent manner. Springerplus 5:41.

Owens DF, Kriegstein AR (1998) Patterns of intracellular calcium fluctuation in precursor cells of the neocortical ventricular zone. J Neurosci 18:5374–5388.

Pan C, Kumar C, Bohl S, Klingmueller U, Mann M (2009) Comparative Proteomic Phenotyping of Cell Lines and Primary Cells to Assess Preservation of Cell Type-specific Functions. Mol Cell Proteomics 8:443–450.

Pang T, Atefy R, Sheen V (2008) Malformations of cortical development. Neurologist 14:141–164.

Pardo LA, del Camino D, Sánchez A, Alves F, Brüggemann A, Beckh S, Stühmer W (1999) Oncogenic potential of EAG K(+) channels. EMBO J 18:5540–5547.

Pardo LA, Stuhmer W (2008) Eag1: An Emerging Oncological Target. Cancer Res 68:1611–1613.

Paxinos G, Hallyday G, Watson C, Koutcherov Y, Wang HH, Halliday GM, Watson C, Koutcherov Y, Wang HH (2007) Atlas of the Developing Mouse Brain at E17.5, P0 and P6, First Edit. Academic Press.

Pian P, Bucchi A, Robinson RB, Siegelbaum S a (2006) Regulation of gating and rundown of HCN hyperpolarization-activated channels by exogenous and

endogenous PIP2. J Gen Physiol 128:593–604.

Picken Bahrey HL, Moody WJ (2002) Early Development of Voltage-Gated Ion Currents and Firing Properties in Neurons of the Mouse Cerebral Cortex. J Neurophysiol 89:1761–1773.

Picken Bahrey HL, Moody WJ (2003) Voltage-gated currents, dye and electrical coupling in the embryonic mouse neocortex. Cereb Cortex 13:239–251.

Piper DR, Mujtaba T, Rao MS, Lucero MT (2000) Immunocytochemical and physiological characterization of a population of cultured human neural precursors. J Neurophysiol 84:534–548.

Platoshyn O, Golovina VA, Bailey CL, Limsuwan A, Krick S, Juhaszova M, Seiden JE, Rubin LJ, Yuan JX-J (2000) Sustained membrane depolarization and pulmonary artery smooth muscle cell proliferation. Am J Physiol Cell Physiol 279:C1540-9.

Proenza C, Angoli D, Agranovich E, Macri V, Accili EA (2002) Pacemaker channels produce an instantaneous current. J Biol Chem 277:5101–5109.

Proenza C, Yellen G (2006) Distinct Populations of HCN Pacemaker Channels Produce Voltage-dependent and Voltage-independent Currents. J Gen Physiol 127:183–190.

Rakic P (1972) Mode of cell migration to the superficial layers of fetal monkey neocortex. J Comp Neurol 145:61–83.

Rakic P (1974) Neurons in Rhesus Monkey Visual Cortex: Systematic Relation between Time of Origin and Eventual Disposition. Science (80-) 183:425–427.

Rakic P (2009) Evolution of the neocortex: a perspective from developmental biology. Nat Rev Neurosci 10:724–735.

Reiprich P, Kilb W, Luhmann HJ (2005) Neonatal NMDA receptor blockade disturbs neuronal migration in rat somatosensory cortex in vivo. Cereb Cortex 15:349–358.

Resende RR, Adhikari A, da Costa JL, Loren??on E, Ladeira MS, Guatimosim S, Kihara AH, Ladeira LO (2010) Influence of spontaneous calcium events on cell-cycle progression in embryonal carcinoma and adult stem cells. Biochim Biophys Acta - Mol Cell Res 1803:246–260.

Riccio O, Jacobshagen M, Golding B, Vutskits L, Jabaudon D, Hornung JP, Dayer a G (2012) Excess of serotonin affects neocortical pyramidal neuron migration. Transl Psychiatry 2:e95.

Rivera C, Voipio J, Payne J a, Ruusuvuori E, Lahtinen H, Lamsa K, Pirvola U, Saarma M, Kaila K (1999) The K+/Cl- co-transporter KCC2 renders GABA hyperpolarizing during neuronal maturation. Nature 397:251–255.

Roccio M, Schmitter D, Knobloch M, Okawa Y, Sage D, Lutolf MP (2013) Predicting

stem cell fate changes by differential cell cycle progression patterns. Development 140:459–470.

Rodrigues ARA, Oertel D (2005) Hyperpolarization-Activated Currents Regulate Excitability in Stellate Cells of the Mammalian Ventral Cochlear Nucleus. J Neurophysiol 95:76–87.

Rodriguez-Gomez JA, Levitsky KL, Lopez-Barneo J (2012) T-type Ca2+ channels in mouse embryonic stem cells: modulation during cell cycle and contribution to self-renewal. AJP Cell Physiol 302:C494–C504.

Rosenberg SS, Spitzer NC (2011) Calcium signaling in neuronal development. Cold Spring Harb Perspect Biol 3:a004259.

Ross ME, Walsh CA (2001) Human brain malformations and their lessons for neuronal migration. Annu Rev Neurosci 24:1041–1070.

Rowitch DH, Kriegstein AR (2010) Developmental genetics of vertebrate glial-cell specification. Nature 468:214–222.

Rueger MA, Backes H, Walberer M, Neumaier B, Ullrich R, Simard ML, Emig B, Fink GR, Hoehn M, Graf R, Schroeter M (2010) Noninvasive Imaging of Endogenous Neural Stem Cell Mobilization In Vivo Using Positron Emission Tomography. J Neurosci 30:6454–6460.

Sachs HG, Stambrook PJ, Ebert JD (1974) Changes in membrane potential during the cell cycle. Exp Cell Res 83:362–366.

Sakaue-Sawano A, Kurokawa H, Morimura T, Hanyu A, Hama H, Osawa H, Kashiwagi S, Fukami K, Miyata T, Miyoshi H, Imamura T, Ogawa M, Masai H, Miyawaki A (2008) Visualizing Spatiotemporal Dynamics of Multicellular Cell-Cycle Progression. Cell 132:487–498.

Sánchez-Alonso JL, Halliwell JV, Colino A (2008) ZD 7288 inhibits T-type calcium current in rat hippocampal pyramidal cells. Neurosci Lett 439:275–280.

Sandke S (2006) Untersuchungen neuronaler H-Kanal Aktivität mit Hilfe transgener Mäuse (Mus musculus). Dissertation, Universität Hamburg.

Santoro B, Chen S, Luthi a, Pavlidis P, Shumyatsky GP, Tibbs GR, Siegelbaum S a (2000) Molecular and functional heterogeneity of hyperpolarization-activated pacemaker channels in the mouse CNS. J Neurosci 20:5264–5275.

Santoro B, Grant SG, Bartsch D, Kandel ER (1997) Interactive cloning with the SH3 domain of N-src identifies a new brain specific ion channel protein, with homology to eag and cyclic nucleotide-gated channels. Proc Natl Acad Sci U S A 94:14815–14820.

Santoro B, Hu L, Liu H, Saponaro A, Pian P, Piskorowski RA, Moroni A, Siegelbaum SA (2011) TRIP8b Regulates HCN1 Channel Trafficking and Gating through Two

Distinct C-Terminal Interaction Sites. J Neurosci 31:4074–4086.

Santoro B, Lee JY, Englot DJ, Gildersleeve S, Piskorowski RA, Siegelbaum SA, Winawer MR, Blumenfeld H (2010) Increased seizure severity and seizure-related death in mice lacking HCN1 channels. Epilepsia 51:1624–1627.

Santoro B, Liu DT, Yao H, Bartsch D, Kandel ER, Siegelbaum SA, Tibbs GR (1998) Identification of a gene encoding a hyperpolarization-activated pacemaker channel of brain. Cell 93:717–729.

Santoro B, Piskorowski RA, Pian P, Hu L, Liu H, Siegelbaum SA (2009) TRIP8b Splice Variants Form a Family of Auxiliary Subunits that Regulate Gating and Trafficking of HCN Channels in the Brain. Neuron 62:802–813.

Santoro B, Wainger BJ, Siegelbaum SA (2004) Regulation of HCN Channel Surface Expression by a Novel C-Terminal Protein-Protein Interaction. J Neurosci 24:10750–10762.

Scarpulla RC (2008) Nuclear Control of Respiratory Chain Expression by Nuclear Respiratory Factors and PGC-1-Related Coactivator. Ann N Y Acad Sci 1147:321–334.

Schaarschmidt G, Wegner F, Schwarz SC, Schmidt H, Schwarz J (2009) Characterization of Voltage-Gated Potassium Channels in Human Neural Progenitor Cells Linden R, ed. PLoS One 4:e6168.

Schlusche AK (2011) Morphologische Charakterisierung zweier H-Strom defizienter Mauslinien. Diplomarbeit, Philipps-Universität Marburg.

Schmalbach B, Lepsveridze E, Djogo N, Papashvili G, Kuang F, Leshchyns'ka I, Sytnyk V, Nikonenko AG, Dityatev A, Jakovcevski I, Schachner M (2015) Age-dependent loss of parvalbumin-expressing hippocampal interneurons in mice deficient in CHL1, a mental retardation and schizophrenia susceptibility gene. J Neurochem 135:830–844.

Schulze-Bahr E, Neu A, Friederich P, Kaupp UB, Breithardt G, Pongs O, Isbrandt D (2003) Pacemaker channel dysfunction in a patient with sinus node disease. J Clin Invest 111:1537–1545.

Seifert R, Scholten a, Gauss R, Mincheva a, Lichter P, Kaupp UB (1999) Molecular characterization of a slowly gating human hyperpolarization-activated channel predominantly expressed in thalamus, heart, and testis. Proc Natl Acad Sci U S A 96:9391–9396.

Seo H, Seol M-J, Lee K (2015) Differential expression of hyperpolarization-activated cyclic nucleotide-gated channel subunits during hippocampal development in the mouse. Mol Brain 8:13.

Shitamukai A, Konno D, Matsuzaki F (2011) Oblique Radial Glial Divisions in the Developing Mouse Neocortex Induce Self-Renewing Progenitors outside the

Germinal Zone That Resemble Primate Outer Subventricular Zone Progenitors. J Neurosci 31:3683–3695.

Siddiqi F, Chen F, Aron a. W, Fiondella CG, Patel K, LoTurco JJ (2014) Fate Mapping by PiggyBac Transposase Reveals That Neocortical GLAST+ Progenitors Generate More Astrocytes Than Nestin+ Progenitors in Rat Neocortex. Cereb Cortex 24:508–520.

Spitzer NC (2006) Electrical activity in early neuronal development. Nature 444:707–712.

Stevens DR, Seifert R, Bufe B, Müller F, Kremmer E, Gauss R, Meyerhof W, Kaupp UB, Lindemann B (2001) Hyperpolarization-activated channels HCN1 and HCN4 mediate responses to sour stimuli. Nature 413:631–635.

Stieber J, Herrmann S, Feil S, Löster J, Feil R, Biel M, Hofmann F, Ludwig A (2003) The hyperpolarization-activated channel HCN4 is required for the generation of pacemaker action potentials in the embryonic heart. Proc Natl Acad Sci U S A 100:15235–15240.

Stieber J, Stöckl G, Herrmann S, Hassfurth B, Hofmann F (2005) Functional expression of the human HCN3 channel. J Biol Chem 280:34635–34643.

Stonehouse AH, Grubb BD, Pringle JH, Norman RI, Stanfield PR, Brammar WJ (2003) Nuclear Immunostaining in Rat Neuronal Cells Using Two Anti-Kir2.2 Ion Channel Polyclonal Antibodies. J Mol Neurosci 20:189–194.

Strick R, Strissel PL, Gavrilov K, Levi-Setti R (2001) Cation–chromatin binding as shown by ion microscopy is essential for the structural integrity of chromosomes. J Cell Biol 155:899–910.

Sundelacruz S, Levin M, Kaplan DL (2008) Membrane Potential Controls Adipogenic and Osteogenic Differentiation of Mesenchymal Stem Cells Giannobile W, ed. PLoS One 3:e3737.

Sundelacruz S, Levin M, Kaplan DL (2013) Depolarization Alters Phenotype, Maintains Plasticity of Predifferentiated Mesenchymal Stem Cells. Tissue Eng Part A 19:1889–1908.

Surges R, Brewster AL, Bender RA, Beck H, Feuerstein TJ, Baram TZ (2006) Regulated expression of HCN channels and cAMP levels shape the properties of the h current in developing rat hippocampus. Eur J Neurosci 24:94–104.

Surges R, Freiman TM, Feuerstein TJ (2003) Gabapentin increases the hyperpolarization-activated cation current Ih in rat CA1 pyramidal cells. Epilepsia 44:150–156.

Takahashi T, Nowakowski RS, Caviness VS (1993) Cell cycle parameters and patterns of nuclear movement in the neocortical proliferative zone of the fetal mouse. J Neurosci 13:820–833.

Takahashi T, Nowakowski RS, Caviness VS (1995) The cell cycle of the pseudostratified ventricular epithelium of the embryonic murine cerebral wall. J Neurosci 15:6046–6057.

Tamm C, Pijuan Galitó S, Annerén C (2013) A Comparative Study of Protocols for Mouse Embryonic Stem Cell Culturing Milstone DS, ed. PLoS One 8:e81156.

Tang B, Sander T, Craven KB, Hempelmann A, Escayg A (2008) Mutation analysis of the hyperpolarization-activated cyclic nucleotide-gated channels HCN1 and HCN2 in idiopathic generalized epilepsy. Neurobiol Dis 29:59–70.

Tang F, Dent EW, Kalil K (2003) Spontaneous calcium transients in developing cortical neurons regulate axon outgrowth. J Neurosci 23:927–936.

Taniguchi Y, Young-Pearse T, Sawa A, Kamiya A (2012) In utero electroporation as a tool for genetic manipulation in vivo to study psychiatric disorders: from genes to circuits and behaviors. Neuroscientist 18:169–179.

Taverna E, Götz M, Huttner WB (2014) The Cell Biology of Neurogenesis: Toward an Understanding of the Development and Evolution of the Neocortex.

Toth AB, Shum AK, Prakriya M (2016) Regulation of neurogenesis by calcium signaling. Cell Calcium 59:124–134.

Tyler WA, Haydar TF (2013) Multiplex genetic fate mapping reveals a novel route of neocortical neurogenesis, which is altered in the Ts65Dn mouse model of down syndrome. Ann Intern Med 158:5106–5119.

Ulens C, Tytgat J (2001) Functional Heteromerization of HCN1 and HCN2 Pacemaker Channels. J Biol Chem 276:6069–6072.

Urrego D, Tomczak AP, Zahed F, Stuhmer W, Pardo LA (2014) Potassium channels in cell cycle and cell proliferation. Philos Trans R Soc B Biol Sci 369:20130094–20130094.

Vallejo M (2009) PACAP signaling to DREAM: A cAMP-dependent pathway that regulates cortical astrogliogenesis. Mol Neurobiol 39:90–100.

Vasilyev D V, Barish ME (2002) Postnatal development of the hyperpolarization-activated excitatory current Ih in mouse hippocampal pyramidal neurons. J Neurosci 22:8992–9004.

Verkerk AO, Wilders R (2015) Pacemaker activity of the human sinoatrial node: An update on the effects of mutations in hcn4 on the hyperpolarization-activated current. Int J Mol Sci 16:3071–3094.

Wahl-Schott C, Baumann L, Zong X, Biel M (2005) An arginine residue in the pore region is a key determinant of chloride dependence in cardiac pacemaker channels. J Biol Chem 280:13694–13700.

Wahl-Schott C, Biel M (2009) HCN channels: Structure, cellular regulation and

physiological function. Cell Mol Life Sci 66:470–494.

Wainger BJ, DeGennaro M, Santoro B, Siegelbaum S a, Tibbs GR (2001) Molecular mechanism of cAMP modulation of HCN pacemaker channels. Nature 411:805–810.

Wang DD, Kriegstein AR (2009) GABA Regulates Excitatory Synapse Formation in the Neocortex via NMDA Receptor Activation. J Neurosci 28:5547–5558.

Wang K, Xue T, Tsang S-Y, Van Huizen R, Wong CW, Lai KW, Ye Z, Cheng L, Au KW, Zhang J, Li G-R, Lau C-P, Tse H-F, Li R a (2005) Electrophysiological properties of pluripotent human and mouse embryonic stem cells. Stem Cells 23:1526–1534.

Wang X, Tsai J-W, LaMonica B, Kriegstein AR (2011) A new subtype of progenitor cell in the mouse embryonic neocortex. Nat Neurosci 14:555–561.

Weissman T a, Riquelme P a, Ivic L, Flint AC, Kriegstein AR (2004) Calcium waves propagate through radial glial cells and modulate proliferation in the developing neocortex. Neuron 43:647–661.

Wicks NL, Wong T, Sun J, Madden Z, Young EC (2010) Cytoplasmic cAMP-sensing domain of hyperpolarization-activated cation (HCN) channels uses two structurally distinct mechanisms to regulate voltage gating. Proc Natl Acad Sci U S A 108:609–614.

Wierschke S, Lehmann TN, Dehnicke C, Horn P, Nitsch R, Deisz RA (2010) Hyperpolarization-activated cation currents in human epileptogenic neocortex. Epilepsia 51:404–414.

Williams SR, Stuart GJ (2000) Site independence of EPSP time course is mediated by dendritic I(h) in neocortical pyramidal neurons. J Neurophysiol 83:3177–3182.

Wonderlin WF, Woodfork KA, Strobl JS (1995) Changes in membrane potential during the progression of MCF-7 human mammary tumor cells through the cell cycle. J Cell Physiol 165:177–185.

Wu X, Liao L, Liu X, Luo F, Yang T, Li C (2012) Is ZD7288 a selective blocker of hyperpolarization-activated cyclic nucleotide-gated channel currents? Channels (Austin) 6:438–442.

Xue T, Marbán E, Li RA (2002) Dominant-negative suppression of HCN1- and HCN2-encoded pacemaker currents by an engineered HCN1 construct: insights into structure-function relationships and multimerization. Circ Res 90:1267–1273.

Yang M, Brackenbury WJ (2013) Membrane potential and cancer progression. Front Physiol 4:185.

Yang SJ, Liang HL, Ning G, Wong-Riley MTT (2004) Ultrastructural study of depolarization-induced translocation of NRF-2 transcription factor in cultured rat visual cortical neurons. Eur J Neurosci 19:1153–1162.

Yasuda T, Bartlett PF, Adams DJ (2008) Kir and Kv channels regulate electrical properties and proliferation of adult neural precursor cells. Mol Cell Neurosci 37:284–297.

Ying S-W, Tibbs GR, Picollo A, Abbas SY, Sanford RL, Accardi A, Hofmann F, Ludwig A, Goldstein P a (2011) PIP2-Mediated HCN3 Channel Gating Is Crucial for Rhythmic Burst Firing in Thalamic Intergeniculate Leaflet Neurons. J Neurosci 31:10412–10423.

Ying SW, Kanda VA, Hu Z, Purtell K, King EC, Abbott GW, Goldstein PA (2012) Targeted deletion of Kcne2 impairs HCN channel function in mouse thalamocortical circuits. PLoS One 7.

Yoshinaka-Niitsu A, Yamagaki T, Harada M, Tachibana K (2012) Solution NMR analysis of the binding mechanism of DIVS6 model peptides of voltage-gated sodium channels and the lipid soluble alkaloid veratridine. Bioorg Med Chem 20:2796–2802.

Zagotta WN, Olivier NB, Black KD, Young EC, Olson R, Gouaux E (2003) Structural basis for modulation and agonist specificity of HCN pacemaker channels. Nature 425:200–205.

Zhou Y, Wong C-O, Cho K -j., van der Hoeven D, Liang H, Thakur DP, Luo J, Babic M, Zinsmaier KE, Zhu MX, Hu H, Venkatachalam K, Hancock JF (2015) Membrane potential modulates plasma membrane phospholipid dynamics and K-Ras signaling. Science (80-) 349:873–876.

Zolles G, Klöcker N, Wenzel D, Weisser-Thomas J, Fleischmann BK, Roeper J, Fakler B (2006) Pacemaking by HCN Channels Requires Interaction with Phosphoinositides. Neuron 52:1027–1036.

Zolles G, Wenzel D, Bildl W, Schulte U, Hofmann A, Müller CS, Thumfart JO, Vlachos A, Deller T, Pfeifer A, Fleischmann BK, Roeper J, Fakler B, Klöcker N (2009) Association with the Auxiliary Subunit PEX5R/Trip8b Controls Responsiveness of HCN Channels to cAMP and Adrenergic Stimulation. Neuron 62:814–825.

Zong X, Eckert C, Yuan H, Wahl-Schott C, Abicht H, Fang L, Li R, Mistrik P, Gerstner A, Much B, Baumann L, Michalakis S, Zeng R, Chen Z, Biel M (2005) A novel mechanism of modulation of hyperpolarization-activated cyclic nucleotide-gated channels by Src kinase. J Biol Chem 280:34224–34232.

Zong X, Stieber J, Ludwig A, Hofmann F, Biel M (2001) A Single Histidine Residue Determines the pH Sensitivity of the Pacemaker Channel HCN2. J Biol Chem 276:6313–6319.

8 List of abbreviations

3D	three dimensional
aIP	apical intermediate progenitors
AMPA	α-amino-3-hydroxy-5-methyl-4-isoxazolepropionic acid
aRG	apical RGs
BAC	bacterial artificial chromosome
BCA	bicinchoninic acid assay
bIP	basal intermediate progenitors
BrdU	5-Bromo-2’-deoxyuridine
bRG	basal RGs
BSA	bovine serum albumin
CA	cornus ammonis region
CAG	cytomegalovirus enhancer combined with chicken beta actin
CaSR	calcium-sensing receptor
CHO	chinese hamster ovary
CISS	constructive interference in steady state
CNBD	cyclic nucleotide-binding domain
CNPAse	2',3'-cyclic-nucleotide 3'-phosphodiesterase
con	control mice
CP	cortical plate
CREB	cAMP response element-binding protein
CT	cycle threshold
dox	doxycycline until P0
E	embryonal day

EAG	ether-à-go-go potassium channel
ER	endoplasmatic reticulum
ERK	extracellular signal-regulated kinase
FACS	fluorescence-activated cell sorting
FGF	fibroblast growth factor
FOV	field of view
FPKM	fragments per kilo base per million reads
FUCCI	fluorescence ubiquitination cell cycle indicator
GABA	γ-aminobutyric acid
GC	guanine-cytosine
GE	ganglionic eminence
GFAP	glial fibrillary acidic protein
GFP	green fluorescent protein
gIP	glial progenitor cells
GYG	glycine – tyrosine – glycine motif
h	human
HA	Hemagglutinin
HCN	hyperpolarization-activated cyclic nucleotide-binding non-selective cation
HCN-DN	dominant negative HCN subunit
HCN-WT	wildtype HCN
HRP	horse radish peroxidase
i.p.	intra peritoneal
I_A	transient, inactivating potassium current
IC_{50}	half maximal inhibitory concentration
I_{DR}	delayed rectifying potassium current

IgG	immunoglobulin G
I_h	hyperpolarization activated current (HCN mediated)
I_{ins}	instantaneous current; voltage-insensitive
I_{IR}	inwardly rectifying potassium current
IP_3	inositol 1,4,5-trisphosphate
IRES	internal ribosomal entry site
I_{ss}	steady-state current
IUE	*in utero* electroporation
IZ	intermediate zone
KCC2	potassium/chloride co-transporter 2
KCR1	potassium channel regulator protein 1
KCTD3	potassium channel tetramerization-domain containing protein 3
KID 1	kinase induced upon depolarization 1
LDH	lactate dehydrogenase
MAPK	mitogen-activated protein kinase
MGE	medial ganglionic eminence
MiRP1	MinK-related protein 1
mut	mutant mice
MZ	marginal zone
NE	neuroepithelium
NeuN	neuronal nucleus antigen
NGS	next generation sequencing
NMDA	N-methyl-D-aspartate
Nrf 2	the nuclear respiratory factor 2
NSC	neural stem cell culture

OCT	optimal cutting temperature compound
OD	optical density
P	postnatal day
PACAP	pituitary adenylate cyclase-activating polypeptide
PB	phosphate buffer
PBS	phosphate buffered saline
PCR	polymerase chain reactions
PFA	paraformaldehyde
PI	propidium iodid
PIP_2	phosphatidylinositol 4,5-bisphosphate
P_{tet}	tetracycline transactivator responsive element
RG	radial glial cells
ROI	region of interest
S	transmembrane domains
SVZ	subventricular zone
TBS	Tris buffered saline
tdTomato	tandem dimer Tomato
TE	echo time
TR	repetition time
TRIP8b	tetratricopeptide repeat containing Rab8b interacting protein
tTA	tetracycline transactivator
TuJ1	class III β-tubulin
VGCC	voltage-gated calcium channels
VZ	ventricular zone
wpc	weeks post conception

9 Acknowledgement

I would like to particularly thank Professor U. B. Kaupp for reviewing this doctoral work and support me with stimulating discussions and remarks. Professor M. Paulsson belongs my heartily gratitude for his unconventionally support and reviewing my doctoral thesis.

Furthermore, I would like to express my gratitude to Professor D. Isbrandt, my supervisor, for giving me the opportunity to work in his lab at this fascinating research project, and his scientific and personal support during the years and especially during the movement from Hamburg to Cologne.

My sincere thanks goes to Professor S. Schoch-McGovern for her support as member of my thesis committee, the generous supply with constructs for further *in utero* electroporation experiments, and her advice and endorsement in my future scientific steps.

I had the great luck to be part of a fruitful collaboration with Dr S. Vay and PD. Dr. A. Rüger from the research group Neural Stem Cells of the University Hospital Cologne. Dr. Vays expertise in cortical stem cell culture and related experiments helped adding valuable contribution to this work.

Dr. M. Florio from the Huttner laboratory at the Max-Plank Institute in Dresden kindly provided me with NGS data.

I was greatly advised and supported at the MRI analysis by Dr. J Sedlacik.

I am grateful of being part of the ENP Team and I would like to thank every one of them for their scientific and personal support during the years. I would like to especially thank Dr. I. Jakovcevski for introducing me to the embryonic world of the brain and supervising me in the last years of the thesis. To Dr. W. Fazeli belongs my gratitude for proof reading this doctoral work and all the great pep talks. I heartily thank K. Sauter for sharing her tips and tricks in the lab with me, her endless knowledge of diverse methods and making incubations times so much fun.

Last but not least I would like to thank my family and friends for watching my back and keeping my chin up.

10 Erklärung

Ich versichere, dass ich die von mir vorgelegte Dissertation selbständig angefertigt, die benutzten Quellen und Hilfsmittel vollständig angegeben und die Stellen der Arbeit – einschließlich Tabellen, Karten und Abbildungen –, die anderen Werken im Wortlaut oder dem Sinn nach entnommen sind, in jedem Einzelfall als Entlehnung kenntlich gemacht habe; dass diese Dissertation noch keiner anderen Fakultät oder Universität zur Prüfung vorgelegen hat; dass sie – abgesehen von unten angegebenen Teilpublikationen – noch nicht veröffentlicht worden ist, sowie, dass ich eine solche Veröffentlichung vor Abschluss des Promotionsverfahrens nicht vornehmen werde. Die Bestimmungen der Promotionsordnung sind mir bekannt. Die von mir vorgelegte Dissertation ist von Herrn Professor Dr. U.B. Kaupp betreut worden.